Swim Like Your Lifecycle Depends On It

Investigating Motility of *Leishmania mexicana*; its Impact on Parasite Lifecycle Progression and Infectivity.

Rachel Christina Findlay

Doctor of Philosophy

University of York

Biology

September 2018

Abstract

The motility of *Leishmania* promastigote parasites is important for survival during host transitions and lifecycle progression. An oscillating flagellum at the anterior end of the promastigotes pulls it through environmental conditions which change significantly during the lifecycle. The parasite morphologically transforms to optimise infection potential.

This study adapts a unique method of high-speed, three-dimensional imaging called digital inline holographic microscopy (DIHM) allowing us to examine the movements of *Leishmania mexicana* promastigotes. We have tracked distinct stages of promastigote parasites over multiple frames to gain information on the swimming patterns of these cells. Quantification of the 3D trajectories reveals stage-specific differences in swimming behaviour.

Using this technique we reveal that mammalian-infective metacyclic promastigotes are more capable of swimming in highly viscous solutions, a result which has interesting implications in the ability of this specific stage to transmit through promastigote secretory gel.

Additionally, the DIHM technique has allowed us to investigate whether these different stages of *Leishmania* promastigote are capable of sensing chemicals in their environment. We reveal how distinct chemotaxic capabilities could play a role in the uptake of parasites by host cells during early infection.

Mathematically quantifying the cell movements of *L. mexicana* within contrasting, biologically relevant environments has revealed swimming mechanisms that are essential for the parasite to remain unencumbered by environmental pressures and adapt their motility to reach preferred conditions.

Contents

List of Figures

Acknowledgements

There are so many people to who I am indebted to and owe a great deal of gratitude for their help and support during the preparation of this thesis. Firstly and foremost I would like to thank my supervisors for without them both this would have been impossible. Dr Pegine Walrad for her passion for parasitology and for always being understanding and supportive. Dr Laurence Wilson for his biophysics expertise and constant encouragement throughout. Additionally, I must thank collaborators of this project; Dr Hermes Gadelha, Dr Matthew Rogers, Dr Helen Price, and TAP members; Dr Thomas Krauss and Dr Jeremy Mottram for the invaluable discussions and feedback. Also the University of York, the Wellcome Trust and everyone involved in the CIDCATS programme for the opportunity. Thanks also to swimmers, biophysics and leishmaniacs groups for fruitful discussions and helpful feedback. Particularly Luis de Pablos and Tiago Ferreira, post docs from the Walrad lab, for always taking time to help me in the lab. Also many thanks to Nik and Katie for providing the perfect office environment for a good rant, I am glad we got through this experience together.

On a less academic level many thanks are owed to caving and the entire caving community for welcoming me into a new family far from home! From exploring new territory abroad to digging grotty holes in the Moors or even just a fun sporting trip in the Dales, each and every one of you have contributed to keeping me motivated to complete this PhD. Many ask me why I go caving and the main reason is the people and true friendships formed in the formidable excluded places we venture to. Thank you all for the escape route when everything got too much and for literally being a bright light in the darkness.

A huge thanks has to go to my family for their continuous support throughout my life leading to this point. Particularly my parents for being a great example of where hard work can get you and encouraging me to do the same. Finally thanks to Nick, I could not have done it without your constant positivity and belief in me.

Authors Declaration

I declare that this thesis is a presentation of original work and I am the sole author. This work has not previously been presented for an award at this, or any other, University. All sources are acknowledged as References.

Chapter 1

Introduction

1.1 Motivation and Aims

Leishmaniasis is a neglected tropical disease affecting 12 million people in 98 countries worldwide [1]. Despite its neglect the disease is responsible for 50 000 deaths annually and hence is the second deadliest parasitic disease after malaria [2]. There are no current 'wide-scale' vaccines in existence to prevent leishmaniasis, yet the World Health Organisation (WHO) have stated their target is to combine detection, prevention and control measures to achieve elimination by 2020 [3]. Our understanding of the eukaryotic parasites causing this disease is surprisingly limited, particularly of the specific promastigote forms involved in transmission from vector to host, increasing the difficulty of meeting this aim.

The *Leishmania* promastigote parasites involved in transmission and early infection in the mammalian host are highly motile due to an appendage located at the anterior of the cell body. This flagellum pulls the cell through different environments which change significantly during the lifecycle. In addition to the varying environments, the parasite transforms itself morphologically, adapting its cell body shape and flagellum length and as a result altering its motility. The motility of these parasites, and hence the mechanisms they use to accomplish these movements, are important for the cyclical progression and host transitions which promote disease development and yet we understand very little of how they achieve this and precisely how motility affects these processes.

This study adapts a unique method of three-dimensional (3D) imaging called digital inline holograpgic microscopy (DIHM) to track the movements of large populations of *L. mexicana* promastigotes. Mathematical quantification of these 3D swimming trajectories allows us to distinguish and compare the swimming patterns of two lifecycle stages, procyclic and metacyclic promastigotes, under varying, biologically-relevant environmental conditions. Investigating the relationship between the motility of the parasites in relation to its infectivity allows us to determine which factors are essential to lifecycle progression and hence survival and transmission.

More specifically the project aims to:

1. Investigate if the different lifecycle stages swim differently, in controlled environments, and characterise distinguishing features.

2. Determine how the mammalian infective metacyclic promastigotes are ca-

pable of transmission through the promastigote secretory gel (PSG) plug by observing and quantifying their movement therein.

3. Determine if a chemical stimulus influences *Leishmania* swimming behaviour to promote leukocyte infection. By designing and developing chemotaxis assays this part of the study aims to determine whether parasites can sense chemical gradients within their surroundings and whether their motility responds to these.

Three-dimensional tracking and mathematical quantification of the cell movements of *Leishmania* procyclic and metacyclic promastigotes may reveal how the parasites use and adapt swimming mechanisms to overcome environmental pressures, promote transmission and perpetuate leishmaniasis worldwide.

1.2 Outline

Chapter 2 provides the necessary biological background details, including an introduction to the disease, leishmaniasis, and highlights the importance of this study. It also includes details of the *Leishmania* parasites, their lifecycle and the different environments and challenges which must be overcome to transmit and propagate disease.
Chapter 3 reviews previous studies analysing the motility of other microorganisms and discusses how *Leishmania* research could benefit from using similar interdisciplinary tools and methods. We also discuss the challenges and complexities of using each method for *Leishmania* including details of how these could be overcome to improve our knowledge of *Leishmania* motility.
Chapter 4 describes the main method used throughout all our experiments to capture three-dimensional swimming tracks of the parasites. This chapter describes the digital inline holographic microscopy (DIHM) technique in detail, giving an overview of its principles, setup, processing procedures and applications.
Chapter 5 concentrates on characterising distinguishing features of the different *Leishmania* promastigote stages motility patterns. Details of methods for defining lifecycle stages, DIHM post-processing and analytical quantification are explained comprehensively before displaying and discussing results. This chapter also includes results exploring the effects of a genetic mutation on the parasites' motility.
Chapter 6 quantifies the effects of promastigote secretory gel and other viscous solutions on the motility of *Leishmania* promastigotes and relates how this has implications in transmission from sandfly vector to mammalian host.
Chapter 7 details a unique, high-throughput assay for analysing chemotaxic capabilities of *Leishmania* promastigotes and discovers the motile methods they use to accomplish taxic behaviour.
Chapter 8 draws conclusions of this work, and details possible future objectives.
Appendix A includes supplementary figures analysing the torsion of the parasites' trajectories in M199 media alone.

Chapter 2

Biological Background Information

This chapter provides an introduction to the disease of interest, leishmaniasis, and highlights the importance of its study. It also includes details of the parasite which causes the disease, its lifecycle and the environmental pressures that the parasite has overcome in order to transmit and propagate disease.

2.1 Leishmaniasis: the motivation behind the research

Leishmaniasis is one of the world's most neglected diseases, largely affecting the poorest areas of the world [1]. Despite its neglect in funding and publicity, it is prevalent in 98 countries across five continents affecting 12 million people worldwide [2]. The disease is responsible for up to 50 000 deaths annually [2], making it the second deadliest parasitic disease after malaria [4]. The distribution of leishmaniasis is expanding and the number of reported cases have increased exponentially over the past two decades [2].

The disease presents itself in three different forms; cutaneous, mucocutaneous and visceral leishmaniasis. Cutaneous leishmaniasis is the most common form, with clinical symptoms appearing in the form of a skin lesion at the site of inoculation [4]. These usually develop into an ulcer (Fig 2.1.1) which heals spontaneously leaving disfiguring scars [5]. Mucocutaneous leishmaniasis causes metastasis of the mucosal tissues of the mouth and upper respiratory tract by lymphatic or haematogenous dissemination [4]. The most fatal form of the disease is visceral leishmaniasis whereby the parasite causing the disease can disseminate to internal organs such as liver, spleen and bone marrow [6]. Symptoms include fever, fatigue, weakness, loss of appetite and weightloss [5].

There are no current 'wide-scale' vaccines in existence to prevent leishmaniasis and progress has been limited [5]. There are several drug treatments available which include oral, parenteral and topical medications. Since the 1940's, pentavalent antimonials have been the main treatment options, however complications arise with adverse, sometimes life-threatening, side effects, resistance (liposomal amphotericin B has replaced antimonials in regions where resistance is common) and costs [1]. Current research into antileishmanial drugs such as miltefosine,

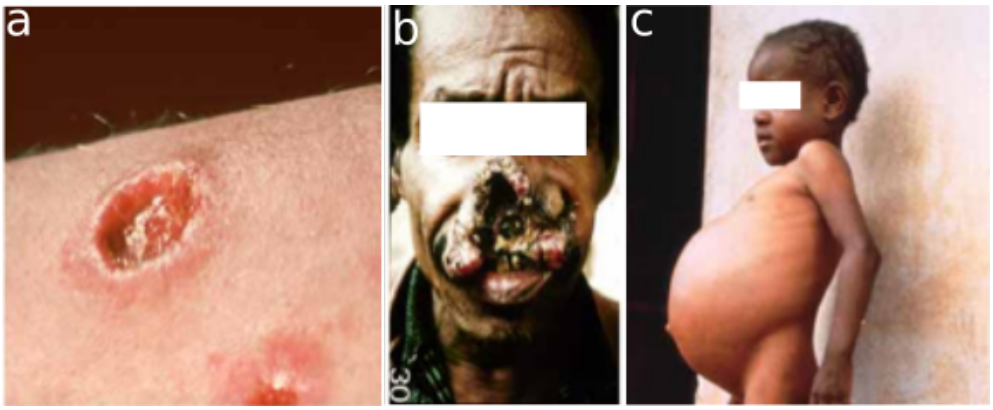

Figure 2.1.1: Symptoms of the three forms of leishmaniasis. **a** Skin lesions caused by cutaneous form. **b** Ulcers develop on the oral or nasal mucosa with mucocutaneous form. **c** Enlargement of spleen and liver is often seen with visceral leishmaniasis.

paromycin and sitamaquine might expand treatment options in the future [5] but new diagnostic tools and treatment strategies will only have an impact on the disease if they are made widely available to patients.

2.2 *Leishmania* Parasites: the source of the disease

Leishmaniasis is caused by infection with one of the 21 species of *Leishmania*, an intracellular protozoan parasite that maintains its lifecycle via transmission between the female phlebotomine sandfly and a mammalian host [6]. Motility plays a crucial role in the lifecycle of *Leishmania* parasites and their trypanosome cousins. They have a single flagellum anchored to the anterior end of the body which allows motility for some or all of their lifecycle [7]. This flagellum not only drags the organism through its environment but there is also evidence of a role in attachment to the sandfly vector's gut [8].

There are two main morphological forms of *Leishmania* parasite:, amastigotes and promastigotes. The amastigotes are small, ellipsoid shaped bodies, approximately 3-5 μm in size [1], which multiply by binary fission at 37°C in the mammalian host cells [9]. This form is an obligate, non-motile parasite. Although they do have a short flagellum, it is not considered to have any role in motility. The single-flagellated, motile forms of *Leishmania* are called promastigotes. These motile organisms are larger and relatively slender, measuring 15-30 μm in length [1] and are mainly found in the gut of the sandfly where they undergo multiple stages of differentiation collectively termed 'metacyclogenesis'.

2.2.1 The Flagella

In promastigotes, the flagellum emerges from an invagination of the plasma membrane called the flagellar pocket [11]. It consists of canonical 9+2 microtubular axoneme and a filamentous paraflagellor rod (PFR) running parallel to the axoneme (Fig 2.2.2b) [12]. Amastigotes although non-motile do have a short flagellum which is potentially involved with sensory perception and cellular or-

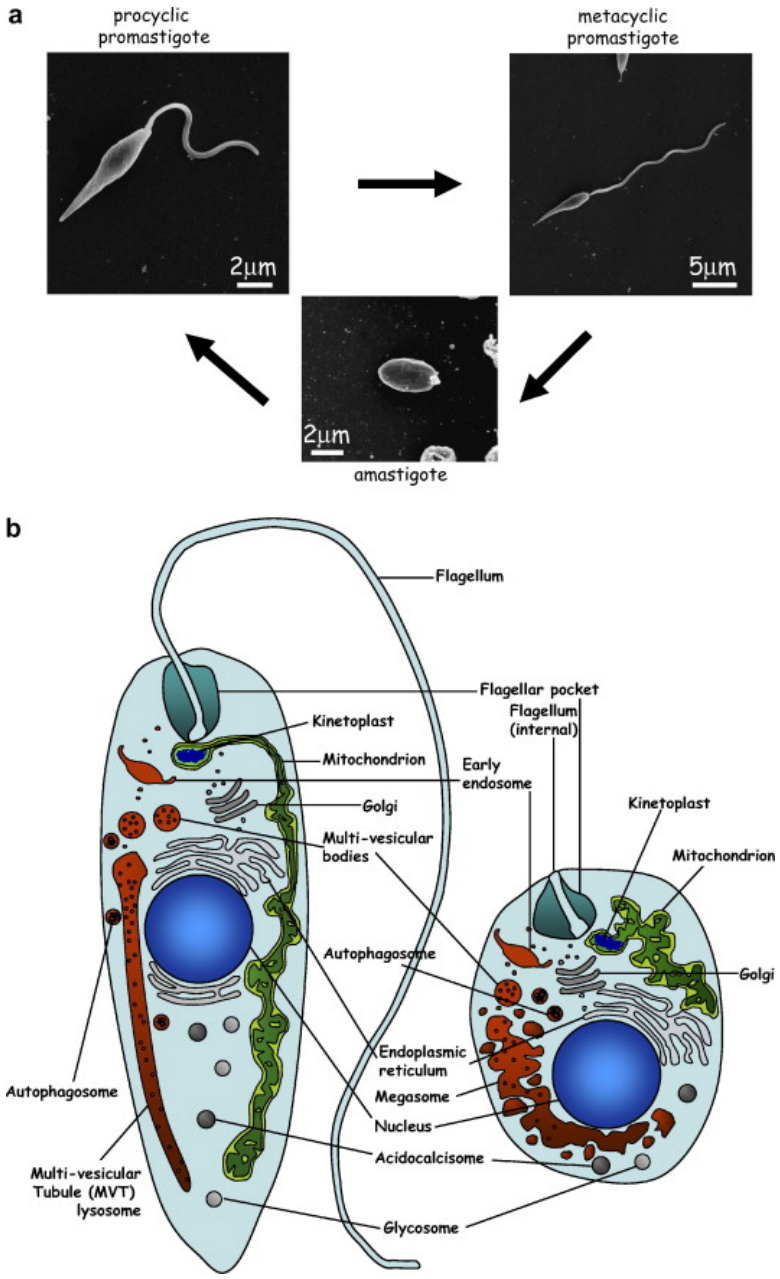

Figure 2.2.1: Changes in cell shape during the *Leishmania* life cycle. **a** Scanning electron microscope images of an amastigote and procyclic and metacyclic promastigotes. **b** Schematic representation of the intracellular organelles in the promastigote (left) and amastigote (right) [10].

ganisation [13]. The amastigotes have no PFR and the 9+2 microtubular pattern is only seen for a short distance beyond the flagellar pocket. Distally, the two central microtubules are absent and one or two outer doublets occupy a more central position instead (Fig 2.2.2a) [12].

How *Leishmania* parasites regulate their flagellum length is another area which has been investigated to an extent. Most eukaryotic flagella, including those of trypanosomatids, requires sophisticated interacting mechanisms for growth and maintenance. Elongation or shortening of the microtubules at the flagellar tip occurs by a highly dynamic process, intraflagellar transport (IFT), which involves the transport of tubulin and other precursors by distinct molecular motors [7].

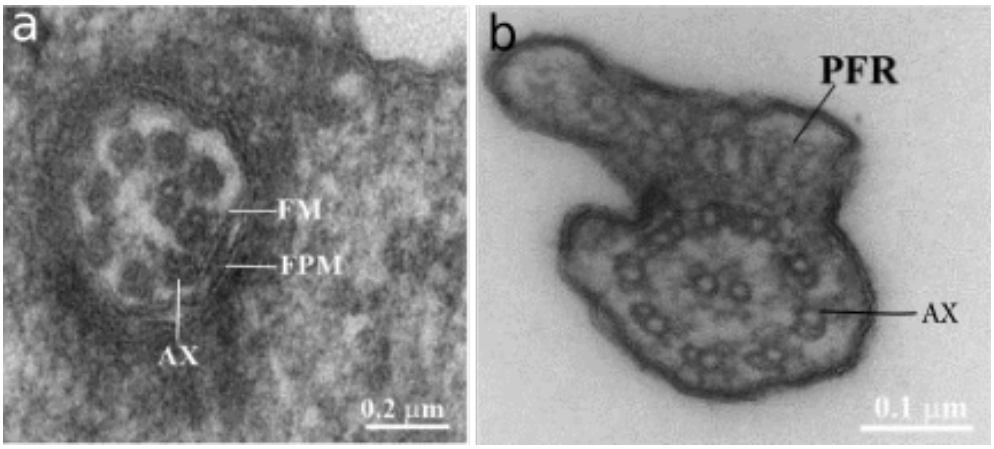

Figure 2.2.2: Cross sectional transmission electron microscopy of *L. amazonensis* parasites. **a** 8+1 axoneme arrangement observed in the distal region of the axoneme of amastigote parasites. **b** An assembled axoneme and paraflagellar rod observed in promastigite flagellum. FM - flagellar membrane, FPM - flagella pocket membrane, AX - axoneme, PFR - paraflagellar rod [12].

2.3 The *Leishmania* Lifecycle

Leishmania parasite transmission occurs through the bite of a sandfly insect vector, essential for the disease to establish infection. The parasites must adapt both themselves and their environments to efficiently progress through the lifecycle. The disease will not be transmitted if the cycle is broken at any point and therefore must be tightly regulated.

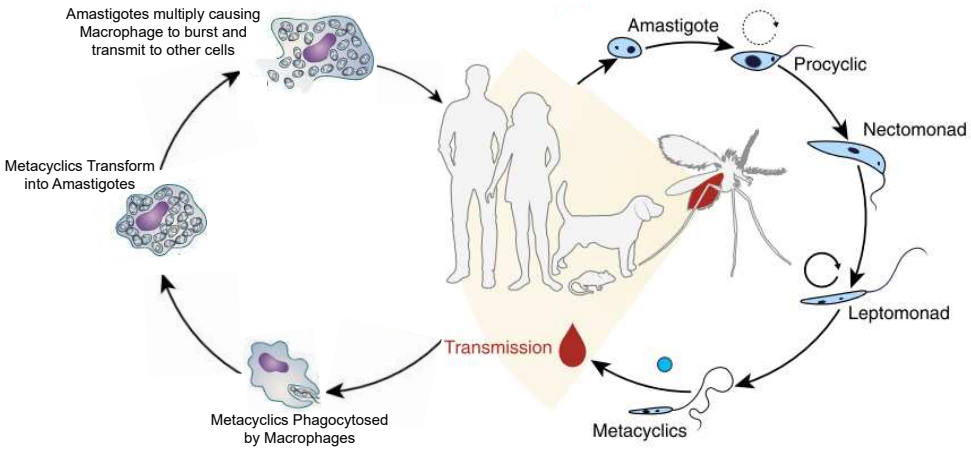

Figure 2.3.1: The complete life cycle of *Leishmania* in the mammalian host and sandfly vector (Adapted from [14] and [15]). Greater detail on the sandfly stages, which are particularly important to this study, can be found in figure 2.3.2b.

2.3.1 Sandfly Vector

Leishmaniasis is a vector-borne disease transmitted by the bite of female phlebotomine sandflies [16]. These dipteran insects belong to the Psychodidae family [17]. It is estimated that out of 700 identified species of sandfly only ∼10% are implicated in the transmission of *Leishmania* parasites [17].

The sandfly belongs to a large group of arthropod vectors known as pool feeders, they acquire parasites when they feed on an infected host while taking a blood meal. They saw into the skin of the infected host with barbed mouthparts, lacerating the dermal capillaries to form a pool of blood [18]. Whilst biting, the sandflies continously secrete saliva into the wound to keep the blood liquid [18]. Blood is then sucked from the pool into the pharyngeal chamber before it is pushed through the stomodeal valve into the midgut (Fig 2.3.2a). Once in the midgut the bloodmeal is encapsulated in a peritrophic matrix to allow digestion to begin [18].

Metacyclogenesis

Within the gut of the fly numerous developmental forms can be observed as they migrate anteriorly from the posterior midgut to the stomodeal valve, which forms a junction with the foregut, in order to become the highly infective metacyclic promastigotes [19]. The first indication of parasite morphogenesis was demonstrated when promastigotes taken from sandflies 3 days after bloodmeal were essentially avirulent, whereas promastigotes taken 7-8 days after were highly virulent in mice [20]. These stages have been characterised morphologically and by functional changes which ensure survival in the sandfly.

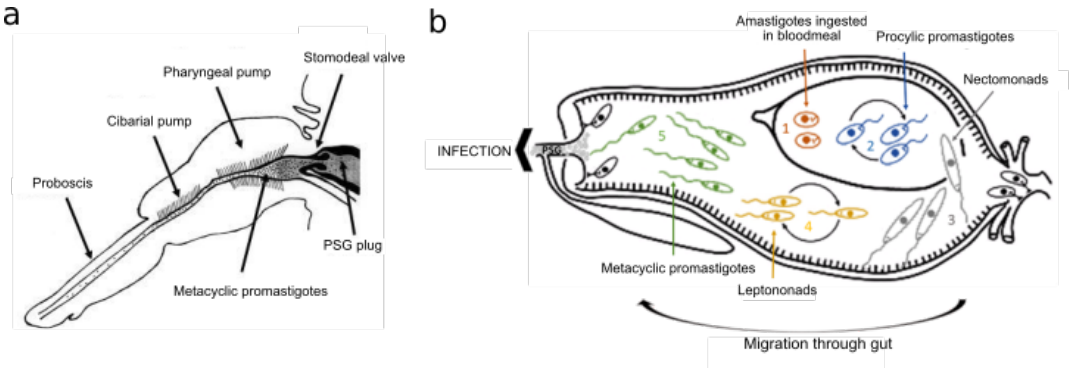

Figure 2.3.2: *Leishmania* within the sandfly vector. **a** Foregut and mouthparts of the sandfly [17]. **b** Lifecycle of *Leishmania* in a the gut of a competent vector. Illustrates time-dependant appearance of distinct morophological form of promastigotes as they migrate through the gut. Adapted from Dostalava et al. (2012) [21].

On taking a bloodmeal the fly acquires the parasites in the ovoid amastigote form. Within 4 hours the infected bloodmeal is contained within a peritrophic matrix (PM) [16]. The PM is a sac of proteins and glycoproteins held together by chitinous microfibrils which surround the bloodmeal forming a barrier that protects the midgut epithelium from abrasive food particles and microbes as well as slowing down the diffusion of digestive proteases into the endoperitrophic space (the space within the PM) [16]. This barrier provides the necessary time to allow the parasite to differentiate into a form which is resistant to midgut proteases, which peak 18-48 hours after blood feeding [16].

These resistant parasites, tranformed from amastigotes, are procyclic promastigotes with a short flagellum, similar in length to the cell body. They begin their first multiplication cycle in the sandfly by binary fission for the next 24-48 hours [16]. By day 2-3, procyclics have developed into nectomonads, large slender forms whose function is to anchor themselves to epithelial cells which line the

midgut and migrate forwards to colonise the anterior midgut. This migration is aided by the degeneration of the PM enabling the nectomonads to escape into the gut lumen. The PM is degraded by chitinases, within 48-72 hours of blood feeding, and expelled along with the undigested bloodmeal. Sandfly chitinases peak at the same time that the nectomonads escape from this barrier. Inhibition of chitinase activity also leads to loss of parasites, presumably because of their inability to escape the PM before defecation [16].

By day 4, leptomonads arise from nectomonads and initiate the second multiplication cycle in the sandfly causing a mass infection at the anterior midgut by day 5-7. Its at this time where the development of haptopmonads appear, whose precursor form is still in question (nectomonads or leptomonads) [16]. This form is a highly specialised, leaf-shaped parasite with a short flagellum. Haptomonads are non-motile and form a plug at the stomodeal valve [16]. The plug is formed as the static parasites attach to each other and the cuticle lining of the valve forming concentric rings of parasites the stop the opening of that valve.

The form which is found in abundance at the stomodeal valve is the highly infective, non-dividing metacyclic promastigote [20, 22]. Differentiated from leptomonads, they have a slender cell body with an elongated flagellum, approximately double the length of its cell body [23]. These mammalian-infective parasites are rapid, free-swimming and highly adapted for transmission and early survival in the vertebrate host.

Some very new research has suggested an additional lifecycle stage caused by the dedifferentitiation of metacyclic promastigotes as an effect of subsequent uninfected bloodmeals by the sandfly [14]. This reverse metacyclogensis results in 'retroleptomonad' promastigotes which are very proliferative and hence multiply rapidly before differentiating to metacyclics and thereby enhancing relative infectiousness. This research shows our understanding of this parasites lifecycle is constantly evolving and progressing. Multiple bloodmeals are shown to have a fundamental role in this cycle and the metacyclic parasites are more plastic than previously thought, which combines to amplify infection.

Metacyclogensis is induced *in vitro* by low pH, anaerobic conditions and decline in a cofactor essential for catalytic activity of nitric oxide synthase, tetrahydrobiopterin [16]. However, *in vivo* the triggers for metacyclogenesis are unknown though some possibilities have been explored [24, 25]. This is an important gap in research of this disease cycle as the transition from replicative, non-infectious procyclic promastigotes, to non-replicating, highly infectious metacyclic promastigotes is a crucial step in the lifecycle of *Leishmania* parasites, promoting infection both within the sandfly vertebrate hosts.

Transmission and the Importance of Promastigote Secretory Gel.

The mechanism for transmission from the sandfly into a mammalian host is thought to follow an adapted 'blocked-fly' hypothesis. The formation of a gel causes an obstruction in the midgut and pharynx of the sandfly [18]. It forces the stomodeal valve open allowing parasites and gel to reach the pharynx and foregut [26]. This promastigote secretory gel (PSG) is highly soluble so when blood is drawn through the parasite-gel obstruction on feeding, a portion of midgut parasites and PSG are regurgitated by backflow into the skin of the

mammal [18]. It regurgitates an estimated $\sim 10^3$ metacyclic promastigotes into the vertebrate host [27].

Leishmania synthesize abundant phophoglycan (PG)-containing molecules including surface lipophosphoglycan (LPG) and surface secreted proteophosphoglycans (PPGs) [18]. PSG is comprised of filamentous PPG (fPPG), the largest molecule secreted by *Leishmania*, specifically leptomonads, (3-6μm diameter, up to 6μm length) [18]. It is a high molecular weight glycoprotein which forms a dense three-dimensional network of PSG [28].

In 1960, a protocol to purify the novel filamentous phosphoglycan-modified secretory compound from *L. major* parasites in culture was determined [28], this has since been developed for other *Leishmania* species. The purification involves passing log/early stationary phase promastigotes ($1 - 1.5 \times 10^8$ cells/ml) through a DE52-cellulose anion exchange chromatography column and eluting the bound PPG with NaCl buffer. The fractions collected were subjected to an ultracentrifugation regime before resuspending the pellet in a CaCl solution [28]. Compositional analysis of the purified PPG showed it contains 4.4% amino acids, 20% phosphate and 75.6% monosaccharides (mainly Man, Gal and Gal-6-phosphate) [28].

The PSG plug obstructing the anterior midgut is packed with promastigote cell bodies [17]. Using scanning electron microscopy (SEM) the PSG plug can be visualised in situ (Fig. 2.3.3). Cells embedded in the plug appear immobile and show little evidence of life. However, when dissected from the sandfly into culture medium the PSG dissolves and the parasites regain motility [17]. The freed promastigotes are predominantly leptomonads, one of the main pieces of evidence that it is this lifecycle stage that is responsible for the secretion of PSG [17].

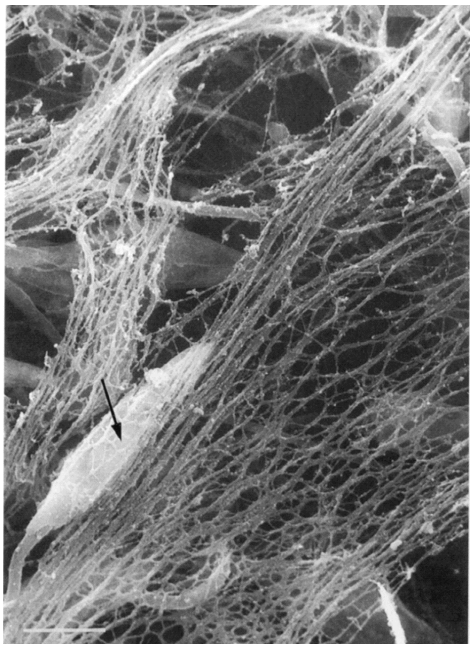

Figure 2.3.3: SEM immunolocalisation and ultrastructure of fPPG in networks produced by and containing *L. mexicana* promastigites (arrow) grown *in vitro*. Scale bar = 2 μm [29].

Metacyclic promastigotes are also closely associated with the plug, mainly located at the poles of the plug: an ideal place for transmission [17]. Distinctively from earlier lifecycle forms, it was observed that metacyclic promastigotes were unencumbered by the gel and swam freely [30]. It is these infective parasites which are expelled, along with PSG, to make a channel for blood to be imbibed (unpublished work on observations by Dr. Matthew Rogers). Consequently, and desirably for the disease cycle, 86-98% of promastigotes egested into the skin are the mammalian-infective metacyclic promastigotes [27].

PSG has also been implicated in accelerating wound healing *in vitro* and ad-

vanced wound closure, early upregulation of inflammatory cytokines and chemokines and promoting alternative activation of macrophages and *Leishmania* infection in mice [31]. This leads to an interesting exploitation of PSG as a novel wound healing therapy and provides a new target for therapeutics.

Along with the completion of metacyclogenesis and formation of the PSG plug, sandfly saliva is a well established disease exacerbation factor. It has potent vasodilatory and antihaemostatic properties making it essential for blood feeding activity [32]. Several studies have shown that co-inoculation of parasites and saliva result in disease exacerbation due to modulation of the immune response to favour the survival and replication of the parasite, promoting lifecycle progression [16].

The timing of delivery into the mammalian host is crucial to successful transmission. Too early and the parasite will not yet have transformed into metacyclic promastigotes in sufficient numbers, too late and the sandfly may not survive the pathogenic effects of infection. At the optimal time for transmission sandflies display an increase in feeding persistence [7]. This led to increased parasite burdens in mice as well as increased probability of biting, and therefore infecting, a second host. The mechanism behind this behavioural manipulation of the vector has not been determined but one hypothesis implicates the presence of PSG as it interferes with blood feeding thus leading to the persistent feeding behaviour observed.

2.3.2 Mammalian Host

The promastigotes which are regurgitated into the mammalian host are next taken up via phagocytosis, a process comprised of two linked events: attachment via low affinity, rapid kinetics interactions; and internalisation following a high-affinity interaction. *Leishmania* spp. uptake has been reported to occur by two types of phagocytosis: classical 'zipper' or 'coiling' [33, 34]. The zipper mechanism involves the attachment of the parasite to receptors on the phagocyte which consequently triggers recruitment of additional receptors from the surrounding membrane, and hence rearrangement of the cytoskeleton. This enables the extension of a pseudopod, which advances along the organism like a zipper, engulfing it into the phagosome. Coiling phagocytosis involves asymmetrical occurrence of pseudopodia coils and other multilayer pseudopod stacks. Importantly, this method of uptake could target the organism to a cytoplasmic compartment aiding their survival.

Two major families of promastigote surface molecules, gp63 and phosphoglycans (as in section 2.3.1), are thought to be the main ligands macrophage attachment. The *Leishmania* phosphoglycan family comprises of glycolipids such as lipophosphoglycan (LPG), and phosphoglycosylated proteins such as proteophosphoglycans (PPG), which covers the entire surface of promastigotes.

Phagocytosis of promastigotes is predominantly triggered by interaction between the host cell and the flagellar tip of the parasite [9]. This results in a pseudopod formation initiating at the tip and extending towards the parasite cell body (Fig 2.3.4). Various properties of the flagellum may contribute to this uptake. The composition of the flagellar membrane has been associated with adhesion and signalling [35, 36]. Surface molecules at the flagellar tip (e.g. LPG

and gp63) have been speculated to account for oriented attachment and entry through receptor-ligand interactions [37]. Alternatively the flagellum may act as a sensory organ releasing parasite proteins during cell attachment to modulate host cell phagocytic activity [38].

Studies have further shown that shape and orientation affect the ability of macrophages to internalise particles [39, 40]. These experiments showed that ellipsoidal particles were weakly phagocytosed compared to spherical beads. This relates to the direct attachment of *Leishmania* via the flagellum tip creating permissive geometry to initiate phagocytic uptake.

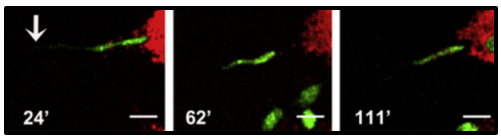

Figure 2.3.4: Lysotracker-positive vesicles (red) and CFSE-labeled parasites (green) at different time points of *Leishmania*-macrophage interaction. Scale bar = 10μm. [9]

The parasites are engulfed into a membrane-bound phagosome that is contiguous with the outer plasma membrane of the macrophage. The phagosome is then modified by fusing with lysosomes to form the phagolysosome or parasitophorous vacuole (PV). The PV is an acidic compartment rich in microbicidal peptides and hydrolytic enzymes. Some of the microbicidal processes of the macrophage are altered during infection with *Leishmania* parasites: the production of superoxide (O_2^-) and H_2O_2 within the PV are inhibited. However, pH is maintained, targeting of hydrolases to the PV is normal, and vesicular traffic is not disturbed.

The macrophage is the main host for the *Leishmania* amastigote but it is also an immune effector cell, its main role is to detect, engulf and destroy pathogens and apoptotic cells. *Leishmania* spp. have developed mechanisms to subvert the microbicidal activity of macrophages. Once inside the macrophage the metacyclic promastigotes undergo significant biochemical and metabolic changes which transforms these into the obligatory intracellular form of the parasite - the amastigote.

Amastigotes are released from macrophages and can re-invade dendritic cells, fibroblasts and new macrophages. The mechanism of exit is unclear. The accepted view has been that the infected macrophage bursts, discharging parasites in the immediate vicinity. However, data obtained by video microscopy suggests that amastigote-containing vacuoles accumulate at the periphery of the infected cell, and the amastigotes are released over several hours in a process similar to exocytosis [34].

2.3.3 The Surface Coat

Covering the exterior of these parasites are many, often stage-specific, surface molecules attached by glycosylphosphatidylinositol (GPI) anchors. These GPI-anchored molecules include proteins such as the parasite surface protease GP63 and proteophosphoglycans (PPGs), as well as short GPI-anchored glycosylinositolphospholipids (GIPLs).

The surface protease abundant in promastigotes is the zinc-metalloprotease GP63 [41]. Studies have shown this protease provides parasite resistance to the

complement-mediated lysis and facilitates parasite engulfment by macrophages [42, 43]. It has also been shown to be responsible for activation of protein tyrosine phosphatases that lead to alteration of major signalling pathways [44, 45]. GP63 is also has the ability to downregulate host macrophage protein synthesis [46]. Together these studies show the importance of GP63 inhibiting microbial signalling and therefore favouring the survival and propagation of the parasite.

Another major surface protein is a large GPI-anchored phosphoglycan called lipophosphoglycan (LPG). The parasites LPG surface coat may protect the promastigotes from lysis by alternative complement cascade and extracellular hydrolases [47]. It has also been shown to be a ligand for insect midgut and mammalian macrophage receptors as well as being essential for infectivity in both insect and mammalian hosts [48, 49, 50]. The structure of LPG varies among *Leishmania* species (defined by number and type of phosphorylated oligosaccharide repeats) [51] and changes as the parasites transform from a procyclic form to the mammalian infective metacyclic form. *lpg3* plays a role in synthesis and assembly of GPI-anchored glycoconjugates including GP63 and LPG, and hence is an essential gene for parasite survival. Recent studies have shown transcripts for *lpg3* were strongly upregulated in procyclic promastigotes and significantly decreased in metacyclic promastigotes [52].

The development of LPG mutants has advanced our understanding of the function of LPG in both sandfly and mammalian hosts. These studies have shown the developmentally regulated *lpg* is essential for releasing the parasites from the sandfly midgut and protecting promastigotes in the mammalian host from immune responses. During metacyclogenesis, the metacyclic form LPG has increased numbers of PG repeats and side-chain galactose residues masked by the addition of terminal arabinose. This modified LPG no longer binds to the sandflies midgut allowing free-swimming metacyclics and hence a transmissable infection [53]. Then once in the mammalian host LPG has multiple roles. It protects the promastigotes against lysis by complement proteins [54]. This is stage specific as procyclic promastigotes are susceptible to this lysis due to the structure of its LPG (half as many repeating units than that of metacyclic promastigotes) [47]. LPG also plays an important role as a ligand during attachment of parasites to macrophages (or neutrophils/dendritic cells) membranes by binding to other proteins such as a mannosefucose receptor expressed by macrophages [55]. It is also involved in inhibiting the synthesis of cytokines related to infection control to allow modulation of macrophage activation leading to parasite survival [54, 56].

The surface coat of Leishmania promastigotes also contains a number of proteophosphoglycans (PPGs) of which their precise function remains unclear. These are discussed in greater detail in section 2.3.1.

2.3.4 Environmental Challenges

During its lifecycle *Leishmania* spp. parasites overcome many challenges in order to transmit and propagate disease which have become clear upon review:

1. After the sandfly has taken an infected bloodmeal the procyclic promastigote parasites must escape the peritrophic matrix to avoid defecation.

2. The parasites must migrate from the posterior midgut to the anterior foregut

and finally the proboscis to be capable of transmission when the sandfly takes another bloodmeal. This includes surviving hydrolytic attack from the sandfly's digestive enzymes and surviving the sandfly's immune response.

3. They must undergo numerous differentiation steps in order to become the human-infective metacyclic promastigotes and transmit to the host.

4. They secrete PSG in order to cause regurgitation of the infective parasites into the mammalian host, additionally the mammalian infective parasites must reach an area within this PSG that will mean they are transmitted along with the gel.

5. They must survive within the laceration caused by the sandfly in the skin before being phagocytosed by leukocytes.

6. Finally they must survive and replicate within macrophages in order to develop disease and be transmitted back to the sandfly vector.

In order to promote the disease these steps must be done efficiently and occur at optimal times without any mistakes. This highlights how tightly controlled this lifecycle is and hence the importance that we gain understanding of each significant step within the parasites' lifecycle.

Chapter 3

Identifying the Mechanisms of *Leishmania* Motility: Methods, Challenges and Perspectives

During the *Leishmania* lifecycle the parasite makes various structural and morphological changes to adapt to shifting environments and as a result its motility is altered. The motility of these parasites, and hence the mechanisms they use to accomplish these movements, are important for the cyclical progression and host transitions which promote disease development. Although the importance of motility to the lifecycle of this parasite is well recognised [9, 57], understanding of *Leishmania* motility has lagged behind that of other swimming eukaryotes. *Chlamydomonas algae* are often used as model 'swimmers' due to relative ease of handling these microorganisms. Even among the trypanosomatids, the motility of species such as *Trypanosoma brucei* have received much more attention from the research community [58].

Bacteria, algae, parasites and other microorganisms live in a microscopic fluid environment which is vastly different to ours. Humans make use of inertia to enable us to swim [59]. Our swimming environment has a Reynolds number (R) of 10^4, this means the ratio of inertial forces to viscous forces is high.

$$R = \frac{a\nu\rho}{\eta} = \frac{Initial forces}{Viscous forces}$$

where a = object dimension, ν = speed, ρ = fluid density, η = dynamic viscosity. The Reynolds number for microorganisms is much lower, 10^{-4}, as viscous forces dominate making inertia irrelevant in microscopic environments. Hence, friction is the only relevant force and the active movement of these microswimmers relies upon the drag force of the oscillating flagellum [60]. This also means cells will not coast before slowing down: it would take approximately 0.6 μs to slow down because only forces exerted on them in that moment have an effect. Displacement of cells must be made using some cyclical deformation of the cell. If these organisms try to swim with reciprocal motion *i.e.* reversing the swimming stroke to return the swimmer to its original shape, it won't go anywhere. Microorganisms have acquired propulsion strategies which successfully overcome and even exploit viscous drag. Propulsion must be non-reciprocal and is instead achieved by sending waves of lateral displacement down their flagellum. In *Escherichia coli* and

other bacteria this is achieved by rotating the flagellum in a corkscrew like manner [61], human sperm cells also use this helical waveform of a single flagellum to deform planar swimming patterns [62], *Chlamydomonas spp.* use asymmetric power and recovery strokes of two flagella [63], *Leishmania's* trypanosome cousins are pulled forward by planar flaglellum beat and use their asymmetrical shaped body to induce rotational motion [64, 65, 66], however the details of the strategy used by *Leishmania* is currently unknown.

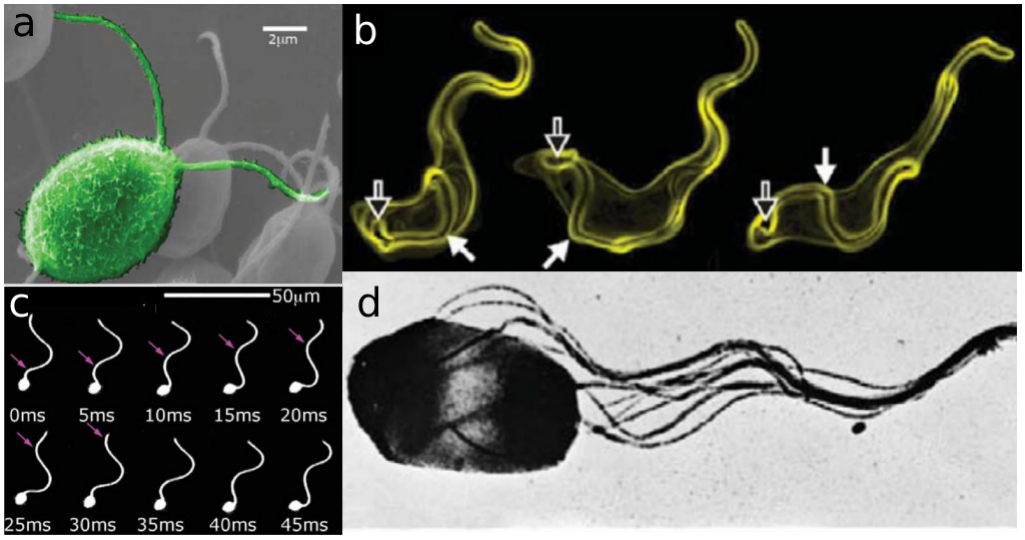

Figure 3.0.1: An illustration of the variety among flagellated cells. **a** Bi-flagellated *Chlamydomonas* swims with breast-stroke like motion [67]. **b** Trypanosomes have a flagellum that protrudes from the flagellar pocket (open arrows) and is attached to the cell body (closed arrows) with an free anterior end [64]. **c** Sperm time series showing the snake-like motion of their flagellum (arrow indicates wave propagation from base-to-tip) [67]. **d** Bacterial cells rotate flagella helically forming a bundle [68].

Propulsion is dependent on the spatial and temporal regulation of the motor proteins within the flagellum to generate different bending patterns [69]. The structure of the eukaryotic flagellum is highly conserved; at its core is a cytoskeletal element, known as the axoneme, which provides a mechanical framework for all the enzymes and mechanical components required to produce bending waves. The axoneme is composed of a central pair of microtubules, surrounded by nine equally spaced microtubule doublets to support the motor proteins, or dyneins, which occur in two forms: inner and outer dyneins. The outer arm dyneins act as amplifiers, increasing the beat frequency and power output [69]. These are tethered to inner arm dyneins which are responsible for the initiation and propagation of flagellum bending. As the proteins are alternately activated on opposite sides of the axoneme they generate sliding between microtubule doublets which is converted into bending of the axoneme by local differences in dynein activation and sliding resistance along the flagellum length.

Although the structure of these appendages is consistent amongst different eukaryotes they vary widely in types of movement generated and hence their resulting swimming trajectories. Moreover, relatively little is known about the control mechanism operating within flagella to produce local differences and generate different bending patterns. In *Leishmania*, motility parameters vary even within a single cell as the structure, length and function of the flagellum is altered

during its lifecycle. This provides an opportunity to study adaptation of the flagellum to facilitate swimming in different environments, within a single species or even a single individual. The procyclic promastigotes, which proliferate in the sandfly vector's midgut, have a short flagellum at the anterior which pulls the cell. Upon differentiation to the highly-infective, non-dividing metacyclic promastigotes, the cell body becomes slender and the flagellum elongated [30] enabling the rapid movements which adapt this lifecycle stage for transmission and early survival in the vertebrate host. These essential physiological changes during the *Leishmania* lifecycle raise several important questions:

1. How is the flagellum structure and motility regulated during the transitions which occur in the *Leishmania* lifecycle?

2. How do these parasites tackle the different challenges and environmental conditions they face to enable them to proliferate?

3. What are the control mechanisms and molecular processes which allow the alteration of the parasites' morphologies and flagellar structure?

These questions have not been answered unequivocally, although important insights have been made in recent studies mentioned throughout this chapter. This chapter gives an overview of what is currently known about *Leishmania* motility, and examines technical challenges in following this line of enquiry.

3.1 Methods to Study Motility

Studying the cell motility of parasites is limited by the availability of experimental tools. In order to determine how *Leishmania* motility impacts disease transmission we must review available tools and examine most efficient usage and potential challenges.

3.1.1 Imaging Techniques

With recent advancements in technology, the ability to image microorganisms has improved. Being able to visually record biological processes is an invaluable resource - from which *Leishmania* research can further benefit. The benefits these techniques have had on closely related parasitic trypanosomatids as well as bacteria, algae and sperm cells suggests that these processes could be adapted for *Leishmania* parasites.

High Speed Videomicroscopy

A key milestone in this field was a comparison study of the flagellar beating of free swimming *L. major* parasites and *Crithidia* species [70]. This study used high speed, phase-contrast videomicroscopy (192 frames s^{-1}) to capture the beating of motile cells allowing a quantitative analysis. The recordings allowed quantification of various parameters of flagellar beating. The first analysis of beat patterns of *Leishmania* flagella, detected important kinematics of the cells' motion. The curvature, wavelength and amplitude of flagellar waves did not detectably change

as the wave travelled from the tip to the base of the flagella. It concluded that the length of the flagellum did not influence the beat frequency but an increase in flagellar length was accompanied by both an increase in wave amplitude and concomitant decrease in curvature. However, this study concentrates particularly on comparing *L. major* procyclic promastigotes to non-parasitic *Crithidia*. The flagellar length of procyclic cells is significantly shorter compared to metacyclics and potential conclusions drawn would benefit from also examining metacyclic promastigotes. This could inform us of differences regarding flagellar beating *in vivo* and the potential involvement of motility in the transmission to mammalian hosts.

Light Sheet Fluorescence Microscopy

In vivo imaging of *Leishmania* parasites in the midgut of the sandfly would provide the field with invaluable information on the parasites' ability to swim and maintain motility in the midgut of the sandfly. This has been made possible in a recent study where they used light sheet fluorescence microscopy to analyse the movements of *Trypanasoma brucei* within its vector, the tsetse fly [71]. High speed recordings of the parasite in its natural environment showed synchronised swarming dynamics for the first time. Using this approach to visualise *Leishmania* in its vector, the phlebotomine sandfly, could be more challenging, as the sandfly and parasite are significantly smaller. Nevertheless, the results would expand our understanding of the parasite's motility and hence its ability to transmit.

Real-time Confocal Microscopy

Imaging has also been an important tool in investigating the dynamics of *Leishmania* motility during the early infection process [9]. Real-time imaging allowed an investigation of the orientation and motion of parasites during infection, as well as interactions with host cells. This study used confocal microscopy videos to find that motile promastigotes enter macrophages almost exclusively by their flagellar tip. The intraflagellar transport activity and heavy beating leads to orientation of the parasite flagellum towards the host cell periphery and results in oscillatory parasite movement. This study showed the importance of parasite motility and polarity in the cell invasion process in the mammalian host and significantly advanced our understanding of *Leishmania* infection. The molecular processes and bending dynamics which occur in the flagellum to allow this are yet to be studied.

High-speed Fluorescence Microscopy

The orientation has also been shown to be important in *T. brucei*. Using another method of imaging, high-speed fluorescence microscopy, to track the flagellum movement showed how the trypanosome is optimised in crowded environments [64]. The authors of this study constructed microfluidic chambers filled with pillars of a variety of sizes and spacings. By examining the swimming speed of the parasites in each case, they determined that the parasites are highly adapted for motility in the bloodstream. The flagellar dynamics changed noticeably when the density of the micro-pillars was further increased to resemble

collagen networks or tissue: the flagellum beat reversed more frequently to allow the cell to swim backwards and avoid becoming trapped. In the absence of any obstacles this beat reversal occurred randomly resulting in irregular waveforms and apparent cell tumbling. This swimming behaviour showed how trypanosomes exploit their surroundings to move efficiently. A similar study would be particularly useful in *Leishmania* to analyse how this parasite has adapted not only to the bloodstream of the vertebrate host, but also to the micro-environment within the midgut of the sandfly allowing it to be transmitted into the mammalian host. Although *Leishmania* and *Trypanosoma* are closely related, there are significant physiological differences. The flagellum of trypanosomes is laterally connected to the cell body along almost its entire length, with only the distal tip extending free of the cell body, whereas the flagellum of *Leishmania* parasites is completely free once it exits the flagellar pocket (site of attachment to the cell body)[72].

Differential Interference-Contrast Microscopy

Differential interference-contrast (DIC) microscopy has been used at millisecond resolution for uncovering some important short-time features of trypanosomes motility [73]. This study discovered that *T. brucei* was driven by bihelical waves with alternating chirality separated by kinks, rather than the helical motion previously thought to be used. This allows *T. brucei* to propagate helically while avoiding the large viscous drag associated with a net rotation of the broad end of its tapering body. While limited in time-scale, this imaging provides insight into the mechanisms of the dynein motor proteins and how these promote the helical waves to create the propulsive movements of microorganisms.

The studies discussed above examine how flagellar beats lead to the motion of individual cells. Another strategy with distinct advantages examines the swimming dynamics of a population of parasites concurrently. Bioimaging has become an increasingly useful tool for studying many biological processes. Moreover, there are some interesting biophysics studies using alternative imaging techniques which could be useful to answer some of the remaining questions about *Leishmania* motility.

Differential Dynamic Microscopy

Differential dynamic microscopy (DDM) is a technique used to measure the isotropic diffusion coefficient of spherical colloids [74] and more recently to study bacterial motility [75]. This method of imaging requires a time series of digital video images acquired using bright-field or phase-contrast microscopy, captured by a high speed camera. An averaged power spectrum of the difference images is then used to describe the dynamics of the system [76]. This fast, high-throughput method characterises a limited number of motility parameters by averaging over many cells in a few minutes [74]. This method has the capacity to monitor the dynamics of a population of *Leishmania* parasites without having to resolve each individual cell, similar to its characterisation of motility dynamics of the bacterium *E. coli* and biflagellate alga *Chlamydomonas reinhardtii* [75]. More recently, this method has been used to characterise the propulsion of microorganisms which swim in non-Newtonian fluids such as high-polymer (highly viscous)

solutions [77]. Results suggest that peculiarities of flagellated bacteria movement in concentrated polymer solutions are due to the fast-rotating flagellum reducing the viscosity in its vicinity. Research into the motility of populations of *Leishmania* parasites could benefit from this method, particularly to examine distinct movement in the different environmental conditions of the parasite lifecycle. Despite this promise, this method is insensitive to the motion of individual cells, inferring that in populations composed of significantly mixed lifecycle stages, DDM should be coupled to cell tracking data for accuracy.

Two-dimensional Cell Tracking

Cell tracking in parasitology, particularly *T. brucei*, has been used previously to analyse the movement patterns of these cells [65, 71, 78, 79]. This is an effective tool which has been used to correlate how the shape of cells effect overall swimming movements in *T. brucei* [65]. As well as characterising different modes of motility, the study determined that cells which are straighter tend to swim more directional and bent cells have a lower net displacement. The ability to relate how cell shape and body rigidity effect persistence of swimming and thereby host invasion and may be applicable to *Leishmania*.

Three-dimensional Imaging - Digital Inline Holographic Microscopy

These imaging methods provide excellent information regarding cell behaviours in two dimensions, but no information pertaining to how parasites swim in three dimensions. A method capable of this was first described about 20 years ago [80], and has since been advanced and developed to allow capture of the shape and swimming behaviours of various microswimmers. Digital Inline Holographic Microscopy (DIHM) allows imaging of microscopic samples in three dimensions. Details on the particulars of this method can be found in Chapter 4 This method has been used for long range tracking at low magnification of a population of cells swimming in a sample, as well as high resolution shape studies to examine the high magnification, three-dimensional shape of individual cells [81, 82, 83].

The former has been used to track the trajectories of *T. brucei* [78]. Three-dimensional quantification of the swimming trajectories exposed two swimming states; swimming and tumbling. This data, similarly to the study using micropillar arrays [64], showed how trypanosomes are adapted to their natural environments in terms of cell motility. Although holography was used here, full advantage was not taken of the technique to characterise the three-dimensional shape of cells in different environments.

DIHM has also been used to study the resulting hydrodynamics or geometrical constraints by the presence of boundaries, which suppresses tumbling in *E. coli* [84]. It has also been used to determine how sperm cells navigate in 3D chemoattractant landscapes [85]. Studying these cells in 3D provided information on how sperm are capable of locating the egg for fertilisation by gradually adjusting their swimming paths. A similar analysis of how *Leishmania* are capable of migration within the sandfly midgut, or locating macrophages once transmitted into a mammalian host would be invaluable toward understanding how to intercept transmission and disease progression.

This method has also been used to analyse the shape of individual cells and reveal the 3D flagellar waveforms of *Plasmodium berghei* microgametes [86]. Examination of the 3D geometry of this waveform allows mapping of differential shear between microtubules. It also questions the hypothesis that chirality in the axoneme structure governs the beat pattern. Geometrical analysis enables the examination of flagellar beat initiation and propagation to distinguish between swimming modes. This study provides great insight into the action of microtubules and the local changes which determine the dynamics of the flagella. Using DIHM for shape studies on *Leishmania* cells would be more challenging due to the presence of a cell body that scatters light more strongly than the flagellum, but could provide insight into the way that these cells move during a critical transmission phase of their lifecycle.

3.1.2 Mathematical Concepts and Modelling

The study of low-Reynolds number swimming has a rich history which began with experimental studies by J. Gray on the motility of swimming organisms such as marine worms, snakes, sperm and cilia [87]. Taylor then analysed the swimming of organisms using small amplitude and low Reynolds number assumptions and compares his work to Gray's experimental studies. Taylor proved that propagated bending waves on a body in a viscous fluid would propel the body [59]. In order to mathematically describe the hydrodynamics of this, mathematical models were introduced.

Hydrodynamics Models

Resistive Force Theory (RFT) was derived to analyse the propulsive velocity of sea urchin sperm [88]. In this approximation of the local drag of a slender filament in Stokes flow in order to explain how a propagating flagellar wave produces a propulsive thrust that is balanced by the drag on the cell body. Slender Body Theory (SBT) is an improved approximation of the RFT. This method generates efficient numerical simulations to allow analysis of surface effects on flagellar hydrodynamic drag. These theories along with high frame rate digital imaging have been used extensively to study the active swimming behaviour of sperm cells and characterise the flagellar movements of migrating sperm resulting in precise spatiotemporal details of the waveform evolution along the flagellum [89]. Examining the relation between kinematic parameters and swimming velocity allowed these studies to conclude that the fluids structure and internal interactions are important in high viscosity liquids where the viscous load on the flagellum induces changes in the waveform [89]. These mathematical frameworks also allow the analysis of planarity, torsion, trajectory and progression per flagellar beat, differential shear, analysis of bending due to combinations of active and passive internal sliding forces and elastic bending stresses. However, exisiting models have yet to give a satisfactory account of motion in 3D.

Geometrical Models

Geometrical simulations are another mathematical modelling technique used widely to understand how shape effects different system. This method has been

used to study both *Leishmania* and *T. brucei* and give insight to how the shape of these parasites affects its motility. In *T. brucei* a triangulated surface model was used combined with multi-particle collision dynamics model to simulate the viscous fluid flow [64]. The stiffness of the trypanosomes cytoskeleton was simulated by allowing bending potentials to be applied along the long axis of the body and the flagellum was defined as a sine wave running from the tip to the base. The simulation analysed the rotation of the cell body and how it resulted in a helical swimming path. The model provided evidence that the course of the flagellum along the cell body as well as the direction of the flagellar waves were responsible for trypanosome motility. This is clearly incomparable to *Leishmania* parasites due to their flagella not being attached to their cell bodies. However, this modelling approach does have a clear predictive advantage in analysing complex behaviour such as cell motility.

Recently, a study using a similar approach has been used to attempt to determine the effective hydrodynamic shape of *T. brucei* and procyclic *L. mexicana* [66]. This approach used a numerical simulation to describe how the cell shape changes as the flagellum beats, based on cell rotation and flagellum beat frequencies. This method concluded that the *T. brucei* cell body shape was chiral whereas *Leishmania* promastigotes were not. Although this study gave a good approximation for how chirality affects *T. brucei* motility it was unable to capture this information for *Leishmania* without a complete three-dimensional description of how the cells shape changes over the course of a flagellar beat. It is also possible the chirality is not due to the cell changing shape but by asymmetries in the body or flagellar beat.

3.1.3 Genetic Tools

Genetics is a powerful tool which has been utilised to understand the molecular mechanisms which regulate many microorganisms; *Leishmania* is no longer an exception. Recent advances in tools to genetically manipulate *Leishmania* have enabled the molecular characterisation of lifecycle progression and host-parasite interactions, including how they regulate their flagellar motility. Levels of specific genes are modified to analyse the impact upon normal parasite growth and cellular function. The use of such tools enables the screening of molecules which contribute to the replication of procyclic promastigotes in culture, the capacity to differentiate sequentially into metacyclic and thereby amastigote forms, as well as relative infection efficiency of parasites into different host environments. Despite significant strides, current tools are less equipped to analyse how the genetic mutations alter the parasites ability to swim. This is due to the lack of a complete model which characterises how the parasite swims without genetic manipulations and therefore an inability to validate distinct variations from the model. An understanding of the regulation of the molecular motors in the flagellum, causing propulsion of the parasite, could clearly benefit from similar methods which have been developed to study the essential regulators of *Leishmania* and combined, these may provide an adequate model to potentiate such investigation.

CRISPR-Cas9

CRISPR/Cas9 is a revolutionary, high-throughput method which can be used in kinetoplastids to genetically manipulate and produce mutant phenotypes. The method uses clustered, regularly interspaced, short, palindromic repeats (CRISPR) and its associated gene 9 (Cas9) [90]. The Cas9 nuclease has a sequence-specificity determined by a single guide RNA (sgRNA) to give precise cleavage of double stranded DNA [90]. Studies have been adapted to exploit the efficiency of this in *Leishmania* [91] and other kinetoplastids and so far this tool has allowed a knock-in of fluorescent protein tags, a modified biotin ligase BirA*, luciferase, HaloTag and small epitope tags allowing study of protein functions and localisation screenings [92]. Perhaps most relevant to motility has been the rapid generation of null mutants in large-scale knockout screens [92]. These large knockout screens can be used to analyse for motility mutants and hence how gene deletions affect the flagellum. A weakness for the application of this technique in kinetoplastid studies is that it is not yet inducible, and can only delete and functionally examine non-essential genes. This is an ideal method to help us gain understanding of parasite motility by characterising how different gene deletions affect the swimming patterns and kinematics of motile *Leishmania*.

RNA Interference

Another method which down regulates gene expression is to use RNA interference (RNAi). This allows a functional analysis of genes by transfecting the parasites with dsRNA to initiate gene silencing. The dsRNA forms into RNA inducing silencing complex (RISC) with the ability to degrade full length transcripts [93]. The RNAi machinery does not exist in most *Leishmania* spp., and attempts to introduce it have been unsuccessful (per E. Ullu, unpublished data). Within the two *Leishmania* species which have the capacity for RNAi, *L. braziliensis* and *L. guyanensis*, it is not inducible and the species are divergent enough that functional conservation cannot be assumed.

Inducible Gene Expression

Tetracycline inducible gene expression has the potential to be used to generate conditional null mutants, where cells contain a tetracycline-inducible ectopic copy of a gene of interest and both allelic copies are replaced by drug resistance genes [94]. Removing tetracycline enables the Tet repressor (TetR) to repress gene expression and hence create a null phenotype which can be examined. This method would require a high expression of exogenous TetR and the T7 polymerase gene. It has been shown these levels are significantly reduced in the metacyclic promastigote stage [95]. As this is clearly an important stage for studying motility relevant to infection, optimisation is needed before this technique could be used for this purpose.

Inducible gene expression can also be mediated by a DiCre recombinase. The antisense gene of interest is flanked with *cis* orientated loxP sites. On activating Cre, loxP recombination induces inversion of the antisense sequence and enables RNA polymerase to mediate transcription while preventing continual recombination and inversion [90]. A conditional mutant overexpression induced dominant

negative phenotypes in promastigotes which can be analysed for motility defects.

Endogenous Tagging

An alternative way to analyse motility would be to regulate the parasite's protein levels rather than altering the gene at the RNA level. This could be done using endogenous tagging, a rapid and scalable method that does not involve cloning [96], or conditional protein destabilisation. The latter regulates protein expression by conferring inducible stability and has been used to analyse the dynamics of flagellum proteins during differentiation in *Leishmania* [97]. In that work, an N-terminal domain caused proteosome-mediated degradation of the protein in absence of a stabilising ligand. This allowed them to analyse flagellar growth throughout the cycle and conclude the shortening of *Leishmania* flagellum switches from a growing to a disassembling state contributing the forming the short flagellum of the amastigotes. Utilising this technique to its full potential and destabilising different proteins has the possibility to explain and develop our understanding of how this parasite alters other aspects of its flagellum during its lifecycle.

In summary, there is a handul of genetic techniques that would require optimisation to be utilised to study *Leishmania* motility and these have already promotes insight into our understanding of the flagellar structure [13, 97]. Coupling this with a method to analyse motility defects which are not visually obvious, *i.e.* impacting speed, waveform kinetics, swimming patterns, would be of great advantage toward understanding *Leishmania* motility.

3.2 Confronting the Challenges of Kinetoplastid Motility Research

There are many tools that would be advantageous to study the motility of *Leishmania* parasites. However, as with any research, studying this complex parasite and its systems comes with challenges. This section discusses what challenges may arise and how it might be possible to overcome them.

To fully characterise *Leishmania* parasites in their natural environment would entail visualising the lifecycle *in vivo*, either within the sandfly or after transmission within the mammalian host. *In vivo* studies in any microorganism are challenging but parasitology comes with bespoke problems. Advances with bioluminescence imaging have improved the ability to analyse chronic *in vivo Leishmania* infections in mouse models [98, 99]. These advances have generated some intriguing data, and show the difficulties associated with in *in vivo* imaging through thick tissue. Light is strongly scattered by most living tissue, severely restricting the depth at which objects can be resolved. Some *in vivo* analysis of malaria infections using multi-photon microscopy has proven to be useful as it is able to penetrate further than conventional confocal microscopy with little tissue damage, owing to the long wavelength of the excitation photons [100]. However, this imaging mode requires a powerful excitation source capable of generating two-photon emission. It also results in relatively low frame rates, up to minutes per

frame depending on the resolution, and so is unsuitable for studying fast-moving cells.

A compromise must be made regarding speed versus penetration depth using these techniques in complex tissues. These parasites swim at high velocities as a result of many oscillations of its flagellum. In order to resolve these oscillations a high spatiotemporal microscopic resolution is needed. Cameras capable of achieving frame rates of several hundred frames per second are now relatively cheap (indeed they are incorporated into cellphones). Balancing this capability with the high sensitivity required by fluorescence-based techniques is an ongoing technological challenge, but one that is likely to reap rewards.

Imaging in the sandfly *in vivo* should be less complex, given recent advancements in light sheet microscopy [71]. However, immobilising the midgut of the sandfly without disturbing the structure and the environment of the parasites is an important challenge to overcome. The midgut tissues, fluid flows and peristaltic movements must all be considered when interpreting experimental data. There are strong incentives to develop new technological and methodological advances to study parasites *in vivo*, and we anticipate that these will eventually provide us with a thorough understanding of the parasite's life within the vector.

Leishmania cells swim in three dimensions, and caution is required when inferring three-dimensional motion from two-dimensional video images. A high fidelity, fully three-dimensional imaging method would be ideal, but no perfect solution is currently known. DIHM provides one option for three dimensional imaging: it is a rapid, non-invasive, high-throughput way of gathering 3D data of motility patterns. It would allow us to analyse the cells and motility mutants in different environments including how different aspects may effect how they swim, such as temperature, viscosity, chemical stimulus. The spatial resolution of DIHM in the direction perpendicular to the optical axis is similar to that offered by bright-field imaging (*i.e.* diffraction-limited imaging). This is more than sufficient for some purposes, such as tracking cells over hundreds of microns. In order to correlate the 3D shape of the cells with the tracks high resolution holography would need to be applied. This has been possible as shown in a recent malaria gamete study to analyse the flagellar waveform which overturned claims that chirality governs overall beat pattern [86]. The challenge with applying this to *Leishmania* lies in the large cell body the flagellum is attached to, absent in Plasmodium gametes. DIHM concept is based on scattered light and the *Leishmania* parasites cell body scatter more light than the flagellum rendering it more difficult to resolve the waveform. This can be overcome using different experimental techniques; including attaching the cell body to limit phase noise and complexity, and optical techniques such as two-colour holographic imaging to reduce artifacts and allow reconstruction of the weakly scattering flagellum in close proximity to the strongly scaterring cell space [101].

Once such challenges are overcome the resulting optimised method can be used to analyse potential motility mutants, albeit with the potential for distinct challenges and complications. The CRISPR/Cas9 system has significantly reduced the challenges associated with deleting genes in *Leishmania*, however it has not overcome the difficulty in interpreting motility phenotypes. Motility phenotypes are not only complicated to detect but it is possible that one gene influences more than one phenotypic trait, displaying functional redundancy. As

a result, discerning between direct, indirect and stage-specific effects could be very complex.

3.3 Concluding Remarks

It is resolutely clear that there are various methods and techniques which the field has not yet utilised to study *Leishmania* motility. This chapter highlights some of the tools which are available and as a result shown the best way to advance the field is using an interdisciplinary approach to explain and resolve the flagellar motility of these complex parasites and how their kinematics, structure, molecular composition allows them to be transmissible and infective. Each of these techniques presents its own challenges, whether thats due to the technique itself or complexities of the parasites. Overcoming these will be worthwhile to facilitate and improve our knowledge of how *Leishmania* parasite motility fluctuates to promote its lifecycle and perpetuate leishmaniasis worldwide.

Chapter 4

Theory of Digital Inline Holographic Microscopy

After reviewing a range of potential methods to study *Leishmania* motility in chapter 3, digital inline holographic microscopy (DIHM) was selected to study this parasite in different environments. DIHM has high-throughput capabilities, capturing swimming behaviour at high speeds in three-dimensions. This added third dimension from the resulting data is important for our understanding of how these cells swim in the three-dimensional environment they experience. This extra information will become clearer in subsequent chapters.

The current chapter describes the DIHM technique in detail, giving an in-depth review of its principles, setup, processing procedures and applications. The post-processing, including numerical refocusing and object localisation, is discussed in chapter 5.

4.1 Principles of Holography

Traditional cell visualisation techniques such as fluorescent tagging or phase-contrast microscopy give excellent information on cell behaviour in two-dimensions, but no information about cells moving in three-dimensions. A method capable of this was first described some 20 years ago [80], and has since been developed due to advances in computing power: digital inline holographic microscopy.

Holography was originally developed by Dennis Gabor [102] as a method of correcting aberration in an electron microscope (in which electrons can be thought of as waves), but has subsequently been applied to optical and acoustic imaging also. The phase and amplitude information that a hologram contains is sufficient to reconstruct the optical field at any point along its propagation direction [103]. There are many methods for achieving reconstruction, but DIHM is one of the simplest and most robust.

Interference between two waves is the central concept: a light wave scattered by an object of interest (object wave) is superimposed onto a wave with a known phase (reference wave) [103]. The reference wave is often a plane wave, in which the phase is constant across any plane perpendicular to the direction of propagation. When the electric fields of the object and reference waves combine, they produce an interference pattern of light and dark fringes, corresponding to constructive or destructive interference. This interference pattern reveals the phase

of the object wave, as compared the quasi-constant reference, and encodes phase differences within the recorded amplitude [103].

There are numerous advantageous of this method: (i) the low cost of apparatus required, (ii) the availability of free software algorithms for post-processing, and (iii) the unique information offered by high-speed, three-dimensional imaging [103]. Other competing methods for three-dimensional imaging, such as rapid scanning of the microscope focal plane [104] are technically demanding and only accessible by dedicated experimental apparatus. Laser scanning confocal microscopy is another approach for three-dimensional imaging of microscopic subjects. This scheme allows high or super-resolution imaging (*i.e.* can resolve details smaller than the classical diffraction limit would allow), but typically requires that the subject is fluorescently labelled. Moreover, confocal schemes require the sample to be mechanically translated between axial sections, restricting the speed at which three-dimensional information can be acquired. In the case of freely-swimming cells, DIHM has the distinct advantage because of its high acquisition rate; this is limited only by the frame rate of the camera used for imaging, and modern cameras with frame rates in excess of 1 kHz at megapixel resolution can be obtained for small fraction of the cost of a confocal scanning system.

However, there are some disadvantages of this technique that have been acknowledged throughout its use. The use of lasers invokes the usual safety concerns, especially where optical instruments are involved: microscopes can concentrate relatively low power laser light to hazardous levels if the appropriate interlocks are not in place. Additionally, the resolution of DIHM is similar to that of standard bright field microscopy [105], although typically with slightly poorer resolution in the axial direction. Improvements in the resolution are bound by the classical diffraction limit.

4.2 Optical Setup

Figure 4.2.1 shows two setup options for an inline holographic microscope (Figure adapted from [103]). Both are based on a standard microscope setup with the exception of the method of illumination. Figure 4.2.1a shows a setup in which an LED is used as a light source, and nearly-closed condenser aperture is used to create a point-like source in the back focal plane of the condenser lens. The lens turns the point-source emission into plane waves at the sample, as indicated. An alternative is that depicted in Figure 4.2.1b, where a laser coupled to a single-mode optical fibre is used for illumination. The fibre is held at a distance of 2-5 cm above the sample, meaning that the optical field is well approximated as a plane wave when it is incident on the sample. The condenser lens is unnecessary in this setup as laser sources can have high intensity and do not require collimation like the LED source. When light passes through either system, some of it is scattered by objects in the sample. This scattered light (object wave) interferes with the remaining unscattered light (reference wave) at the image plane. This method is described as 'inline' holographic microscopy due to the fact the object and reference waves both take the same path through the imaging system.

The two configurations described take advantage of different levels of optical coherence. The fundamentals of optical coherence are somewhat nuanced [106];

for the purposes of this thesis, coherence is best thought of as deviations that the object wave can take from the reference wave while still producing interference fringes. An LED source has low inherent coherence, hence the need for the 'pinhole' condenser aperture, which introduces a small level of coherence. Holography using an LED required that the object and reference waves must only have a small optical path length difference in order to produce fringes. This means that only a small thickness of sample volume can be imaged at one time, as indicated in the red highlighted region in the lower panels of Fig 4.2.1. A laser is highly coherent and so can be used to image much thicker sample volumes, at both high and low magnification. A laser therefore increases the size of 'sensitive volume', however this also means it will include unwanted contributions from dust particles that cross the optical path during experiments, irregularities on the surface of the sample chamber, and other sources that can produce a confounding signal. The optical setup used throughout the following research was that shown in Fig 4.2.1b, utilising the lasers ability to sample large volumes. Some of the unwanted noise was filtered out during post processing. More details of this can be found in chapter 5.

4.3 Data Processing

Raw DIHM images are two-dimensional and look similar to out-of-focus bright field microscope images. These images contain information about the three-dimensional positions and shapes of the cells in the sample chamber. There are several computational processing schemes for extracting three-dimensional information from holographic images [107, 108], the most convenient being the Rayleigh-Sommerfield back-propagation method [109]. This method is particularly useful for 3D localisation of weakly scattered objects while being fast and highly flexible. It treats the holographic image as a plane in three-dimensional space. It takes each pixel in the raw image as a source of light waves, each with the same phase, and an amplitude set by the pixel value (a light pixel is a strong source, a dark pixel is a weak one). By summing the contributions from all sources at a particular point across a plane parallel to the holographic image, we 'numerically refocus' the raw image at an arbitrary distance within the sample.

This method typically produces a stack of images which replicates manually scanning the microscope's focal plane through a sample, taking images at different depths. Weakly-scattering objects appear to have bright or dark centres, depending on which side of the focal plane they lie on. An object's appearance changes (from light to dark or vice versa) when it passes through the focal plane [109]. Regions where this light-dark transition occurs in a short distance in the axial (z) direction are therefore associated with scattering regions and are used to localise objects in the three-dimensional volume. Each small volume of the object hit by the laser light will scatter some light, and the total scattered field can then me measured as the sum of the individual contributions. This approach is an approximation of the light scattering physics known as they Rayleigh-Gans-Debye (RGD) approximation. RGD scattering is strictly appropriate when the scatterer's refractive index relative to the suspending medium ($m = \frac{n_s}{n_m}$) and a characteristic dimension, d, adhere to the following conditions:

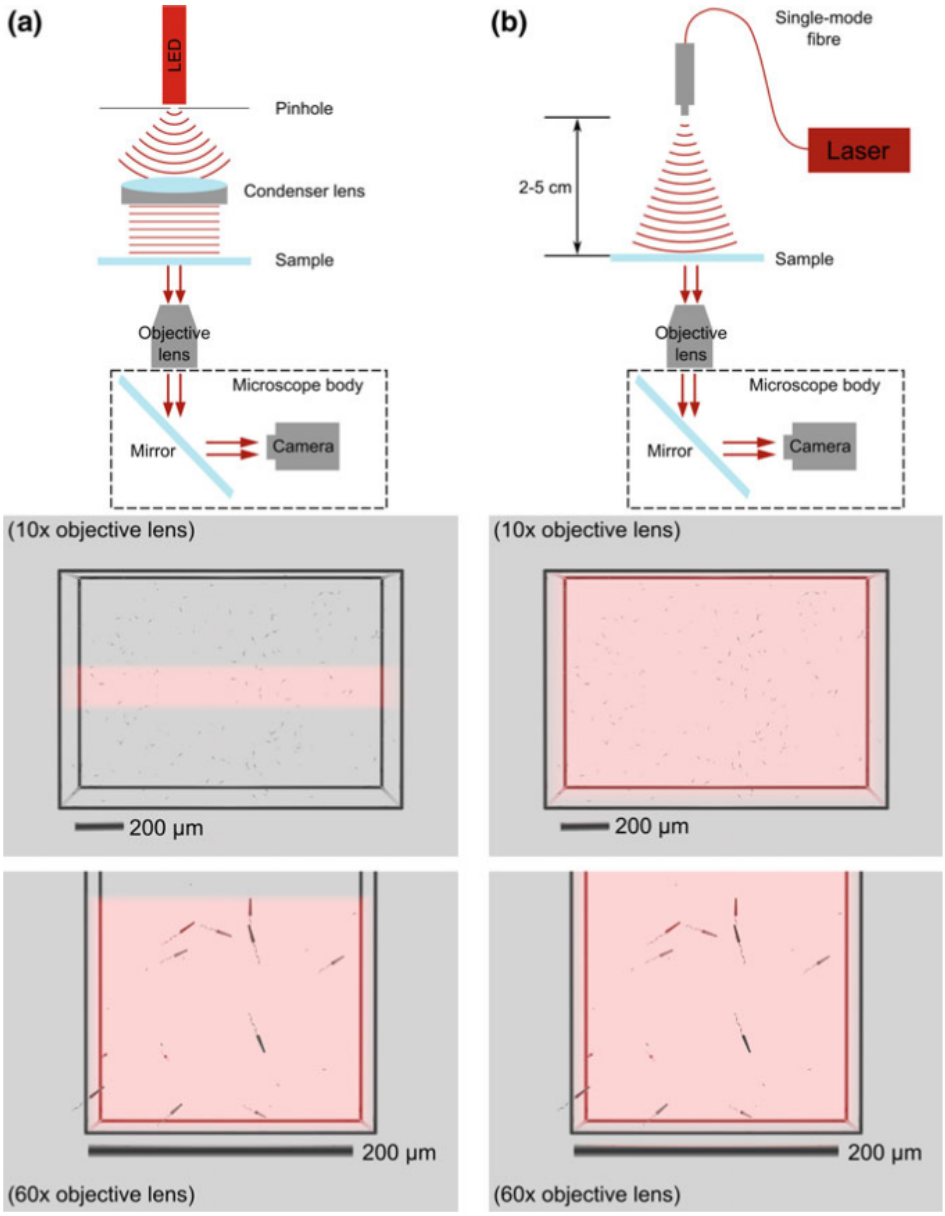

Figure 4.2.1: Two layouts for DIHM. At the bottom of each panel are two 'cartoon' images of the sample, highlighting the volume from which data is recorded, using typical 10× and 60× objective lenses. These lower four panels contain 'cartoon' cells, drawn to scale, to represent *Leishmania mexicana*. The system in panel **a** uses an LED and a pinhole (nearly-closed condenser aperture) for quasi-coherent illumination. Panel **b** uses a diode laser coupled to a single mode fibre, which eliminates the need for a pinhole [103].

$$| m - 1 | \ll 1, \text{ and } kd \, | m - 1 | \ll 1, \tag{4.3.1}$$

where the wavenumber $k = \frac{2\pi n_m}{\lambda}$, and λ is the illumination wavelength. Under this assumption each small portion of the subject behaves as an independent scattering centre, scattering light as if isolated from the rest of the sample. This independence means that each notional scattering centre appears in the refocussed image stack as a localised region in which there is a dark-to-light transition as the image is numerically focussed. These dark-to-light transitions are isolated in an image stack using a three-dimensional image processing filter based on the

two-dimensional Sobel-Feldman operator [109], discussed further in 5.

4.4 DIHM Applications

The holographic recording and reconstruction process results in data that can be analysed at a range of different length scales. Previous studies have broadly taken one of two approaches: examining the shape of single cells at high resolution, or establish a 'centroid' position within the cell and track this over time, the latter of which is our main focus during this particular research of *Leishmania* motility (chapters 5, 6, 7).

At higher magnification, the shape of individual cells can be examined in three dimensions. Eukaryotic flagella are an ideal subject for this kind of analysis, as they are weakly scattering, ensuring that the RGD scattering limit is valid. DIHM has previously been used on *P. berghei* microgametes [86] to examine the shape of the flagellum, giving insight into local changes that alter the flagellar dynamics (section 3.1.1). This has also been attempted for *Leishmania* flagellum [101], however it is more challenging due to the presence of the cell body that scatters light more strongly than the flagellum.

At low magnification and high video frame rates, individual points can be tracked simultaneously over multiple frames, to provide information on the swimming patterns of cells [85]. This tracking information can offer insight into how cells spread into new territory, and interact with each other and their environment.

For example, this technique has been used to track *E. coli* cells close to surfaces [110]. Understanding how bacterial cells move near surfaces is important for many microbial processes such as biofilm formation, bacterial dispersion and pathogenic infections. Using DIHM this study demonstrated that aside from physical constraints, cell biophysics is also affected by the presence of a nearby wall, which suppresses tumbling events. These findings imply that tumbling does not provide an effective means to escape trapping near surfaces.

Another important area of research where DIHM has been applied is to identify the principal features of sperm navigation in 3D chemoattractant gradients. Sperm require a sense of direction to locate the egg for fertilization. They follow gradients of chemical and physical cues provided by the egg or the oviduct but the principles of how they navigate were unknown. This technique showed sperm produce two different steering responses - incremental corrections and sharp turns [85].

DIHM has also been applied to track the displacement of *T. brucei* [78]. 3D quantification of the swimming patterns established two swimming states; swimming and tumbling as well as switching between the two states. Similarly to *Leishmania*, this research has implications in understanding the infection process and is indicative of adaptation of the trypansomsomes to their natural environments involving a change in swimming mode.

In the following results chapters, this DIHM technique is used to track ensembles of individual *Leishmania* parasites in different conditions. The result gives us 3D displacement information so we can understand and compare swimming patterns and mechanisms, elucidating how motility is important during transmission and infection.

Chapter 5

Tracking Different Lifecycle Stages Reveals Distinct Swimming Patterns

This chapter concentrates on characterising the different motility patterns of the motile promastigote parasites *in vitro*. By exploring the *L. mexicana* promastigotes' behaviour in an environment they are metabolically optimal in (culture media), we can gain information regarding the different lifecycle stages and characterise their distinctive motility. We then use this analysis as control data, providing comparative data for experiments carried out in other environments (chapters 6, 7).

Firstly, I will describe the methods used for parasite culture and characterisation that will define the lifecycle stages studied. Secondly, I will describe and explain post-processing details of the DIHM data into three-dimensional tracks, a method which is also relevant to the other results chapters. We then describe multiple methods necessary to quantify the motility and swimming patterns of the cells and prove that the two promastigote lifecycle stages investigated swim differently. We further use these methods to explore the effects of a genetic mutation on the parasites' motility, quantitatively validating a severe motility defect.

5.1 Experimental Methods and Post Processing

5.1.1 Promastigote Parasite Culture

Promastigote parasites of *Leishmania mexicana* (strain M379) were cultured at 26°C in Medium 199 (M199 - HEPES modification with Hanks' Salts, Gibco) supplemented with 10% foetal bovine serum, 40mM HEPES, penicillin, streptomycin, adenine and 0.005% Hemin; consistent with previous studies [111, 112]. All cells were cultured up to passage 10 or less. Procyclic promastigotes were harvested in mid logarithmic phase at concentrations of approximately 5×10^6 cells/ml. This stock sample was diluted by a factor of 100 into fresh M199 medium for holographic tracking.

To generate metacyclic promastigotes the procyclic culture was passaged into Grace's insect media at pH 5.5. The cells were cultured in Grace's for 7 days at 26°C. To ensure a purified population of metacyclic promastigotes, a 10% Ficoll

gradient was used, adapted from G. F. Spaeth et al. (2001) [113]. This density-gradient centrifugation creates an enriched population of metacyclic promastigotes (as defined by morphology, molecular markers and infectivity to macrophages). The purified population of metacyclics were transferred into fresh M199 medium and diluted to a concentration the same as that of the procyclic promastigotes, for holographic tracking.

With known stage-specific molecular markers ([114] and Walrad lab unpublished data) we were able to confirm these populations of procyclic and metacyclic promastigotes with qPCR, a method to quantitavely measure gene expression.

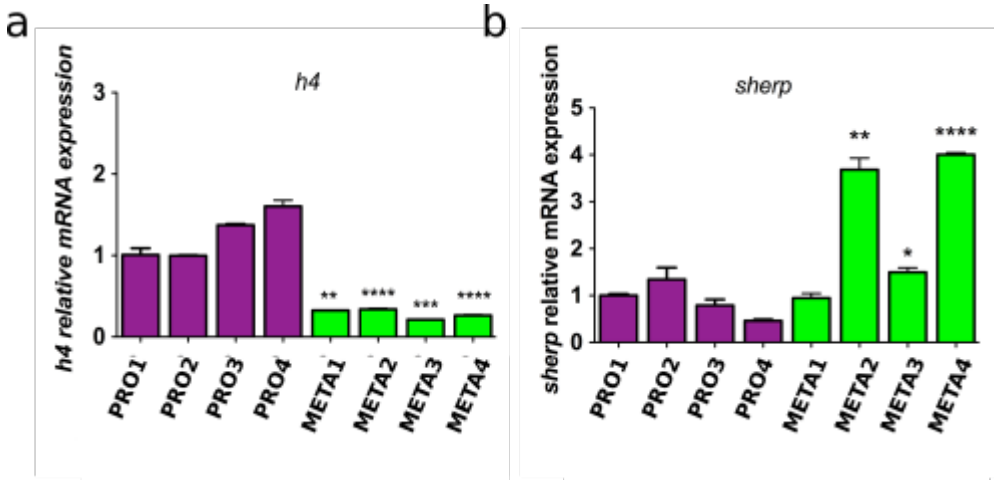

Figure 5.1.1: **a** qPCR results showing upregulation of histone H4 gene expression in procyclic populations 1-4 (purple bars) in comparison with metacyclic populations 1-4 (green bars). **b** qPCR results showing upregulation of sherp gene expression in metacyclic populations in comparison with procyclics.[1]

Histone H4 gene expression was shown to be upregulated in *L. major* procyclics [52] and was hence used as a marker to confirm procyclic promastigotes and distinguish from the metacyclic promastigote stage. There is a higher quantity of the histone H4 gene expression shown in figure 5.1.1a as these parasites have not yet differentiated to the later lifecycle stages and remain predominantly in the log-phase, as procyclic promastigotes.

SHERP is a small, hydrophillic endoplasmic reticulum-associated protein upregulated in the stationary phase parasites and hence has been used as a stage specific marker for metacyclic parasites [114]. Figure 5.1.1b shows upregulation of this genes expression in Meta 2 and 4, hence these populations of cells were used for cell tracking of metacyclics. [1]

5.1.2 DIHM Post Processing

In order to track the three-dimensional position of these cultured cells described in the previous section, digital inline holographic microscopy was implemented. The theory and setup of this technique has been described in detail in Chapter 4. This technique was used to track the centre of the cell body of freely swimming cells in custom-made sample chambers with approximate dimensions 26×6×1.5 mm. A coverslip was affixed to the chamber with UV-curable epoxy

[1]The qPCR was kindly carried out by Tiago Ferreira from the Walrad lab.

(Norland 63). Approximately 300μl of cells were then added to the chambers and sealed with petroleum jelly to reduce air flow causing and unwanted artefacts such as evaporation, and consequent convection currents. The chambers were either imaged immediately at room temperature ($\sim 20 \pm 3$°C) or kept in 26°C incubator until required.

Due to the volume of the sample being relatively large, the optical setup used was that shown in figure 4.2.1b in chapter 4. A laser with peak emission wavelength of 642 nm was spacially filtered with single mode optical fibre. Experiments were performed on a Nikon Eclipse E600 upright microscope, with a 10× magnification objective lens.

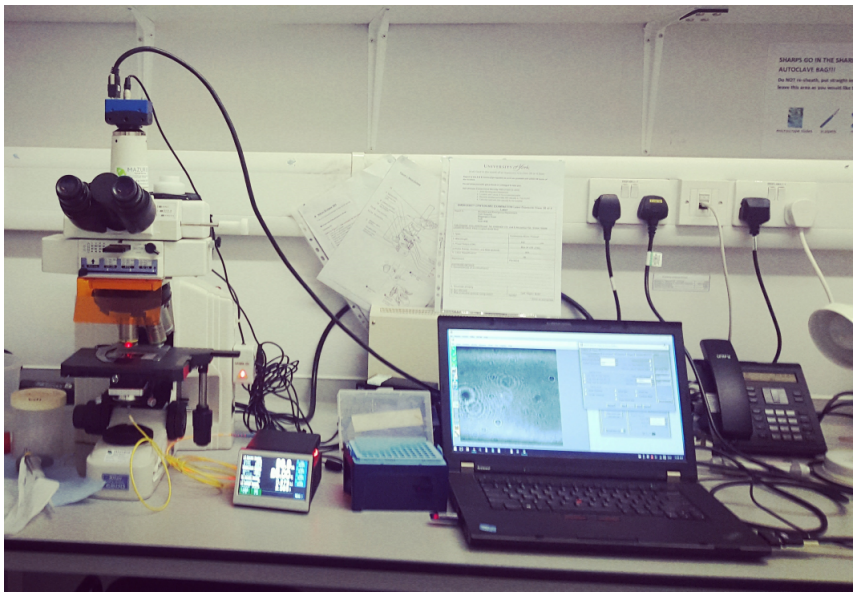

Figure 5.1.2: Photographic image showing microscope, camera and laser setup linked to laptop for data acquisition.

A Mikrotron MC-1362 CMOS camera was used to record video images. The video data was acquired at 50 Hz with an exposure time of 50 μsec which was completely sufficient to capture the motility dynamics with short exposure time to minimise blurring from the parasites motion. Each video captured 3000 frames (1 minute) with 1444×1444 μm^2 field of view. From these videos, three-dimensional swimming paths were reconstructed in several steps using in house programmes from the Wilson Lab, written and adapted in LabVIEW. The following steps describe the 'offline' post-processing of the videos acquired during experiments.

- **Step 1: Normalisation.** A median background image was calculated from each video sequence. This image contains the static background features (e.g. fixed-pattern noise, marks on the sample chamber surfaces) without any of the motile cells. Each video frame was divided by the background image to remove these artefacts.

- **Step 2: Calculating the image stack.** We applied the Rayleigh-Sommerfield back-propagation scheme to numerically refocus each background-free hologram (more details in 4.3).

- **Step 3: 3D image segmentation.** The resulting image stacks from step 2 were then subjected to various types of processing. Firstly, a spatial bandpass filter was applied in the $x - y$ plane to reduce single pixel noise from the camera during capture. Next, a three-dimensional processing filter, based on the two-dimensional Sobel-Feldman operator [109], was applied. This operator transforms a stack of numerically refocussed images into one in which axial intensity gradients are picked out as bright objects on a dark background. The objects are then isolated by performing a thresholding operation on the image stack. This reduces the filtered image stack to a sparse form that is empty (zero) in all x-y positions except those where the parasites are located. The z-position of the parasites was then determined for each non-zero column of pixels using LabVIEW's built-in quadratic peak-detection algorithm. The result of this process is a list of (x, y, z) coordinates for each cell in the frame.

- **Step 4: Compile Tracks.** Another in-house LabVIEW programme is then used to link the position of the parasites in each frame, creating tracks. From the first (x, y, z) coordinate, the programme searches the next frame for the closest coordinate in a given radius. It continues to do this for each frame until it no longer finds a coordinate within this radius, ending the track. In addition to this, it removes tracks which are not longer than a specific length set by the user, mainly tracks at the edge of the field of view.

- **Step 5: Spline Smoothing.** A cubic spline fitting tool is then used to smooth the data according to a user-set balance parameter, which sets the balance between smoothness of the cubic spline fit and accuracy with which it fits the data. This programme fits observations between sets of three points by minimising the function:

$$A(x) = p\sum_{i=0}^{n-1} W_i(y_i - f((x_i))^2 + (1-p)\int_{x_0}^{x_{n-1}} \lambda(x)(f''(x))^2\,dx \qquad (5.1.1)$$

  where p is the balance parameter and W is the weight of each data point (automatically set to 1). $f''(x)$ is the second-order derivative of the cubic spline function, $f(x)$. $\lambda(x)$ is the piecewise constant function:

$$\lambda(x) = \lambda_i, \quad x_i \leq x < x_{i+1}, \quad i = 0, 1, \ldots, n-2 \qquad (5.1.2)$$

  where λ_i is the ith element of smoothness. The result of using this algorithm gave a smoothed track which accurately preserves the main trend of the data.

  The balance parameter must fall within the range [0, 1]. If balance parameter is 0, the cubic spline fit is equivalent to a linear fit. If balance parameter is 1, the cubic spline fit interpolates between the data points. The balance parameters determined for this study and used throughout were 0.95 and 0.9 for procyclic and metacyclic promastigotes respectively. These were chosen by varying the balance parameter and comparing approximately 100 tracks before and after spline fitting (Fig 5.1.3). The parameter was

chosen as close to one as possible to remove noise while minimising the removal of any swimming characteristics in the tracks. It was noticable that metacyclic promastigotes scattered less light, probably due to their slimmer body shape, and hence a stiffer balance parameter was required to combat the noisier data produced.

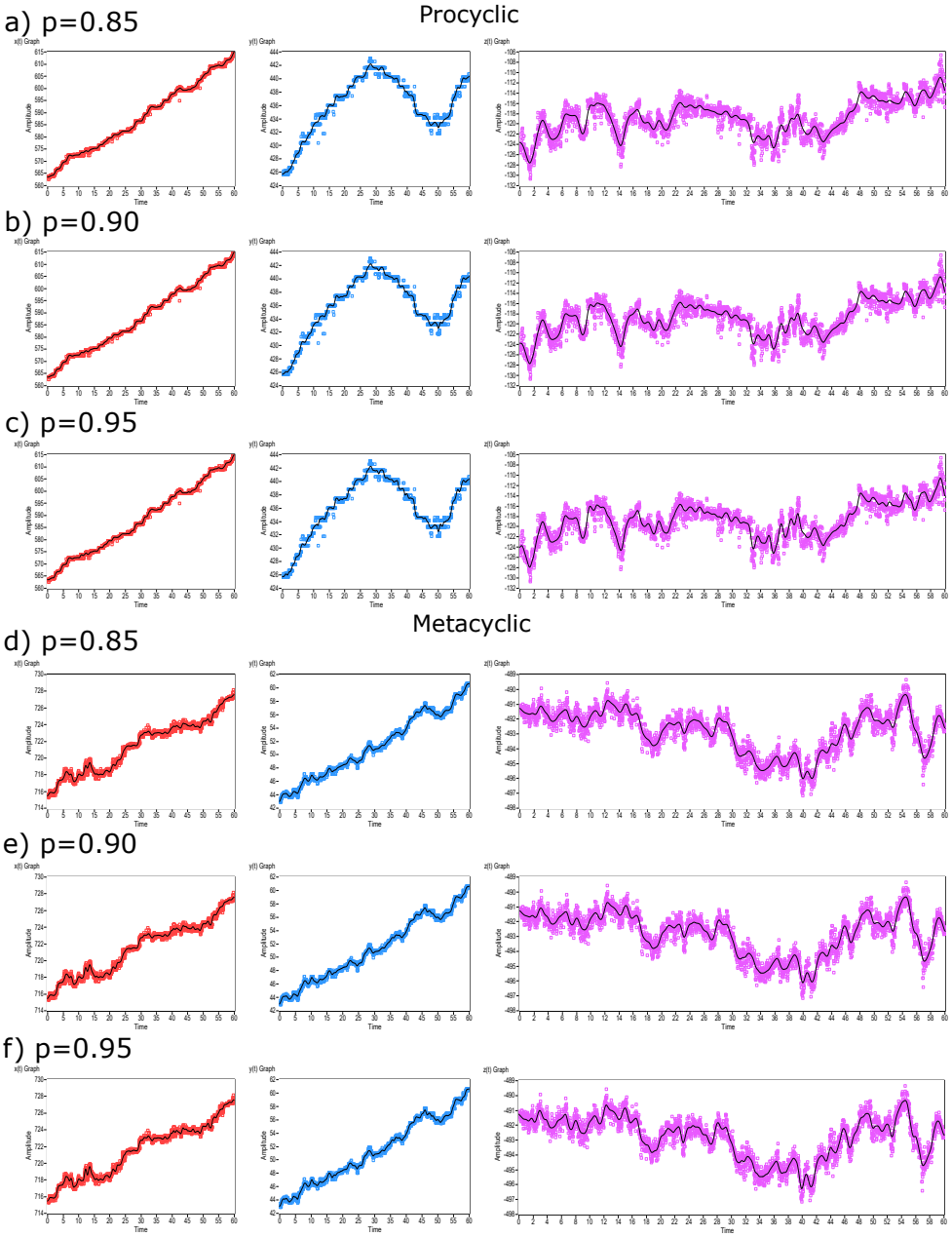

Figure 5.1.3: Testing of different balance parameters for an example procyclic track (**a, b, c**) and metacyclic track (**d, e, f**). Plotting the raw data (x(t) - red, y(t) - blue, z(t) - pink) with the smoothed spline fitting line allows visual determination of how the smoothed fit compares to the raw data. This analysis was used to visualise approximately 100 tracks of each cell type to ensure distinct features of the track were not lost during smoothing. The fit parameter in **c** and **e** were chosen for procyclic and metacyclic respectively.

- **Step 6: Swimmers vs. Diffusers.** A large proportion of the parasites tracked will be exhibiting only brownian motion, a random diffusive behaviour with no preferred direction. In order to analyse the parasites

propulsively swimming we use a filter to remove these diffusers. Calculating the mean squared displacement for each track, a measurement of the deviation of the cell with respect to a reference position over time, allows us to measure the extent of random motion.

$$\text{MSD} \equiv \langle (x - x_0)^2 \rangle = \frac{1}{N} \sum_{n=1}^{N} (x_n(t) - x_n(0))^2 \tag{5.1.3}$$

where N is the number of cells to be averaged, $x_n(0) = x_0$ is the reference position of each cell, $x_n(t)$ is the position of each cell in determined time t. This measurement of displacement over time determines if a cell is spreading solely due to diffusion or if another force is contributing. By setting the criteria of the MSD gradient and displacement we select for cells which are only swimming, the parameters chosen for different lifecycle stages are shown in Table 5.1.

	MSD slope	log MSD amplitude
Procyclic	1.4	2
Metacyclic	1	2.5

Table 5.1: Mean squared displacement parameters for procyclic and metacyclic swimmers.

The statistical average of an ideal swimmer would have a slope of two on a log-log distance vs. time graph; and for a diffuser the average slope would be one. As not every cell gives exactly the average the MSD slope parameter is the minimum value it must meet i.e. procyclic cells with slope greater than or equal to 1.4 would meet this first criteria to be classed as a swimmer. However, some short and particularly noisy tracks may also be capable of meeting this criteria. Hence, in order to ensure accurate determination a second critera has been imposed on the tracks - a minimum limit on the distance travelled in a delay time window set to two seconds. Hence, on average, the procyclic tracks displacement must be greater than two at the last time point within the window (Fig 5.1.4). Similarly to the first criteria, a very small, highly scattered particle may be able to cross this total displacement threshold. As both criteria must be met it would have a slope too low to be classed as a swimmer. The exact parameters for procyclic and metacyclic parameters were chosen by watching LabVIEW scans through approximately 100 tracks on preliminary processing.

- **Step 7: Data Analysis.** Various methods have been applied to extract the motility parameters and bending patterns of these tracks. Each of these methods will be explained in detail in the next section.

5.1.3 Mathematical Framework

Frenet-Serret Apparatus for Analysing Curvature and Torsion

The three-dimensional trajectories, representing the promastigotes swimming patterns, can be described effectively by velocity (detailed in results section), curvature and torsion. We are able to to determine exactly how they differ and

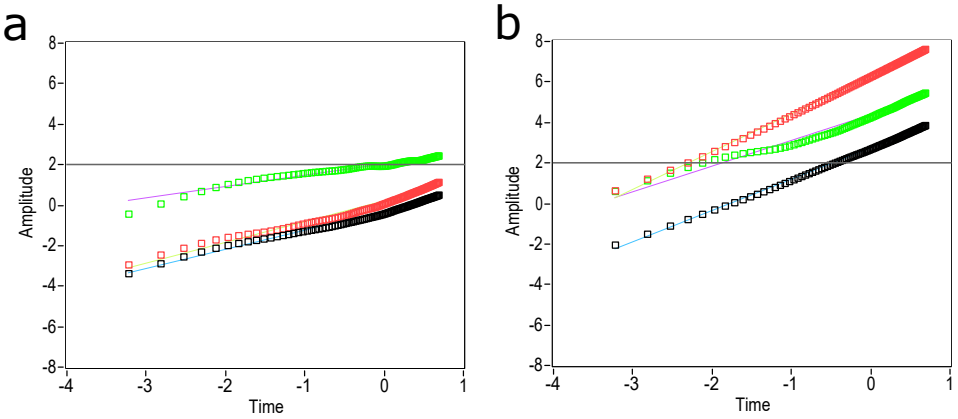

Figure 5.1.4: A procyclic track is split up using a specific time window and the displacement over time plotted. If the final point in this time window is below the threshold amplitude of two this track will be counted as a diffuser **(a)**. Otherwise the track will pass this criteria for being a swimmer **(b)**.

quantify the shape mathematically by a scalar variable, κ, that measures the curvature as a function of arc length along the cell track. The curvature is the amount by which the track deviates from being straight, or equivalently, the rate of change of the unit tangent vector [115]. The torsion, τ, measures the amount by which the curve is coming out of the plane which it lies. These parameters can be described mathematically using the Frenet-Serret apparatus, formulas to describe the rate of change of the orthogonal triad of unit vectors: tangent, normal, and binormal, in terms of each other (Fig 5.1.5a). A curve in space can be defined by a continuous series of points $\mathbf{P}$(s) where $\mathbf{P}$ represents a vector from the origin of a global XYZ coordinate system and s measures the arc length along the curve. $\widehat{\mathbf{T}}$ is the unit vector tangent to the curve and points in the direction of motion. $\widehat{\mathbf{N}}$ is the normal unit vector, the derivative of $\widehat{\mathbf{T}}$ with respect to arclength (s) of the curve. $\widehat{\mathbf{B}}$ is the binormal unit vector, the cross product of $\widehat{\mathbf{T}}$ and $\widehat{\mathbf{N}}$. These definitions result in:

$$\frac{d\widehat{\mathbf{T}}}{ds} = \kappa\widehat{\mathbf{N}} \tag{5.1.4}$$

$$\frac{d\mathbf{N}}{ds} = -\kappa\widehat{\mathbf{T}} + \tau\widehat{\mathbf{B}} \tag{5.1.5}$$

$$\frac{d\mathbf{B}}{ds} = -\tau\widehat{\mathbf{N}} \tag{5.1.6}$$

where the scalar variables, κ and τ - curvature and torsion respectively, are sufficient to describe the change in the local coordinate system as it moves along the curve. Hence, this apparatus is sufficient to describe the shape of the trajectories.

The curvature can be defined by:

$$\frac{d\widehat{\mathbf{T}}}{ds} = \frac{d^2\widehat{\mathbf{P}}}{ds^2} = \kappa\widehat{\mathbf{N}} \tag{5.1.7}$$

In the case of our trajectories we have a series of points, $\mathbf{P}$[j] for j = 0...N, with constant spacing Δs between $\mathbf{P}$[j] and $\mathbf{P}$[j-1]. Then we can estimate the magnitude of the curvature at joint j by vector subtraction:

$$\kappa[j] = \frac{|\mathbf{T}[j+1] - \mathbf{T}[j]|}{\Delta s^3} = \arcsin \frac{\frac{\mathbf{T}[j+1] \wedge \mathbf{T}[j]}{\Delta s^2}}{\Delta s} \tag{5.1.8}$$

Δs^3 is used instead of Δs because the $\mathbf{T}$ vectors are not unit vectors. Torsion can be estimated in a similar manner:

$$\tau[j+1] = \frac{-|\mathbf{B}[j+1] - \mathbf{B}[j] \mid \mathbf{T}[j+1]}{\Delta s} \tag{5.1.9}$$

These steps give the tangent vector and torsion for a segment, while the curvature is calculated for a joint. Using this approximation we have calculated and analysed the instantaneous curvature and torsion over time for each individual parasites three-dimensional swimming trajectories.

Helicity

The helicity, or chirality, is also only accessible due to the 3D nature of our data. This local chirality, H, is defined using three contiguous segments of the track. It is the angle between a segment ($\mathbf{T}_j$) and the plane formed by the two previous segments $\mathbf{T}_{j-2} \wedge \mathbf{T}_{j-1}$ (Fig. 5.1.5b, c). The sign of H is positive (right-handed) if $\mathbf{T}_j$ lies in the same half-space as the cross product of $\mathbf{T}_{j-2}$ and $\mathbf{T}_{j-1}$ and negative (left-handed) if not [86]. This allows us to determine whether the cells are more likely to swim in a clockwise or anticlockwise helical manner.

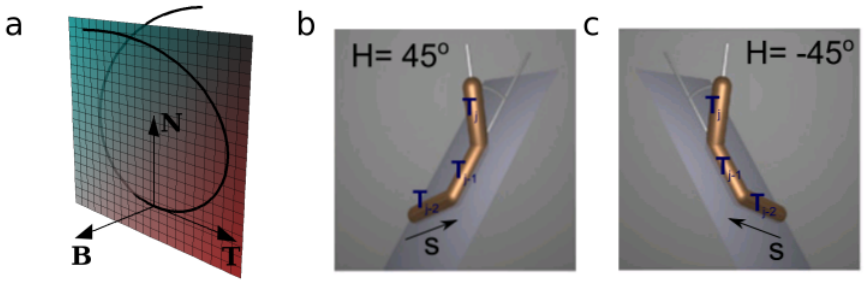

Figure 5.1.5: **a** A curve in space followed by the Frenet-Serret apparatus - triad of vectors **T**, **N**, **B**. Diagram also includes the plane spanned by **T** and **N**. **b,c** Representation of how local helicity is defined using three contiguous segments. **a** The H angle is positive and hence swimming right-handed. **b** Helicity if negative and hence left-handed [86].

5.2 Results

Initially the data was analysed through rendering in POV-ray to allow visualisation of the cell tracks in 3D. Figure 5.2.1 allows us to see by eye, clear distinctions between how these distinct populations of *L. mexicana* promastigote parasites swim in a optimised culture medium environment. However, in order to precisely analyse these differences we have used various tools to quantify their motility parameters.

First, we measured the instantaneous swimming speed of the different populations of parasites. This has been previously analysed for general promastigote populations in a few studies using differing methods. Using phase contrast

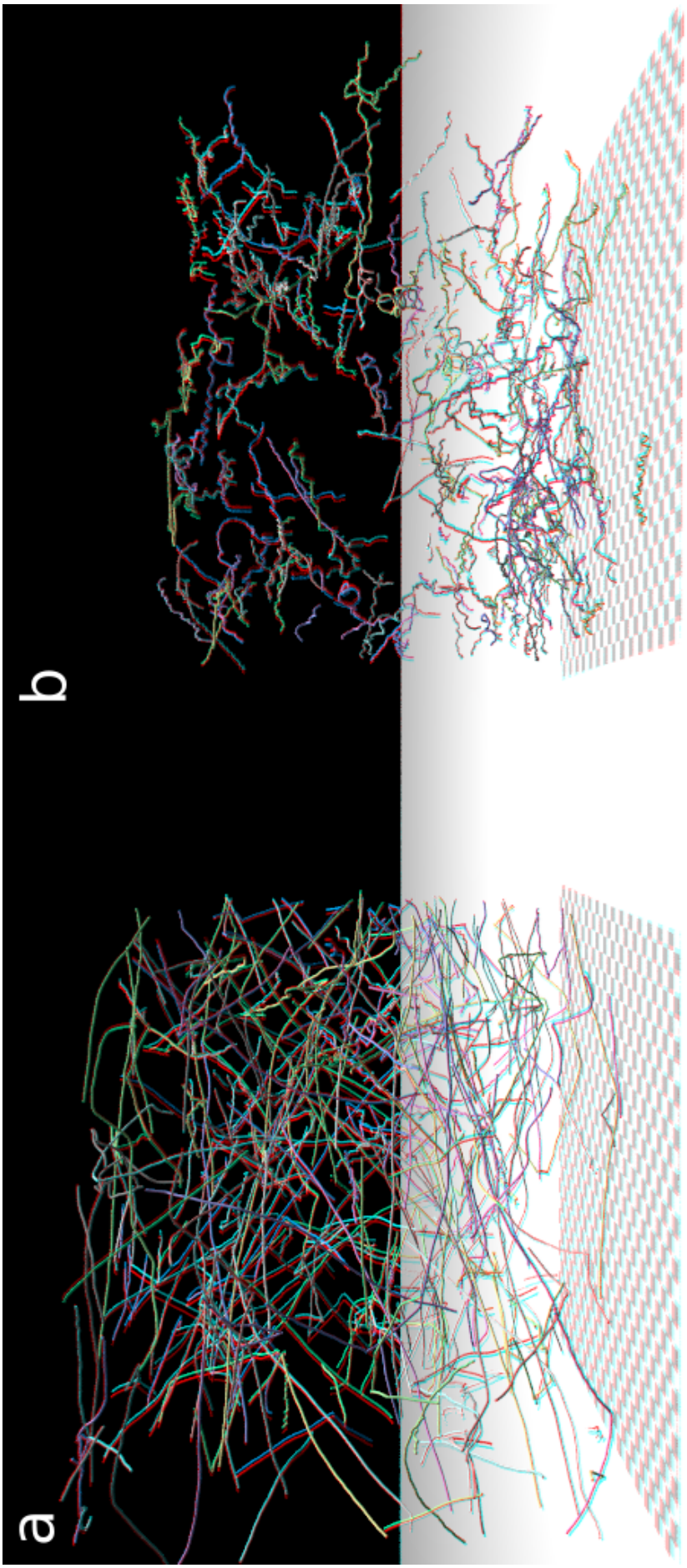

Figure 5.2.1: Rendered images show $\frac{1}{10}$th of the tracks in culture media in order to cleanly visualise them in a 1.5 mm^3 volume. Each square on the chequerboard at the base of each sample volume represents 50 μm. **a** Metacyclic promastigotes, mammalian infective cells, swimming in M199 culture media and similarly, **b** the procyclic promastigotes.

videomicroscopy of individual, long-term cultured *Leishmania major* cells the Gadelha (2007) et. al. [70] study found the cell propagation speed to be around 36 μms^{-1}. More recently, Reddy (2017) et. al. [116], calculated the speed of *Leishmania donovani* promastigote parasites. Perhaps understandably due to analysis of a different species in different media and uncharacterised populations the mean speed found by this study was significantly lower at around 26 μms^{-1}. Apparently, the speed of metacyclic promastigotes has not been identified previous to this study.

We used a high throughput method (DIHM) to collect data for a large population of cells compared with previous studies with the additional three-dimensional aspect giving us a more complete data set. Instantaneous velocities were calculated from individual positions $\mathbf{P}(t)$ by dividing displacement by time:

$$v(t) = \frac{|\mathbf{P}(t + \Delta t) - \mathbf{P}(t)|}{\Delta t} \tag{5.2.1}$$

Figure 5.2.2a and d shows the corresponding histograms when the instantaneous speed is averaged for each track to remove any bias of track length (*i.e.* each track is given the same weighting on the result independent of how long the track is). This resulted in an average speed for *Leishmania mexicana* procyclic cells of 19 μms^{-1}. Although this speed is lower than those observed in other studies, previous work focused on different species (*L. donovani* and *L. major*). The average speed of the metacyclic promastigotes was considerably faster than the procyclic cells, at 31 μms^{-1}. The significant difference in speed could be explained by the hydrodynamic drag on the cell body of the parasites. The width of the procyclic cell body is approximately 5-7 μm, 2-3 times wider than the more streamlined metacyclic cell body. This narrower body results in significantly less hyrdrodynamic drag upon the metacyclics allowing them the more rapid speed we analyse here. Their rapid speed is perhaps expected and biologically relevant given the metayclics main aim of being transmitted into the mammalian host. The metacyclics use a more rapid motile action than the procyclics, the motility of which is optimised according to different criteria in the crowded midgut of the sandfly. Other environmental factors affecting speed are presented in forthcoming chapters.

Additionally, there is a noticeable difference in the shape of these speed histograms and the corresponding distribution fitting. A traditional log-normal probability distribution appropriately fits the procyclic speed data. This is mainly due to the data being left-skewed suggesting asymmetric variability. Interestingly, the metacyclic speed histogram fits a bell shaped, Gaussian curve suggesting symmetrical variability around the mean. The difference in the shape of the graphs indicates that these populations are using different mechanisms to achieve motility. The log-normal fit for procyclic promastigotes suggests there may be limiting factors to their swimming speed in comparison to metacyclics. A potential limitation could be the available energy - a large proportion of the procyclic cells analysed will be undergoing division. This may reduce the energy available for motility unlike metacyclic promastigotes which are non-replicative. Results suggests the metacyclic cells can use various speeds in this homogeneous *in vitro* environment we tested within. Therefore, hypothetically *in vivo* it may also be possible for them to exhibit a diverse range of speeds making them more capable

of adjusting their speed according to different heterogeneous environments. However, it would be interesting to analyse whether alternative environments result in a similar limited response that we have seen here with the procyclics.

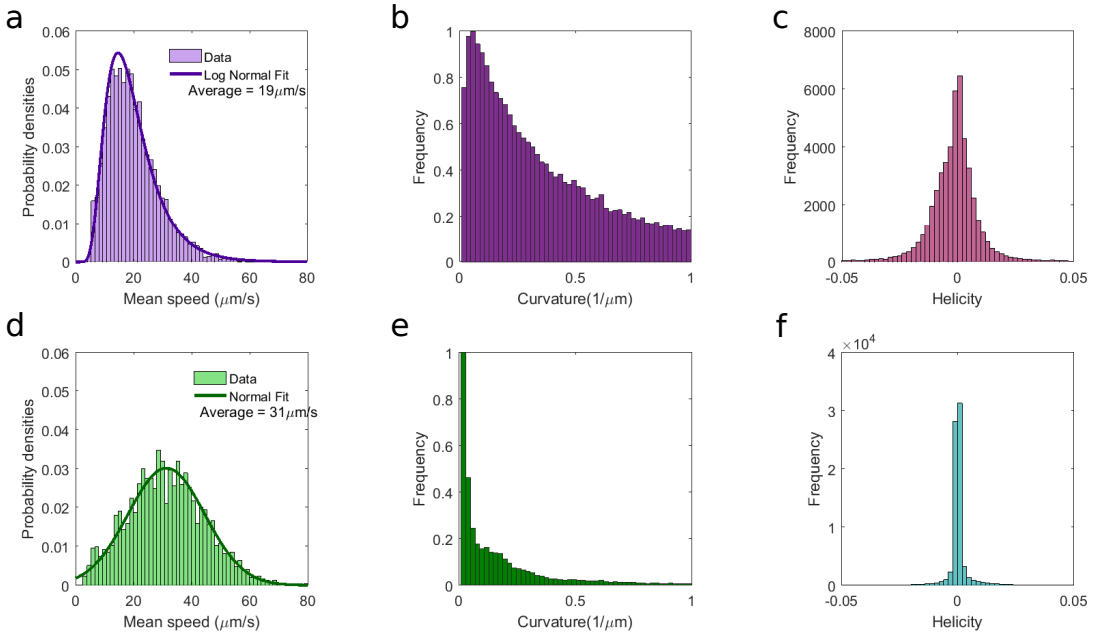

Figure 5.2.2: **a, b, c** Histograms of speed, curvature and helicity for population of procyclic tracks in M199, n = 3231. **d, e, f** Histograms of speed, curvature and helicity for metacyclic promastigotes in M199, n = 2202.

In order to rule out ambiguities stemming from sample to sample variation, I explored the possibility of systematic variations between biological and technical experimental replicates. The experimental design was optimised to reduce variation by including at least three biological and technical replicates for each experimental condition. As a result of both the high-throughput method and high number of replicates the motile fraction captured for the procyclic and metacyclic populations was n = 3231 and n = 2202 respectively. Plotting the distribution of speed for different experimental replicates in figure 5.2.3 shows the shape of the distribution is comparable, and hence the variation within our data is negligible.

5.2.1 Quantification of bending patterns reveals substantial differences in motile behaviour.

The results of curvature analysis (described in section 5.1.3 is shown using histograms in figure 5.2.2b for procyclic promastigotes and 5.2.2e for metacyclic promastigotes. This quantification allowed us to verify that the metacyclic tracks have a predominantly lower curvature than the procyclic tracks. This corresponds with what we see visually in figure 5.2.1 as the metacyclic tracks are predominantly straight lines whereas the procyclics tend to swim in a helical manner. Due to the three-dimensionality of our tracks we were also able to calculate the inherently 3D parameter, torsion. However, this quantity is not ideal for our purposes as it is difficult to interpret and determine how it is relevant biologically.[2]

[2]Some example torsion histograms can be found in Appendix A.

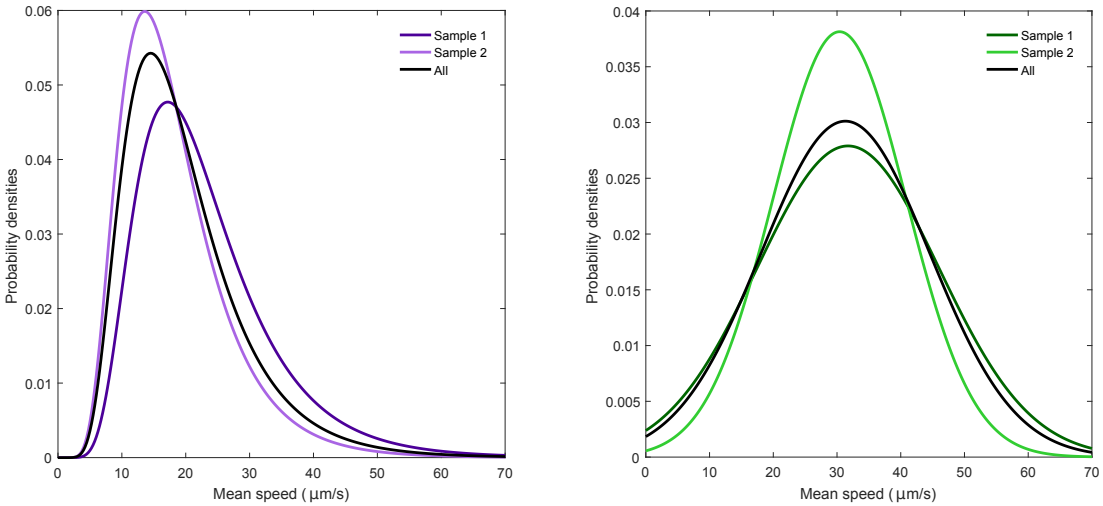

Figure 5.2.3: **a** Probability distribution for 2 biological replicates of procyclic promastigotes (different shades of purple lines) and the overall distribution in black. **b** Similarly for metacyclic promastigotes.

The final histograms in figure 5.2.2c and 5.2.2f show the helicity for our populations of procyclic and metacyclic cells, respectively. Unlike the speed histograms, the helicity has not been averaged for each track and instead each local chirality is used in the graph. This means longer tracks will have more data points and hence a bias in the graph, but it is assumed the helicity will not have a dependence on track length.

The helicity histograms of both procyclic and metacyclic promastigotes display generally symmetrical distributions with no significant bias towards positive or negative handedness. The distribution of procyclic helicity is wider than that of metacyclics, possibly as a result of metacyclics not swimming in a helical manner and is represented by low values of helicity. The slightly higher helicity values are therefore coming from elsewhere, potentially in the form of a 'tumble'. The data so far is conducive to metacyclic cells being capable of run and tumble behaviour. Run and tumble behaviour was first seen in *E. coli* cells as a method of navigation in Brownian motion and is linked to chemotaxis. Although this will be discussed further in chapter 7, Berg et. al (1972) [117] describe a 'tumble' as a change in direction whilst also slowing down or coming to a complete halt, but whilst they are 'running', they are persistently swimming in one direction and the speed is nearly uniform. This mechanism that bacteria use will be tested for *Leishmania* in chapter 7 but in the meantime these potential 'tumbles' could be an explanation for the helicity we see in metacyclic tracks.

5.2.2 Conclusions

Our data concludes that in comparison with the procyclic promastigotes, the metacyclic cells swim faster and straighter. Perhaps it is this rapid, more direct method of motility that enables them for transmission, a process irrelevant to procyclics. The result of higher curvature and chirality results in the procyclic cells swimming in a helical manner. Although these experiments have been done *in vitro* it would be interesting to see whether this corkscrew motile pattern is also seen *in vivo*. If this is the case it would suggest the procyclics use a helical

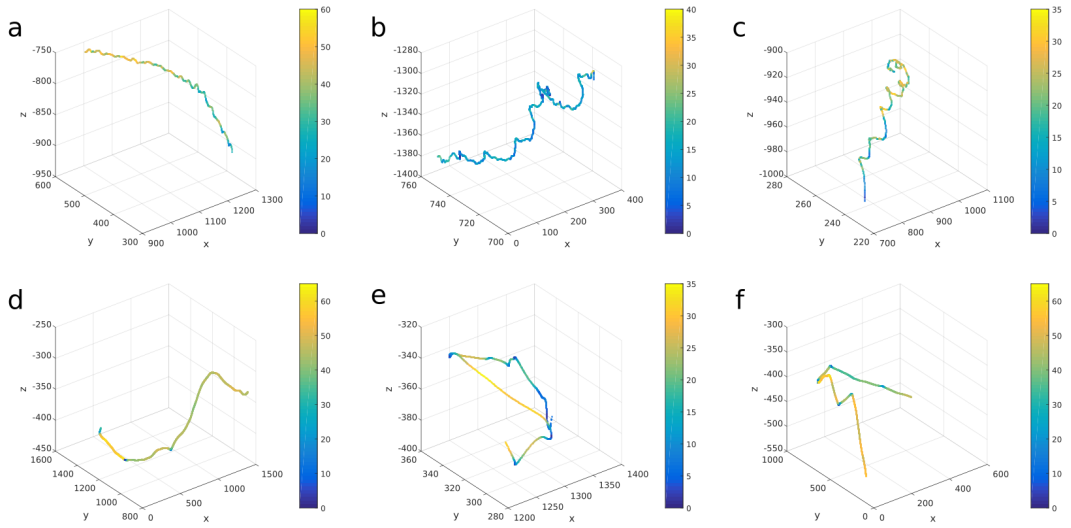

Figure 5.2.4: Individual representative tracks plotted with colourmap showing instantaneous speed. Note: Each colourmap is different to highlight minimum-maximum range effectively and the x,y,z axes aren't to scale intentionally in order to capture the broader trends in track shape. **a-c** are the helical tracking patterns of procyclic promastigotes. **d-f** are all metacyclic tracks, notice the speed of the cells slows upon changing direction similar to bacterial 'run and tumble' behaviour.

swimming mechanism to escape from the bloodmeal and progress through the harsh gut environment of the phlebotomine sandfly.

Ultimately, we have found that the procyclic and metacyclic promastigotes swim with distinct motility parameters in comparison with each other. These parasites are therefore capable of altering the mechanisms used to achieve their motility during differentiation. This energy-consuming process would not occur if it was not of importance during the lifecycle - the specifics of which are unknown at this point of the thesis but will be developed throughout following chapters. The data in this chapter, and the corresponding analyses, will be used throughout the following chapters as control data. It will give us a comparison of precisely how the motility patterns are altered when the parasites are in the different situations and environmental conditions that we have tested them in.

5.3 Tracking Genetic Mutant Parasites

We have shown this technique can give a well-rounded picture of the motility of *Leishmania* parasites and how it differs between lifecycle stages. The next obvious step is to use it to analyse parasites with genetic mutations that may result in motility defects. One area of interest is the BBSome complex, a protein complex required for specific trafficking events to and from the primary cilia (non-motile cilia, usually emanating from the cell surface which houses multiple signalling pathways necessary for normal cellular homoeostasis and development [118]). Previous research in the *Leishmania* field has concentrated on the BBS1 subunit [119]. Although the infectivity was reduced when a knockout of BBS1 was created, there was no apparent defects in growth, flagellum assembly, motility or differentiation. However, the lab of Dr. Helen Price (Keele University) have also

generated a knockout of another BBSome subunit, BBS9, which was suggested to impact some features of the parasites morphology and motility. Morphologically, the mutant cells appear rounder, fatter and have a shortened flagellum. This section applies the optimised techniques used in the previous sections to analyse the motility of the BBS9 knockout mutants and characterise how the absence of levels may impact swimming capacity.

5.3.1 Cell culture

BBS9-/- *L. mexicana* (from Price lab) procyclic promastigotes were cultured and harvested similarly to section 5.1.1. However, the mutant metacyclic promastigotes were cultured differently because when culturing in Grace's media they differentiate to the non-motile amastigote form. Although, interesting from a cell development point of view this differentiation is irrelevant to this motility study and is instead being pursued by our collaborators in the Price lab. We therefore cultured the cells for seven days in M199 until in stationary phase and then carried out the Ficoll gradient described previously (section 5.1.1). These cells will be referred to as stationary phase parasites instead of metacyclic parasites as they cannot be confirmed as a pure metacyclic population. Wildtype cells, also from the Price lab, were also cultured exactly the same as the mutant cells as a biological control.

5.3.2 Results

After performing DIHM on the mutant and wildtype samples and reconstructing the corresponding tracks, we initially calculated the motile fraction of our populations. This corresponds to the number of diffusers versus the number of swimmers from the filter described in 5.1.2, step 6. These numbers have also been confirmed by calculating the maximum intensity projection (MIP) for each frame and using ImageJ to create a projection in the z-direction of the MIP stack. Cells which are swimming will show up as a line (*i.e.* the cell track in two dimensions), while those not progressing will present as dots (Fig 5.3.1b). The lines/swimmers could be counted easily by eye, the dots/diffusers were counted using an in-built object counter in ImageJ and altering the threshold to count the total population of cells in the sample and subtracting the number of lines (Fig 5.3.1a). The percentage of swimmers from both the filter and the verification MIP analyses were similar.

The result of calculating the motile fraction (Fig. 5.3.2 e, f) showed that the number of cells in both populations, procyclic and stationary phase, were substantially lower than the wildtype population. Hence, this mutation of BBS9 has an impact on the ability of the parasites to swim in culture media.

For those cells that are progressively swimming, we also calculated their speed. We concluded that the procyclic BBS9-/- cells swim slower than the wildtype procyclic cells. This reaffirms the result that the mutant procyclic parasites are less capable of swimming. However, the stationary phase parasites' speed did not differ between the wildtype and mutant cells. This is interesting as those cells which are capable of swimming are not impeded in any way, according to this measure. However, overall the stationary phase parasites speed is much slower

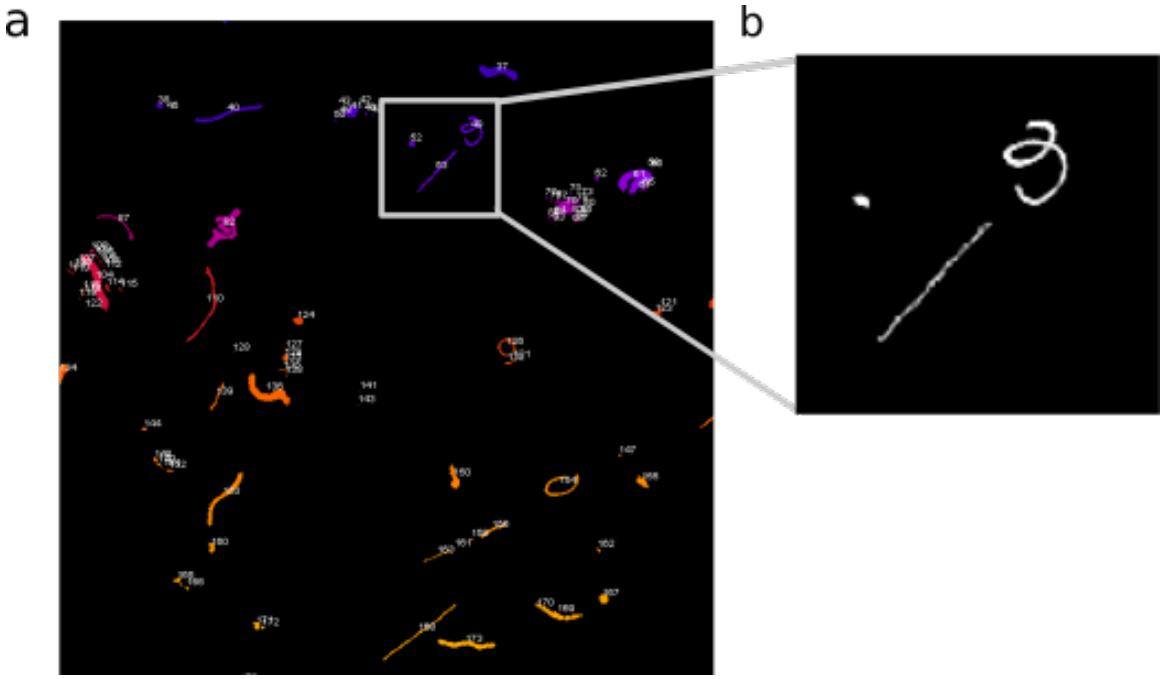

Figure 5.3.1: **a** Using ImageJ's Z-project function we can create a projection of tracks in two dimensions. The ImageJ object counter function uses blob detection algorithms to allow us to count the total number of parasites in each sample. **b** Then the motile fraction can be calculated by the percentage of the sample which are lines (swimmers). This magnified image shows two swimmers (lines) and one diffusers (dot).

than previously seen by our wildtype metacyclic promastigotes (Fig 5.2.2d). This suggests that the inability to culture 'true' metacyclic parasites using Grace's media has had an impact on our results.

Regardless, the data confirms a mutation of the BBS9 subunit of the BBSome impacts the parasites ability to swim and results in severe motility defects up to the extent of being unable to swim at all. Further research is needed biologically to characterise precisely what the BBS9-/- is causing before we can conclude how exactly it is affecting the parasites motility. However, these experiments give a good example of how quantitative studies integrate with genetics to create a holistic picture of parasite motility.

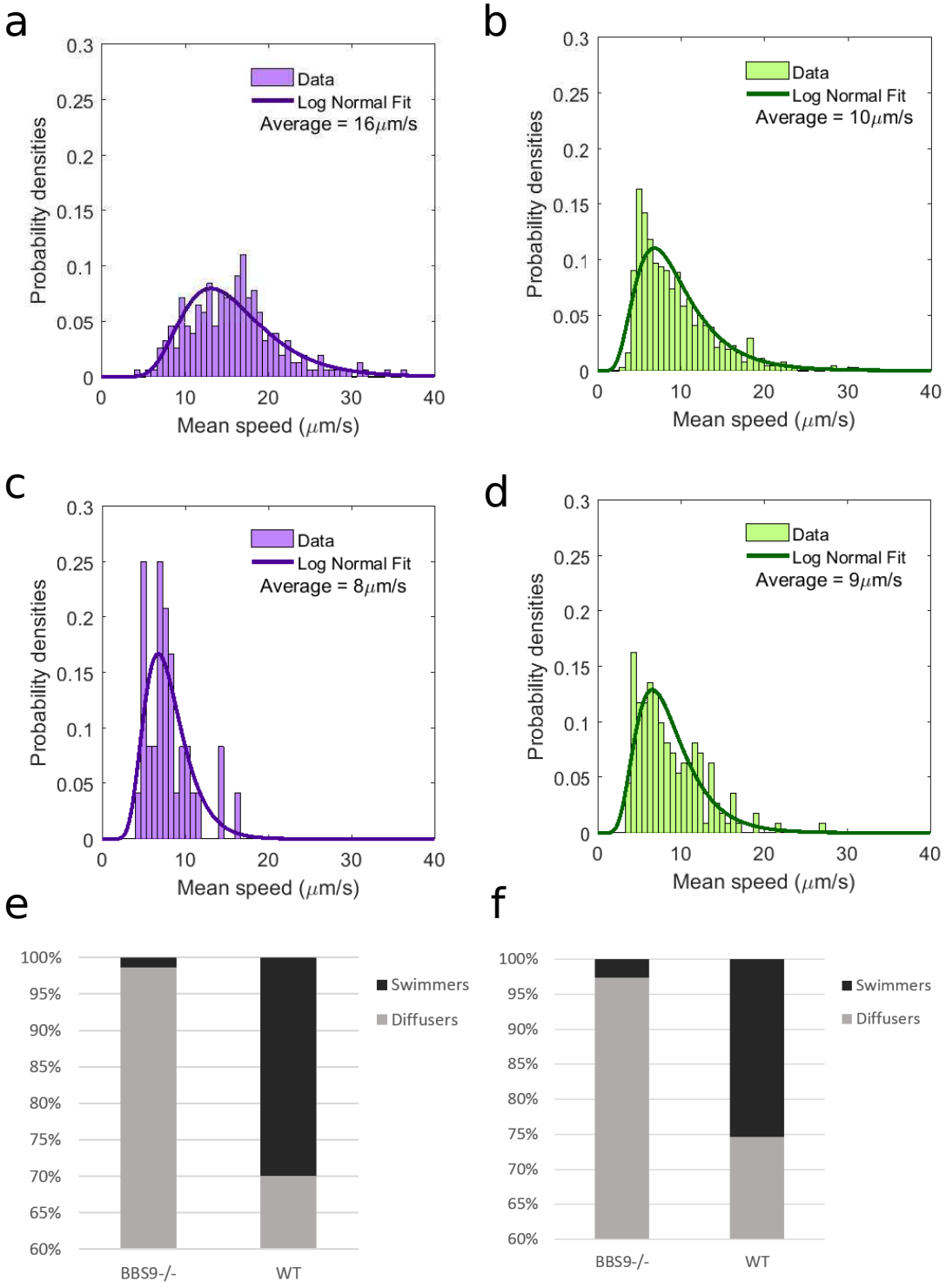

Figure 5.3.2: Analysis of BBS9-/- procyclic promastigotes **a, c, e** and metacyclic promastigotes **b, d, f**. **a** and **c** are speed histograms of procyclic mutant and wildtype populations, proving the mutant procyclics swim slower. **b** and **d** are speed histograms for the metacyclic parasites where there is little difference in how fast they are able to swim. **e** and **f** show the % motility of mutant cells is much lower than the wildtype sample.

Chapter 6

Effects of Promastigote Secretory Gel on Promastigote Motility

The transmission of *Leishmania* parasites from the sandfly into a mammalian host is exacerbated by formation of a gel-like substance[18, 112]. This promastigote secretory gel (PSG) is secreted by leptomonad promastigotes and causes an obstruction in the midgut and pharynx of the sandfly. It forces the stomodeal valve open and causes the fly to regurgitate the parasites along with the PSG upon taking a bloodmeal [26]. Metacyclic promastigotes are strongly associated with the plug as both are located in the foregut of the sandfly's digestive tract [17]. Distinctive from earlier lifecycle forms, metacyclic promastigotes are unencumbered by the gel and swim freely [30]. Metacyclics are expelled, along with part of the PSG, when a sandfly takes a blood meal [17]. Blood is then drawn through a thin channel in the PSG plug (personal communication with M. E. Rogers and previously mentioned as unpublished in P.A. Bates (2007) [17]), limiting its flow and increasing the likelihood of longer, more frequent blood meals in infected sandflies [120]. Consequently, and desirably for the disease cycle, 86-98% of promastigotes egested into the skin are the mammalian-infective metacyclic promastigotes [27].

This PSG is mainly comprised of filamentous proteophosphoglycans (fPPG), a high molecular weight ($\sim$100 kDa) glycoprotein which forms a dense three-dimensional network [28]. This network is formed by interactions between different molecules in the fluid and has an impact on the substance's viscosity [28]. Viscosity is a measurement of the fluid's resistance to flow, and so determines the energy required to make the fluid flow, or to allow cells to swim through it. It has not been determined whether the physical aspect of viscosity impacts the parasites' motility in PSG. Hence, this chapter analyses the effects of viscosity by tracking the motility of promastigotes in 3D, using DIHM as described in chapter 4, in viscous substances. Within the sandfly's midgut, metacyclogenesis occurs [121]. This process is the ability of cells to remodel their cell shape and flagellum length from the short, rounded procyclic promastigotes to the slender, elongated flagellum observed in metacyclic promastigote populations. Metacyclogenesis is energy expensive for the parasites and represents an important part of their lifecycle within the sandfly vector. We compare the different morphologies of both procyclic and metacyclic promastigotes under the main hypothesis that metacyclics remain more motile in higher viscosity solutions that other promastigotes.

The biological nature of PSG suggests that it may be highly variable and difficult to characterise. Although the main component is known, many of the other molecules and proteins it contains have not yet been identified [18]. Additionally, it is challenging and time consuming to extract in large volumes. Henceforth, we tested the parasites' reaction to well-characterised polymer solutions allowing comparisons of the relative properties. Polymers are large molecules created by polymerisation of many small molecules (monomers). Their large molecular mass relative to the monomers produces unique physical properties such as viscoelasticity and toughness.

We used the polymers Ficoll and Polyvinylpyrrolidone (PVP), as these have been characterised fairly extensively elsewhere [77]. Ficoll is a neutral, highly branched, high-mass, hydrophilic polysaccharide which dissolves readily in aqueous solutions (Fig 6.0.1a). Ficoll radii range from 2-7 nm. It is prepared by reaction of a polysaccharide with epichlorohydrin. Increasing the concentration of Ficoll by dissolving more of the Ficoll powder in a fixed volume of fluid increases the viscosity of the sample. PVP is a water-soluble polymer made from the monomer N-vinylpyrrolidone. It creates a loose, quasi-rigid network consisting of long, linear polymer molecules (Fig 6.0.1b). Increasing the concentration of PVP not only increases the viscosity, but also the elasticity (hence 'viscoelasticity') allowing us to test the effects of viscous and elastic characteristics on the parasites. Viscous fluids, such as water and in this case the Ficoll polymer solution, flow (deform) at a constant rate as they resist shear flow and strain linearly with time when a stress is applied [122]. Viscosity is a measurement of this resistance of fluids to shear stress, hence less viscous fluids deform more easily with applied shear. Elastic materials strain when stretched and immediately return to their original state when the stress is removed. Viscoelastic solutions, such as honey or aqeous solution of PVP, have elements of both viscous and elastic properties and, as a result, exhibit time-dependent strain. The bonds within the substance are gradually disrupted and the force required to maintain a constant deformation gradually decreases exponentially over time. This distinction between viscous and viscoelastic solutions is particularly useful as we do not know which best represents the natural response of PSG.

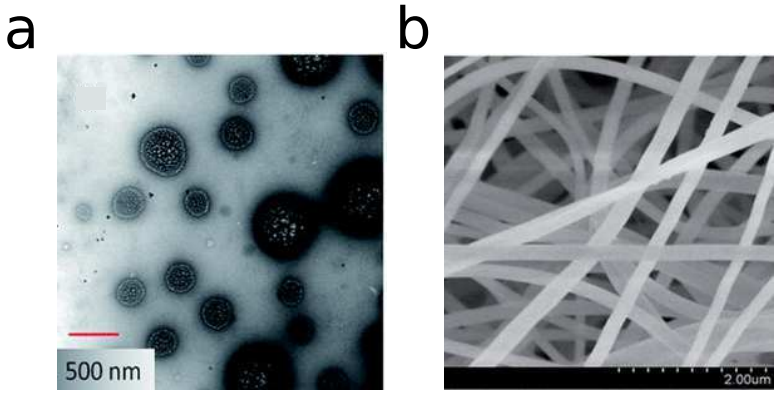

Figure 6.0.1: **a** Transmission electron micropgraph showing structure of Ficoll polymer [123]. **b** Scanning electron micrograph of PVP [124].

Although caution must be used in comparing the behaviour of bacteria and eukaryotes, given their vastly different mechanisms for achieveing motility, rep-

resentatives of both domains are found in similar (or even the same) physical and hydrodynamic environments. In light of this it may be of interest that some bacteria have been observed to swim at a higher speed at a particular viscosity. For example the swimming speed of *Pseudomonas aeruginosa* (a bacterium with a single polar flagellum) increases with viscosity up to a characteristic point and thereafter decreases (Fig. 6.0.2). This has also been shown to occur in various other bacterial species [125]. This phenomenon is caused by the structure of the polymer solutions. The polymers which form a linear network (PVP) perturb the motion of bacteria less than branched polymers (Ficoll) of the same apparent viscosity [126]. The bacteria are capable of pushing polymer chains out of the way and move more than they do in pure solvents or branched polysaccharides. It also suggests that bacteria swimming has evolved to be particularly efficient for a specific viscosity. By similar examination of procyclic and metacyclic promastigotes in an array of viscosities could give insight into whether *Leishmania* promastigotes, similar to bacteria, are optimised for a particular viscosity. We can then infer details of the parasites' ability to swim in biologically-relevant environments such as PSG, the rheology of which is not easily obtainable.

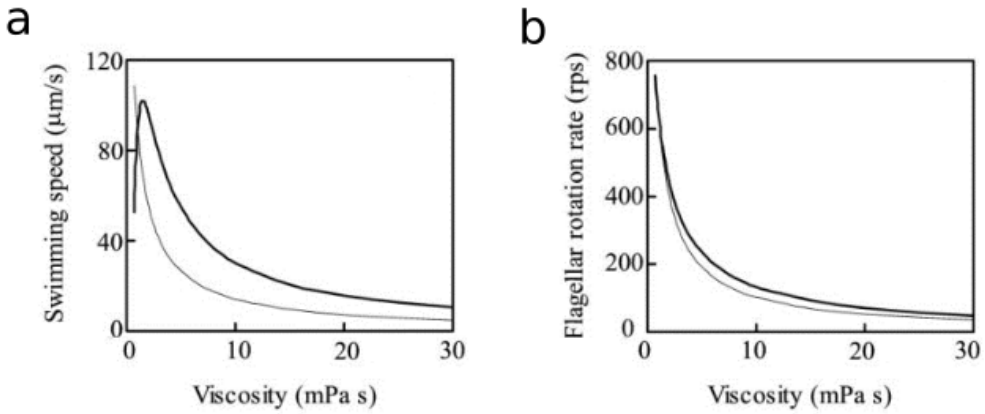

Figure 6.0.2: **a** Bacteria swimming speed and **b** flagellar rotation rates of *Pseudomonas aeriginosa* in varying viscosities of PVP [127]. The bacteria exhibit fastest swimming speed at viscosity of approximately 2 cP (*i.e.* double the viscosity of M199 media alone) before decreasing.

6.1 Methods

6.1.1 Parasite Culture

Procyclic and metacyclic promastigotes were cultured, isolated and molecularly validated as described in section 5.1.1. They were used at a final concentration of approximately 5×10^4 cells/ml. This concentration is consistent throughout all experiments described within this thesis allowing straightforward comparisons between measurements.

6.1.2 Polymer Composition and Characterisation

Ficoll (viscous) and PVP (viscoelastic) were used at molecular weights of 400 kDa and 360 kDa respectively, these polymers are well characterised in compar-

ison to other more complicated polymers [77]. Both were dissolved in supplemented M199 media using a slow magnetic stirring on a low heat. The PVP stock solution was dialysed in dialysis tubing with 14 mm diameter and a 12 kDa cut off against the supplemented M199 (ensuring no important factors of M199 were removed). The dialysis was performed over 8 days, changing the M199 every second day. This should remove low molecular weight impurities; we follow Martinez et al. [77] and omit this step for Ficoll, to ensure our rheology measurements is comparable with theirs. The final concentration of the polymers was determined by measuring the weight loss of a sample during drying in a speedvac; this instrument allowed us to create a vacuum, spin at 250 g and keep a constant temperature of 50°C for 8 hours to evaporate solvent, leaving a dry residue of polymer and media components. Previous studies of polymers dissolved in water, but in our experiments we dissolve in M199 media to remain consistent with our other experiments and also to keep the parasites alive. Hence, the M199 without polymer was also dried and subtracted from the weight of the other samples to analyse to ratio of polymer to M199 and precisely measure the polymer weight. Ficoll was used at 5% and 10% whereas PVP was used at 2.5% and 5%. All concentrations are given as % w/v.

The viscosity of these different concentrations of polymer, dissolved in M199, were measured using a Brookfield Ametek LV DV-E viscometer. The viscometer measures viscosity around 15 cP and above. As our expected range is lower we enhanced the viscometer using a Ultra Low (UL) adapter spindle to measure viscosities as low as 1-10 cP. The viscosity (cP) of 16 ml of each polymer solution was measured at room temperature at different shear rates (Hz) which were altered by changing the rotation speed of the UL spindle.

Figures 6.1.1b, c show how the viscosity varies with shear rate. Both polymers of varying concentrations have a relatively constant viscosity when altering the shear rate. On average, at comparable weights the PVP has higher viscosity than Ficoll (Fig. 6.1.1a). The average viscosity of Ficoll increases more linearly with weight whereas PVP trends towards an exponential increase. The viscosity of PVP measured can be compared with measurement from previous studies [77, 125]. Schneider et al. [125] found the viscosity of PVP to be much lower than the values we found. This could be due to different methods of dissolving PVP and use of a different solution. In contrast, our results are consistent with findings by Martinez et al. [77] which analyse viscosity using two methods - rheometry and microrheology. Rheometry is the traditional method which we use in our study. A new way of measuring the rheological properties, such as microviscosity, is microrheology. This measures the trajectory of a flow tracer such as micrometre-sized particles. As our method of measurement is comparable to the rheometry measurements in the Martinez et al. study, as expected we found equivalent results.

Confirming the viscosity of these polymers allows us to analyse how the parasites react to a range of different viscosities and different polymer structures, *i.e.* from low viscosity branched (Ficoll) to high viscosity linear (PVP). Assuming the viscosity and structure of PSG is within this range we will have comparable measurements.

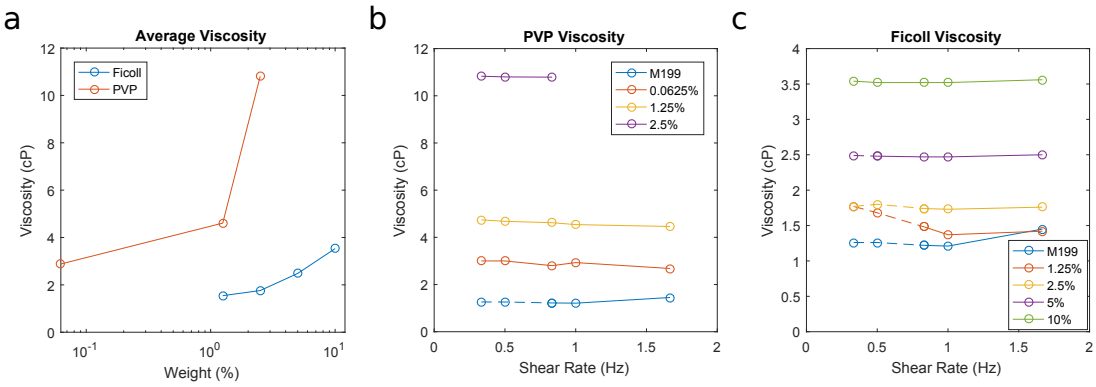

Figure 6.1.1: **a** Average viscosity (cP) for Ficoll and PVP polymers of different weights. **b, c** Show how the viscosity of Ficoll **b** and PVP **c** varies when increasing the shear rate. For comparison, the measured M199 viscosity is also shown in blue on both graphs. The dashed lines are measurements below the reliable torque range (∼10%) as recommended by the viscometers guidelines.

6.1.3 PSG

PSG was acquired from female *Lutzomyia longipalpis* flies infected with *L. mexicana* amastigotes (M. E. Rogers, LSHTM). Flies were maintained to allow full development of the parasite infection within the fly as described in [128]. The PSG plug at the anterior midgut is isolated when the infection is mature. The gut is sliced in a longitudinal direction and the plug lifted out with entomological needles.

This experiment used approximately 200 μl of 0.2 μg/μl PSG. A 1:5 serial dilution of the stock solution of PSG was carried out four times, in supplemented M199, resulting in 5 different concentrations for testing - 0.2, 0.04, 0.008, 0.0016, 0.00032 μg/μl.

6.1.4 Assay Setup

Assay 1 - Polymers

The assay testing parasites in polymer solutions was set up identically to the basic motility assays in chapter 5. 300μl of a suspension containing 5×10^4 cells/ml plus polymer were added to a sample chamber and sealed with petroleum jelly. The cells were immediately imaged using DIHM. This experiment was repeated across all polymer concentrations with at least three biological replicates, each with three technical replicates. The results were then colated for analysis.

Assay 2 - PSG

The assay using different concentrations of PSG was identical to assay 1 described above with the exception of the sample chamber dimensions. As described above obtaining PSG, especially in large volumes, is very challenging. For this reason altered chamber slides were constructed to allow only 20 μl to be used for each replicate. Hence, the width and depth of the sample chambers were kept the same, but the length was reduced from 26 mm to approximately 5 mm (final dimensions of $5\times6\times1.5$ mm). The new dimensions did not effect imaging as this was ample area to capture the same field of view ($\sim 1.4\times1.4$ mm) as previously.

Due to difficult logistics and inadequate PSG volumes, only technical replicates were used for this experiment. The outcome still resulted in an ample population for accurate analysis.

6.1.5 Analysis

Post-processing was carried out in the same way as described in the previous chapter, section 5.1.2. The motility of the parasites was characterised by the velocity, motile fractions and bending patterns also described previously in section 5.1.3. Using identical analysis to quantify the swimming patterns allows us to compare these results to those already described in 5.

6.2 Results - Metacyclics are more capable of motility in high viscosity solutions

Renders of the three-dimensional tracks in two different polymers of varying viscous properties are visualised in figures 6.2.2a, b, c and 6.2.2d, e, f for procyclic and metacyclic promastigotes respectively. To analyse the motility of these parasites in the different solutions we quantified their speed, curvature, and motile fraction of the population comparable to analysis in M199 alone (chapter 5).

Initial analysis determined how the swimming speed is affected by viscosity (Fig. 6.2.3). Within Ficoll, as the concentration of polymer and thus the viscosity was increased, the procyclic parasites slowed. An apparent anomaly is that the average swimming speed of cells in 5% Ficoll is slightly faster (∼10%) than that in M199 media alone. Although this result is similar to that previously seen in bacteria in viscoelastic polymers [125], the result is somewhat unexpected in the purely viscous Ficoll solution. This higher average speed could be a result of procyclic cells being more efficient in swimming in slightly higher viscosity (approximately 1.25 cP more) than M199 media. Alternatively, the Ficoll may inhibit slower cells from remaining motile hence raising the average speed.

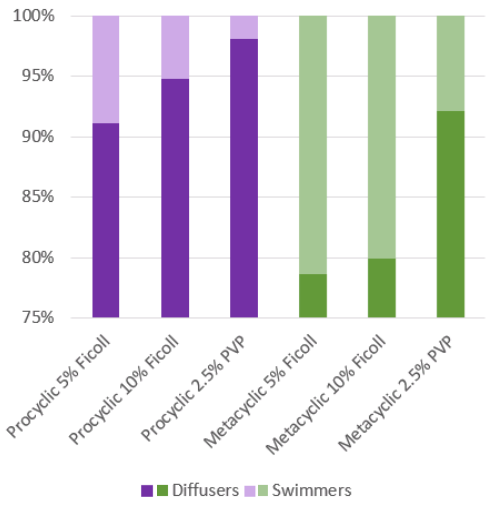

Figure 6.2.1: Analysing the percentage of swimmers (light colours) versus the percentage of diffusers (dark colours) allows analysis of the motile fraction of the samples. Calculated for procyclic (purple) and metacyclic (green) in various polymer solutions tested shows % motile decreases with viscosity.

In comparison, the metacyclic speed in different Ficoll viscosities tested remains the same. In 2.5% w/v PVP polymer, both promastigotes' speed were substantially decreased. The cells are still capable of maintaining some motility in PVP even though it has much higher viscosity in Ficoll. This is probably due to the structure and elasticity of the polymer. Experiments were attempted in

5% PVP solutions but no motile cells were evident from either population.

These speed results coincide with the motile fraction detected within the experiments, shown in figure 6.2.1. As the viscosity is increased the motile fraction of both promastigote populations decrease, albeit less so among the metacyclics. The motile fraction in both Ficoll solutions is comparable to media only results (20% motile cells in media for procyclic and metacyclic). In PVP the motile fraction is approximately half, but is four times more than procyclics.

We were also able to characterise the swimming kinematics of these cells similarly to the media-only analysis (section 5.1.3). As described previously, the main distinction between these two lifecycle stages is the curvature of the tracks. Procyclic cells have a helical swimming pattern hence have a higher curvature than metacyclics which tend to swim in a straight line. Analysis in Ficoll solutions gave the same result for both promastigotes. However in PVP, more of the metacyclic tracks exhibit higher curvature, as evident from figure 6.2.2f. Potential reasons for this change in curvature are discussed below, in section 6.4.

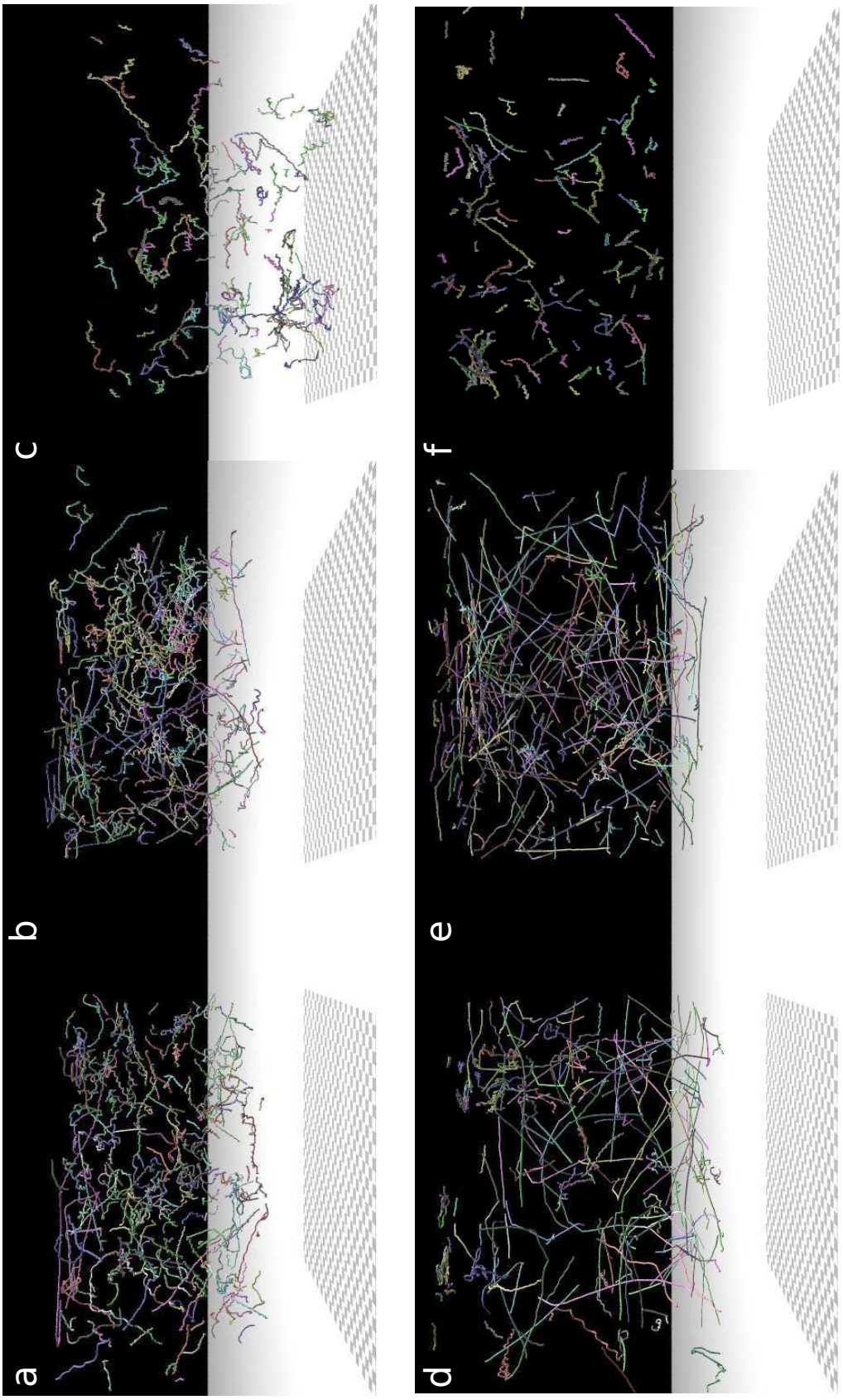

Figure 6.2.2: Rendered images show the procyclic (**a, b, c**) and metacyclic (**d, e, f**) tracks in polymer solutions giving a clear visualisation of their location in 1.5 mm^3 volume sample. Each square on the chequerboard at the base of each sample volume represents 50 μm. The parasites are in **a, d** 5% Ficoll, **b, e** 10% Ficoll, and **c, f** 2.5% PVP.

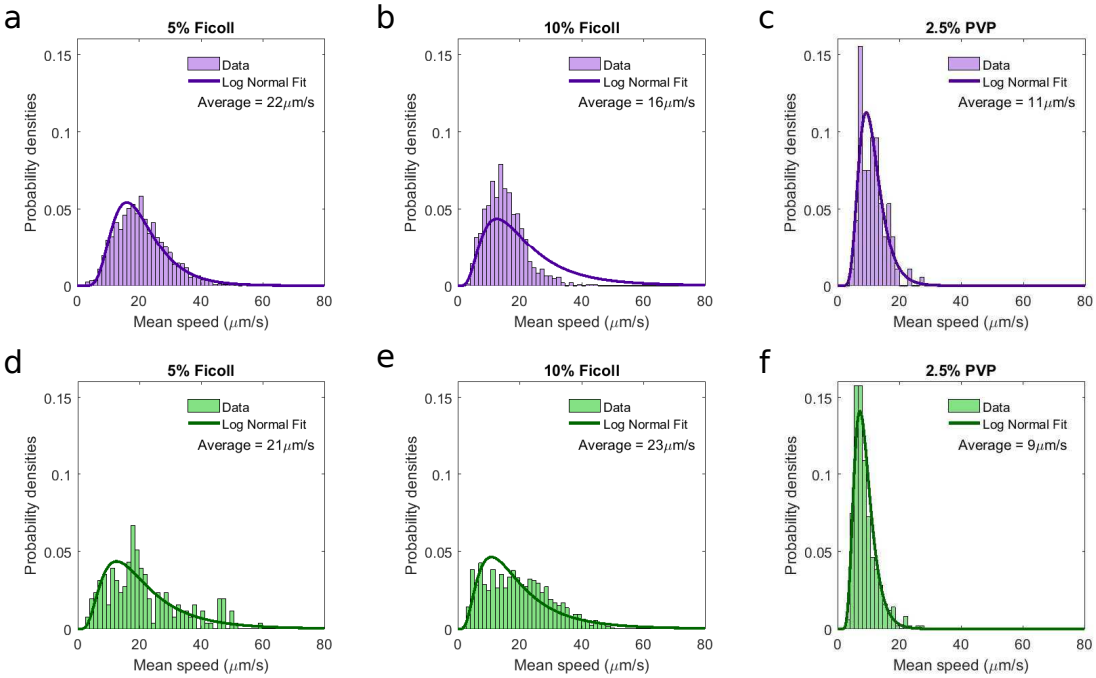

Figure 6.2.3: Histograms detailing the speed of the parasites tracked in polymer solutions of different viscosities. **a, b, c** Purple histograms correspond to procyclic promastigotes and **d, e, f** green histograms are the results of metacyclic promastigotes. The first column (**a, d**) are in 5% Ficoll, the second column (**b, e**) in 10% Ficoll and the final column (**c, f**) is in 2.5% PVP. Ficoll reduces the speed of procyclics but does not alter metacyclic speed. PVP reduces the swimming speed of both promastigotes.

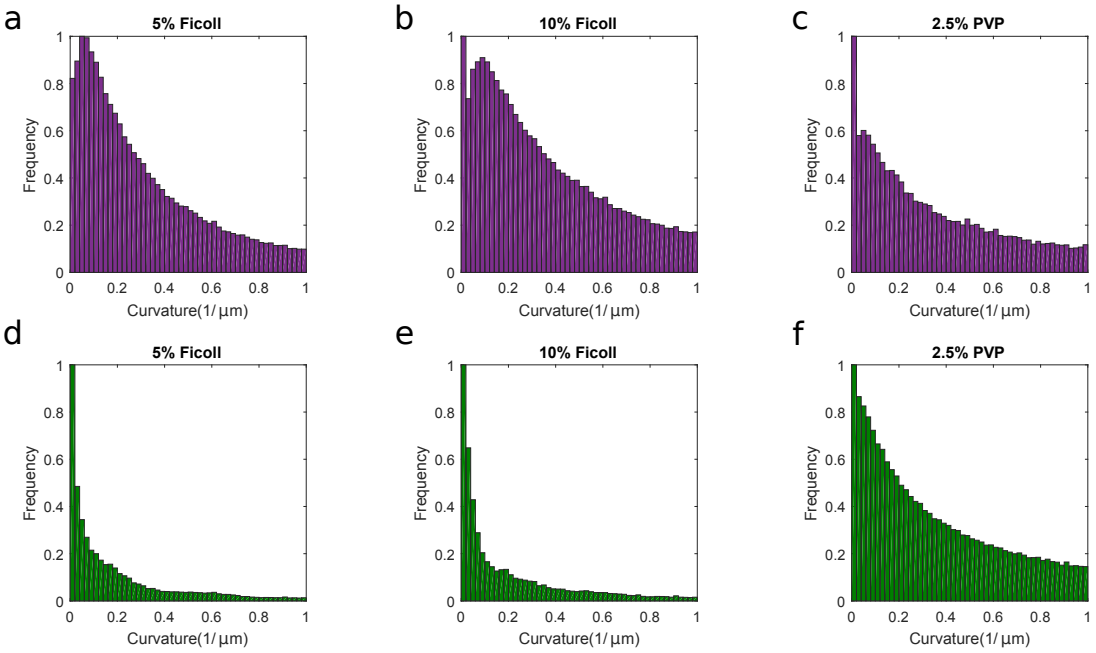

Figure 6.2.4: Histograms displaying the variation of curvature of procyclic (**a, b, c**) and metacyclic (**d, e, f**) in polymer solutions. These have all been normalised by dividing the data by the largest frequency value for each graph allowing easier comparison. The first column (**a, d**) are in 5% Ficoll, the second column (**b, e**) in 10% Ficoll and the final column (**c, f**) is in 2.5% PVP. The results are equivalent other than (**f**), in which the curvature displayed by metacyclics is increased.

6.3 Results - Metacyclics are inhibited by increasing PSG viscosity

The final experiment in this section yielded 3D tracks of both procyclic and metacyclic parasites swimming in five different concentrations of PSG. This experiment is more biologically relevant than the tests in polymer solutions and could help us to understand how motility is implicated in transmission from the female phlebotomine sandfly to the mammal. However, this biological relevance comes with additional complications. As a result of some experimental complication (causing unwanted convection currents) our analysis omits results for the two highest concentration PSG samples for metacyclic promastigotes. This anomaly was not due to the concentration of PSG and is instead a coincidence that it affected these two samples. Due to insufficient volumes of PSG we were unfortunately unable to repeat for these conditions.

Analysis of the average swimming speed of these cells led to the first interesting outcome. The different dilutions of PSG do not appear to impact the speed of the procyclic promastigotes (Fig. 6.3.1). The speed of these cells in the most concentrated PSG is comparable to that in $\sim$10 cP PVP whereas all other dilutions are comparable to high viscous Ficoll solutions. The biological relevance of testing this lifecycle stage in PSG is limited, due to the fact they never encounter PSG. They are located at the opposite end of the sandfly's gut and either undergo differentiation to migrate to the anterior end [121] or are defecated along with the bloodmeal [129]. However, it is still interesting that they do not appear to be affected, this result could have implications on understanding the mechanisms used to remain motile in PSG.

For the metacyclic samples the speed with regard to PSG concentration is varied (Fig. 6.3.2). The highest concentration result (0.008 μg/μl - Fig. 6.3.2a) reduces both the speed and the motile fraction (Fig. 6.3.2d), having a larger impact on the cells than the Ficoll and therefore an effect more comparable to our results in PVP. This impact is reduced with PSG as the rheological behaviour of the surrounding media becomes more like that of the 'bare' solvent.

On similar analysis of the curvature of the tracks, the procyclic cells exhibit comparable curvature to previous analysis. Of these cells curvature does not appear to be altered by viscosity. However, some of the metacyclic cells exhibit higher curvature in PSG. The result was not as pronounced as within PVP but is still significant. Reasons for these results and corresponding analysis of promastigote swimming in PSG are discussed in more detail in the conclusions section for this chapter (section 6.4).

6.4 Conclusions

The results of our first assay, testing in polymer solutions with relatively well-characterised viscoelastic properties, concluded that the metacyclic promastigotes are more capable of swimming in higher polymer concentrations than the procyclic promastigotes. This result was derived by analysis of how the speed and motile fraction is affected. Overall, metacyclics retain speed and motility better than procyclic promastigotes upon increasing polymer concentration. In

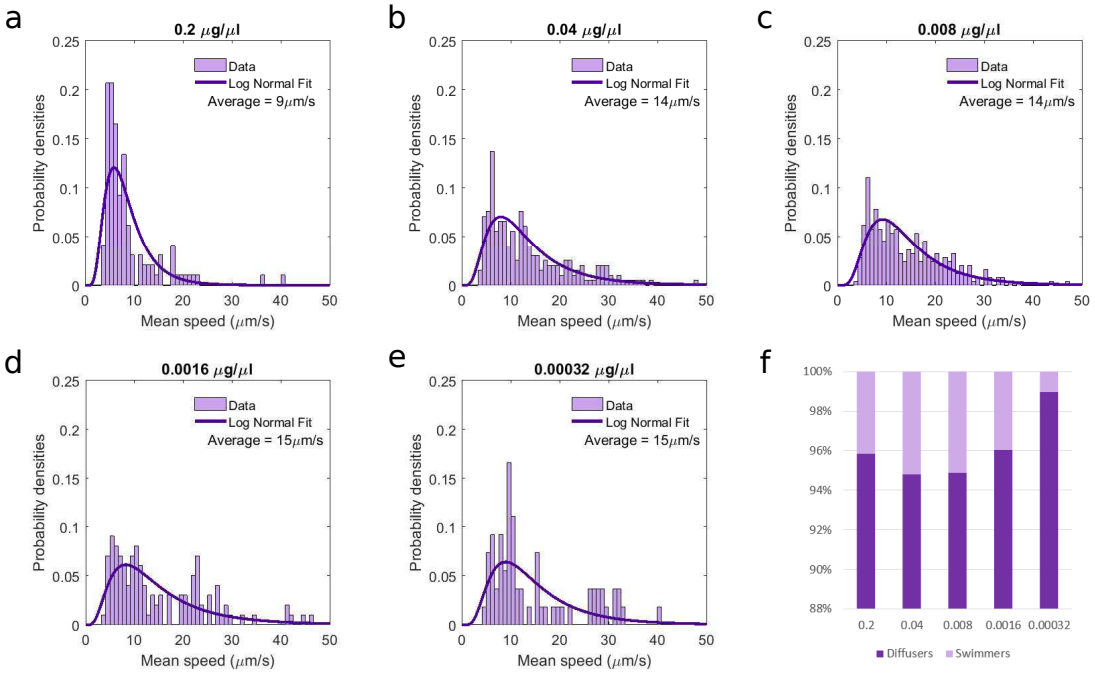

Figure 6.3.1: Histograms detailing the speed of procyclic promastigotes in PSG concentrations ($\mu g/\mu l$) **a** 0.2, **b** 0.04, **c** 0.008, **d** 0.0016, and **e** 0.00032. **f** Displays the percentage of swimmers versus diffusers giving us the motile fraction in various concentrations of PSG.

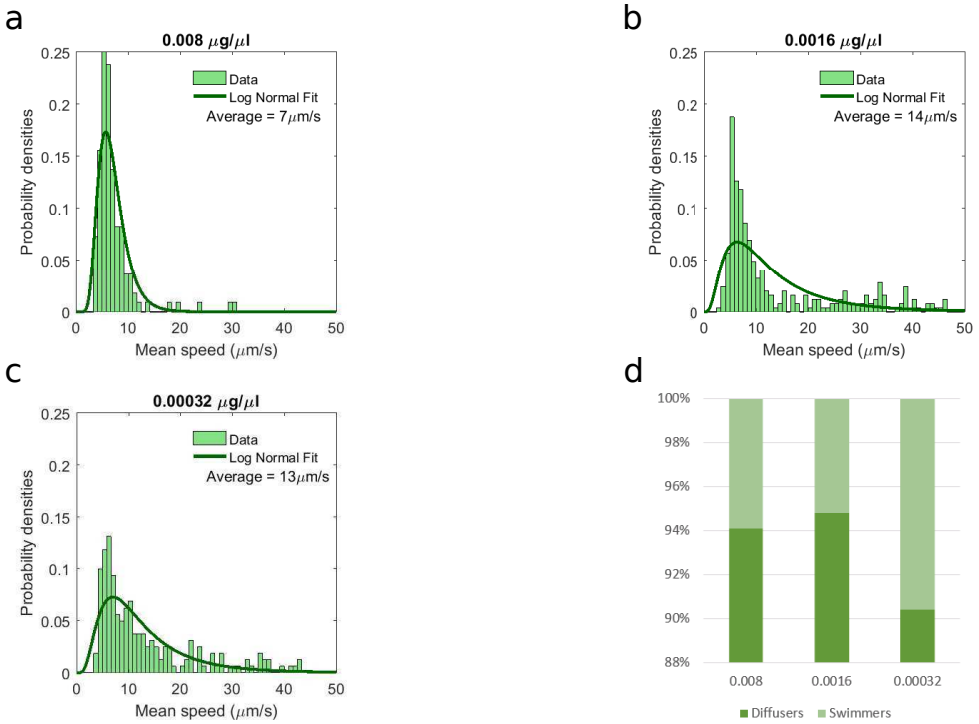

Figure 6.3.2: Histograms detailing the speed of metacyclic promastigotes in PSG concentrations ($\mu g/\mu l$) **a** 0.008, **b** 0.0016, and **c** 0.00032. **d** The percentage of swimmers versus diffusing metacyclic parasites giving us the motile fraction for the concentrations of PSG tested.

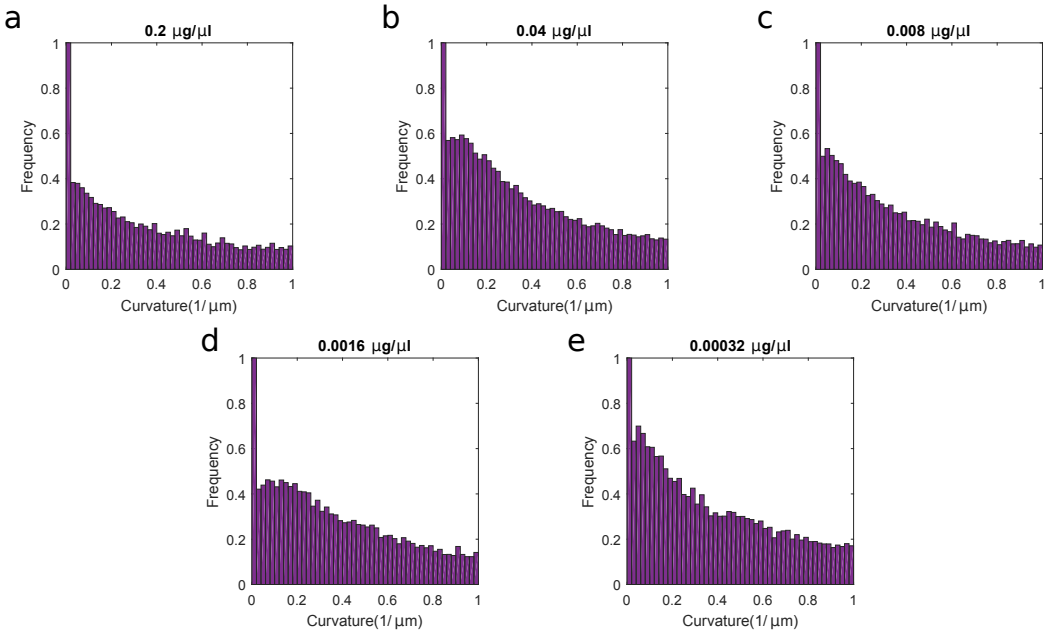

Figure 6.3.3: Histograms showing the curvature of procyclic cells in PSG with concentration (μg/μl) **a** 0.2, **b** 0.04, **c** 0.008, **d** 0.0016, and **e** 0.00032. The concentration, and hence viscosity, does not appear to affect the curvature of the procyclics.

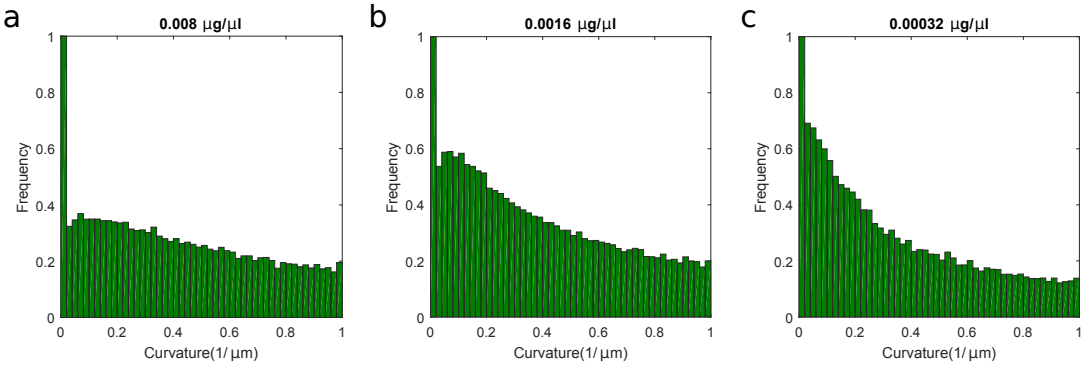

Figure 6.3.4: Histograms showing the curvature of metacyclic cells in PSG with concentration (μg/μl) **a** 0.008, **b** 0.0016, **c** 0.00032. Metacyclic cells exhibit higher curvature values while swimming in PSG.

addition, the metacyclic promastigotes adjust swimming patterns when in the viscoelastic polymer PVP. We observe that metacyclic cells swim with higher curvature, similar to that of procyclics, suggesting they are obstructed from their normal straight line swimming pattern. It is possible that the polymer structure is 'trapping' these cells so they are incapable of continuing in a straight line and the time between changing direction, or run duration, is reduced. Alternatively, these cells may adjust their swimming mechanism in order to remain motile in higher viscosity environments.

Intriguingly, the results seen in polymers were not necessarily replicated within PSG. The concentration of PSG within the *in vivo* environment of the sandfly is highly variable and dependent on the initial parasite infection [112]. Hence we analysed various concentrations of PSG, all of which could be biologically relevant. The procyclic cells do not physically encounter PSG *in vivo* so although not biologically relevant, the procyclic cells appear to be uninhibited by PSG. During our analysis in polymers we observed the procyclics can be affected by viscosity, suggesting that there is something other than physical forces which are affecting parasite motility.

The speed and motile fraction of metacyclic cells are reduced with PSG concentration. However, some metacyclic cells are capable of remaining motile, possibly due to the higher curvature and lower speed that we have examined. The trajectories of these cells are closer to what we see in the procyclic population in the absence of polymers or PSG. It is unclear whether the cells are altering their motility in response to the environment or whether the environment is forcing a different swimming pattern. More testing is necessary to decide whether these parasites are capable of rapidly remodelling their swimming mechanisms, or whether distinct swimming capabilities are hard-wired during differentiation. At this point, the bulk of the evidence appears to point towards the latter.

In conclusion, the procyclics are not affected by PSG to the same extent as metacyclics. A better comparison would be to compare isolated leptomonads or nectomonads. They differentiate into the infective metacyclics but are not infective themselves and hence are the most important cell types to be inhibited by PSG during transmission. These cells have not been analysed due to difficulties in obtaining purified populations, although advancements in identifying molecular markers for these cells types may make this possible in the future [52].

Although biological levels of PSG are varied, comparing the results of swimming patterns in polymers and PSG has been difficult due to the unknown viscosity of PSG used for our experiments. The viscometer used to determine the viscosity of polymers required 16 ml for accuracy. It would not be possible to measure the viscosity of PSG using this method as acquiring this volume of PSG would not be possible, requiring too many sandflies and a significant amount of dissection time. It may be possible to establish the viscosity using previously mentioned microrheology experiments, such as those described in the study analysing bacteria in polymers [77]. This method analyses the low-shear viscosity by calculating the mean square displacement of tracer particles under controlled stress forces. This can then be related to the resistance of the beads due to the viscous forces and hence rheology of the solution.

Chapter 7

Chemotaxic Responses of Promastigotes

Motile organisms typically respond to specific environmental stimuli by directed movement, a phenomenon called taxis. As previously described, in order for *Leishmania* to infect a mammalian host the promastigote must move from its main site of multiplication in the hindgut or midgut of the phlebotomine sandfly up the alimentary canal to the pharynx and proboscis, where is must enter the mammalian skin [130]. Once in the skin it is still necessary for the promastigote to gain entry in a macrophage, where it will transform into an amastigote and multiply. The first hours after infection are crucial for the obligate intracellular parasites to rapidly localise phagocytes, it must do this quickly as human sera will kill it within 30 minutes [131]. One method which has been suggested is the use of neutrophils as a trojan horse before they enter macrophages. Laskay et. al. suggest that parasites are phagocytosed first by neutrophils which are the first responders of the innate immune response, infiltrating the skin rapidly upon infection (although the trigger for this is unknown)[132]. Hence, they will encounter the parasites first allowing them to uptake the parasites and present them to macrophages when they undergo apoptosis, potentially preparing the parasites for macrophage uptake and survival. Two photon intravital imaging has shown this process of uptake of parasites by neutrophils *in vivo* [133]. However, it is possible that the neutrophils are only scavenging parasites which have been ignored [6]. Additional information of this trojan horse hypothesis, as well as the unknown pathways for parasites to travel to the lymph, bone marrow and to be distributed throughout the skin in visceral species [134], could be determined with advanced parasite tracking techniques. For example, the time lapse images in Peters et. al. were taken at a rate of one per minute, as speed fit for the neutrophils but not for the promastigote parasites. High speed *in vivo* tracking of fluorescently labelled parasites could allow counts and localisations of parasites in infections.

The internalisation into macrophages is controlled through interaction with many different receptors. LPG, being one of these receptors, plays an important role during attachment and invasion of macrophages. LPG coat protects the parasites from complement-mediated lysis and induces complement activation thus promoting parasite phagocytosis [135]. It is possible that chemotaxis, directional movement of cells in response to chemical stimulus, has an involvement in this

internalisation process assisting the parasites in their aim to transmit and infect. We investigate this, presenting the methods and results in this chapter.

Chemotaxis and osmotaxis (where a gradient in osmotic pressure is the directing factor), in non-specified *Leishmania* promastigotes has been investigated in various studies previously. An overview of this work and its limitations is presented first. These previous experiments give an excellent foundation for our experiments and allow us to direct and optimise them to gain more efficient and conclusive results however they do not distinguish between procyclic and metacyclic promastigotes. This chapter details two experiments - one to investigate whether cell swimming is biased towards potential chemoattractants and the second using the previously described DIHM technique to analyse the parasites' 3D motility patterns in chemical gradients to determine whether swimming behaviour is altered.

7.1 Previous Evidence of Taxic Responses of *Leishmania* Promastigotes

The chemotaxic response of *Leishmania* promastigotes (unspecified stages of four species *L. mexicana, L. major, L. donovani, L. tropica*) and macrophages were first investigated *in vitro* by R.S Bray [136]. The method used involved introducing a promastigote suspension to a chamber slide made of a sawn-off, disposable 1 ml Tuberculin syringe covered by a Millipore filter, also known as the Boyden chamber system. The apparatus is then immersed in a suspension of parasites in the putative chemotaxic fluids; including sugars, serum components, culture supernatants, haemoglobin and murine peritoneal macrophages.

For murine peritoneal macrophages the results indicated that serum was necessary for attraction between promastigotes and macrophages and that the attraction was exerted upon the macrophages as opposed to the motile promastigotes. The promastigotes activate serum to produce a gradient of a factor that is attractive to macrophages, and which is destroyed by heating to 56°C for 30 minutes and inhibited by EDTA [136]. In the absence of serum, promastigotes do not produce a chemotaxin for macrophages, and dilution of the serum available for promastigote activation dimishes the chemotaxic effect upon macrophages (Fig. 7.1.1 [136]).

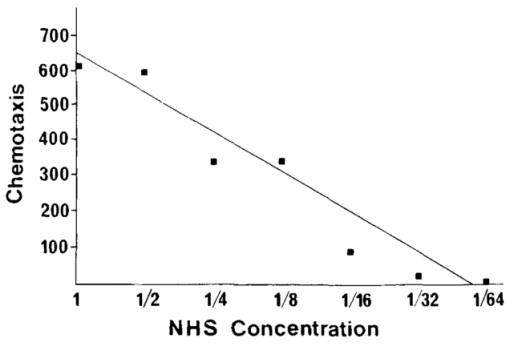

Figure 7.1.1: Chemotaxic response (number of macrophages below the filter) of mouse unelicited peritoneal macrophages to varying concentrations of normal human serum (NHS) by 4×10^7 promastigotes of *L. mexicana* for 3 hours in the Boyden chamber system [136].

This work highlighted that chemotaxic influences upon the promastigote were relevant to its life in the invertebrate host and in the inflammatory skin site. The chemotaxic effect of several sugars were also shown, which could contribute significantly to movement of the parasite within the alimentary canal of the sandfly

and also within the bloodstream of the mammalian host. The sugars, such as raffinose, maltose, mannose, fructose, sucrose and melibiose, are in high concentration near the pharynx where promastigotes congregate during late infection and glucose is prevalent in blood.

Although it was possible to detect chemotaxic responses by the method used by R.S. Bray, it proved to be insensitive and require high concentrations of attractant ($\geqslant$ 20 mM). Even at high concentrations, this method was ineffective in demonstrating the chemotaxis effect exercised by carbohydrates, such as glucose and fructose, considered to be important in the diet of phlebotomine sandflies. Additionally, the study suggests the attraction was exerted upon macrophages without considering the difference in speed between them and the promastigotes. Although macrophages have been observed to respond to inflammatory signals more rapidly with a migration speed of $0.1\mu\text{ms}^{-1}$ [137] this is still considerably slower than promastigotes (from our *in vitro* calculations, fig. 5.2.2a,d).

Distinguishing between promastigote stages

A more sensitive method was developed by J.S. Oliveira et al. [138] to study chemotaxis in *Leishmania* (species *L. chagasi* and *L. amazonensis*) in greater detail. A gradient of the assayed substances was produced inside capillary tubes submerged in promastigote suspension [138]. The different stages were defined by two different growth phases (logarithmic phase and stationary phase). Due to their division rate (or lack of), historically the procyclic stage was associated with log-phase and the metacyclic stage with stationary phase. After an incubation period, the attractiveness was measured by counting the number of parasites in the capillaries using a haemocytometer. The chemotaxic bias to the carbohydrates tested were expressed as chemotaxic capability (CC), calculated as the number of promastigotes attracted to each test capillary decided by the number present in the respective control tube.

Chemotaxic Capability of Some Carbohydrates on Promastigotes of *Leishmania amazonensis* and *L. chagasi*

	Chemotaxic capability (CC) ± SE							
Carbohydrate	Glucose	Fructose	Sucrose	Raffinose	Manose	Galactose	Maltose	Melibiose
L amazonensis PH8 (log phase)	2.4 ± 0.1	2.4 ± 0.1	4.2 ± 2.1	3.0 ± 1.1	—	—	—	—
L amazonensis PH8 (stationary phase)	7.5 ± 1.4	7.7 ± 0.8	5.2 ± 2.0	4.4 ± 2.1	—	—	—	—
L amazonensis BH6 (log phase)	7.1 ± 0.2	5.6 ± 0.7	7.5 ± 0.1	6.8 ± 1.0	2.8 ± 0.7	4.0 ± 1.2	7.0 ± 1.2	3.9 ± 0.3
L chagasi BH46 (log phase)	3.1 ± 1.4	3.1 ± 1.3	2.7 ± 0.5	2.8 ± 0.5	2.7 ± 1.1	2.4 ± 0.6	3.1 ± 0.9	4.2 ± 1.2

Figure 7.1.2: Chemotaxic response to various carbohydrates of log and stationary phase promastigotes (*L. amazonensis* and *L. chagasi* species). The chemotaxis capacity (CC) represents how many times the number of attracted promastigote cells was greater than the number present in the respective control [138].

Figure 7.1.2 shows different responses were obtained when the test was performed using promastigotes of the same strain in two different physiological states (log and stationary phase). The stationary phase cells showed enhanced chemotaxic capability [138]. It is possible that this can be explained by the stationary phase cultures consisting of many metacyclic promastigotes which have greater mobility than other promastigotes.

Chemotaxis or Osmotaxis?

The results from J. S. Oliviera et al. (2000) [138] were interpreted as evidence of sugar chemotaxis, although absence of a control substance that was not attractive to parasites left open the possibility that promastigotes were moving towards an osmotic gradient rather than, or in addition to, a chemical one. G. Leslie et al. [139] adapted this assay into a simple taxis assay which directly measured the number of *L. mexicana* promastigotes (of unspecified stages) that move, over a period of 1 hour, from a buffered cell suspension into the open end of a capillary tube containing an agarose gel matrix plus a source of the putative chemoattractant [139]. Diffusion of this substance from the capillary tube establishes a concentration gradient diffusing from its open end [138].

The test compound L-glucose is not a substrate for *Leishmania* hexose transporters and is not metabolised by *Leishmania* promastigotes [139]. It is also not abundant in the diet of the sandfly host and not likely to be encountered by *Leishmania*. However, it elicited the same taxic response as D-glucose, which is a major energy source for promastigotes *in vitro* and a major component of the sandfly diet. This raised the possibility that *Leishmania* promastigotes could exhibit osmotaxis, a phenomenon not previously described in eukaryotes. This was confirmed under conditions where solute levels were equimolar (*i.e.* in the absence of an osmotic gradient),experiments showed no accumulation of promastigotes in the capillary tubes [139].

This report of osmotaxis in eukaryotes could explain how promastigotes migrate in the anterior region of the insect gut, or it could be an adaptation by which parasites avoid osmotic stress. Either way, motility and consequent migration are critical to the parasite life cycle and the presence of a chemical stimulus is a plausible way of orienting the cells' migration.

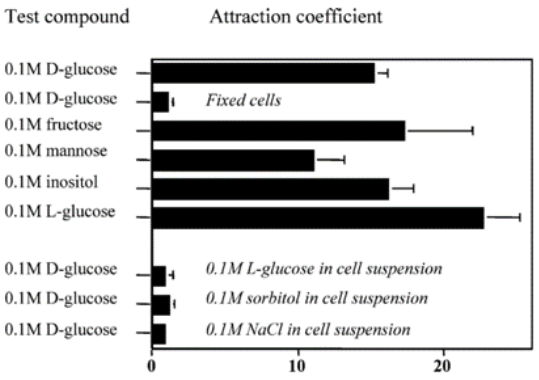

Figure 7.1.3: Movement of promastigotes in the presence or absence of solute gradients. Attraction coefficient was calculated as the mean number of cells moving into a capillary tube containing the indicated test compounds [139].

A complementary study by A. A. Ahmed et al. [140] provides evidence of *Leishmania* parasites' ability to attract macrophages. They studied the chemotaxic activities of live, killed and sonicated *L. major* promastigotes with murine macrophages. They hypothesised that chemoattraction of the host target cell towards the parasite not only ensures the parasites' entry into the right type of cell, but also minimises extracellullar existence of parasites and hence also lysis or uptake and killing by neutrophils. However, more recent studies suggest uptake by neutrophils is beneficial for *L. major* and increases their chances of infection [133].

One result from this study conclusively showed that preincubation of macrophages with promastigotes for 2 hours completely abolished the chemotaxic capacity of the cells towards living parasites [140]. This indicates that the chemoattractant activity of living promastigotes is a receptor-mediated process, which possibly becomes saturated during the incubation period, resulting in the abolishment of the

chemotaxic capacity towards parasites. Also, paraformaldehyde-killed promastigotes significantly inhibited macrophage chemotaxic activity, indicating that living promastigote chemotaxic factor(s) may be proteinacious. Moreover, living promastigotes were the most efficient attractants for macrophages compared with other forms of the parasites. Therefore the viability of the parasites is essential for effective attraction of macrophages.

First analysis of parasite movement during chemotaxis

The studies previously discussed all use the Boyden chamber, or a variation thereof, to distinguish the occurence of chemotaxis or osmotaxis. A study that used a different method is that by Barros et al. [141]. They used an approach previously used in bacteria [142] to track the parasite (*L. amazonensis*) and measure the mean time of straight line movement (TSLM) in the presence or absence of taxic agents. This study was the first in the *Leishmania* field to hint that the promastigotes may be capable of 'tumbling' - an abrupt change in direction similar to that exhibited by peritrichously flagellated bacteria such as *E. coli*. In essence they were measuring the duration of the run during possible 'run and tumble' dynamics, a mechanism we will explore further in our own results. This study confirmed the promastigotes show taxic responses (longer TSLM) to low concentrations of sucrose, lactose, mannitol and glycine but not to the same molar concentrations of NaCl, Hepes and guanosine (Fig. 7.1.4). This suggests that the taxic response is not due to positive osmotaxis as proposed by Leslie et al. [139], because osmotaxis would elicit the same taxic response to all solutions under the same experimental conditions if the osmotic pressure was similar (NaCl ionizes to Na^+ and Cl^- hence has double the osmotic pressure to the same molar concentration of sucrose or any other non-ionising substance).

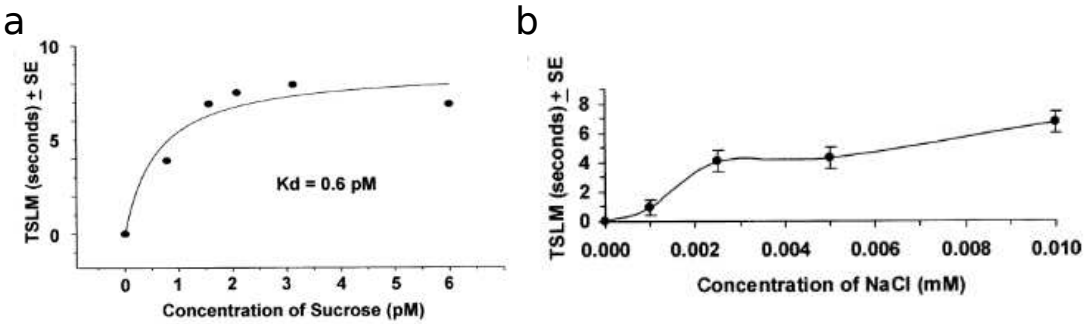

Figure 7.1.4: Mean time of straight line movement (TSLM) of *L. amazonensis* promastigotes in different concentrations of **a** sucrose and **b** NaCl [141].

Limitations

Although all of these studies mentioned have advanced *Leishmania* chemo/osmotaxis research, each has its limitations. These studies are labour intensive: only a small number of cells can be analysed in each individual experiment. They are mostly qualitative, giving positive or negative results, but not the precise details of how those results occur. Only log and stationary phase parasites have been analysed, as purifying metacyclics has only been developed recently [113] the response of the important mammalian infective cells has not yet been characterised.

Table 7.1: Glossary of taxic terms

Chemotaxis	Directional movement in response to chemical stimulus.
Osmotaxis	Directional movement in response to osmotic pressure.
Chemokinesis	Change in organisms swimming behaviour by chemical stimulus but not necessarily its direction, *i.e.* change of speed, frequency and migratory behaviour.
Orthokinesis	Form of chemokinesis altering the speed or frequency of cells in response to stimulus.
Klinokinesis	Form of chemokinesis altering the amount of turning the cells does in response to stimulus.

This is especially important in the studies involving macrophages since these are the lifecycle stage involved. Additionally, many of these studies do not consider the possibility of the involvement of chemokinesis. Chemokinesis is a random cell movement (rather than directional movement exhibited during chemotaxis) that occurs in the absence of a concentration gradient of chemoattractants, chemotaxic agents that induce a cell to migrate toward them. It can occur in two forms - orthokinesis and klinokinesis. In orthokinesis, the speed or frequency of locomotion is determined by the magnitude of the stimulus, *i.e.* the attractant concentration. In klinokinesis the amount of turning the cell does is determined by the magnitude of the stimulus. Orthokinesis is thus a straightforward acceleration or deceleration of cells in response to stimuli and is important in leukocytes. Klinokinesis is of uncertain importance in leukocytes, but in bacteria such as *E. coli*, a chemical gradient can cause the cells to change direction more frequently [143]. The studies described above are limited to only analysing the number of cells in comparison to a control experiment and do not consider speed or direction of the parasites swimming. Hence they would not be able to determine whether the motility mechanism is chemotaxis or chemokinesis. Although Barros et al. [141] begin to analyse the cell movement they only calculate TSLM and infer that a fall in the TSLM indicates an increase in the rate of change in direction suggesting the cells are searching. They do not consider the speed of the cells or the overall direction of the cell path.

In our study we are interested in the way that the parasites' motility changes during taxis (arguably osmo-,chemo-taxis or chemokinesis). The importance of discovering the mechanisms used by bacteria and sperm during chemotaxis has advanced the studies of these microswimmers substantially [85, 117, 144]. It has also allowed the modification of these organisms to inhibit chemotaxis [117] and gain a better understanding of how these organisms use motility for various reasons. *Leishmania* research would greatly benefit from this analysis and directed inhibition of motility to block transmission would clearly be beneficial in the fight against leishmaniasis.

7.2 Initial Experiments Demonstrate Directional Bias Towards Macrophages

This simple investigation of chemotaxic behaviour gave additional motivation for the later, more detailed experiments.

7.2.1 Methods

Cell Culture

Procyclic and metacyclic parasites were cultured using the methods described in section 5.1.1. J774.2 macrophages [145], an immortalised mouse cell line, were maintained in Dulbecco's Modified Eagle Medium (DMEM) supplemented with 10% heat-inactivated calf serum, 1% Penicillin-Streptomycin and 1% glutamine. They were incubated at 37°C with 10% CO_2 and passaged into new media every 3 days.

7.2.2 Assay Setup

The initial assay involved the use of a choice chamber, designed using a microfluidic chamber slide ('Ibidi y-shaped μ-slide'). The shape of this slide allowed for a control substrate (complete M199 media only) to be added to one of the wells, as indicated in figure 7.2.1. 60μl of J774.2 macrophages, with concentration of 5×10^6 cells/ml, were added to the well at the other end of the slide and were left overnight at an angle within a humidity chamber to adhere to the bottom of the microfluidic slide. The slides were filled with M199 from the control-only side, without washing was to ensure that any stimulus emitted from the adhered macrophages was not removed.

The slides were also adapted to include two extra central wells (as seen in Fig 7.2.1) where the parasites could be added. 1 μl of metacyclic and procyclic parasites were added to these wells simultaneously at an approximate concentration 5×10^6 cells/ml. The slides were then imaged at various positions along the y-shaped arms of the slide, towards the macrophages and towards the control well as indicated in figure 7.2.1 (both cell types were studied at the same positions although for clarity, these are only marked on the procyclic side of the figure. The images were taken almost immediately after inoculation, and again 30 minutes post-inoculation. Using 20× magnification on an Nikon Eclipse E600 upright microscope, images were captured using a Mikrotron MC-1362 CMOS camera. Between image acquisitions, the slides were incubated in a humidity chamber at 27°C.

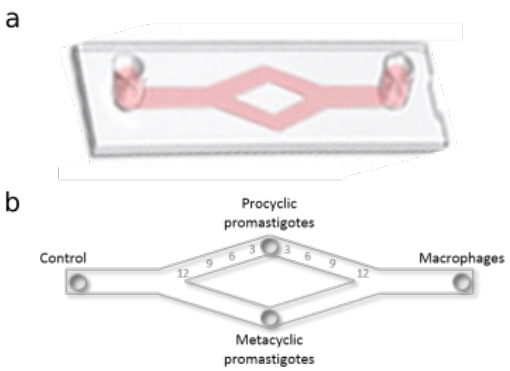

Figure 7.2.1: **a** Image of the 'Ibidi y-shaped μ-slide' used during the initial chemotaxis assay. **b** Diagrammatically shows which cells were added to which wells in the slide. It also shows the distances along the slides where images were taken (at 3, 6, 9, and 12 mm).

Using the ImageJ object counter (previously described in 5.3.2) the number of parasites in each image were calculated allowing comparisons in bias towards either the control or the macrophages.

7.2.3 Results

As shown in figure 7.2.2a, we consistently found a higher number of parasites in the macrophage channel versus the media control. Procyclic parasites never encounter macrophages so this bias was not expected. However, it is possible that they still have the capability of detecting chemical or osmotic gradients. For example, if this is a receptor-mediated response, the procyclics may already have the receptors and mechanisms to alter their motility before differentiating to metacyclics.

From this data we were also capable of calculating the 'index of chemokinesis' to further analyse the effect of the macrophage stimulus:

$$\chi = \frac{N_{test}}{N_{test} + N_{control}}$$

where N_{test} is the number of parasites in the macrophage channel and $N_{control}$ is the number in the media control channel. If $\chi = 1$ all parasites are drawn towards the macrophages at the test side. The reverse of this is if $\chi = 0$, the stimulus is repelling the parasites and are all positioned in the control channel. A null result, where they are neither attracted of repelled would result in $\chi = 0.5$. Figure 7.2.2b shows the index of chemokinesis and how it varies at different distances from the initial insertion well. The grey line at $\chi = 0.5$ marks the position corresponding to a null result. The majority of results are between $0.5 < \chi \leq 1$ proving there is some attraction towards macrophages. This is with the exception of 12 mm distance for procyclic parasites where the majority are being repelled, suggesting metacyclics may be more attracted than procyclics.

The data has also been broken down into boxplots to display variation in the experiments without making assumptions of statistical distribution (Fig 7.2.2c-f). The larger boxes in the metacyclic data suggest the variation between experiments is higher. This is a result of noise: the metacyclics are thinner, smaller cells that are more difficult to see using 20× magnification. This may have resulted in higher cell counting errors and hence more variability. This data also allows us to observe that, as expected due to difference in swimming speed, the metacyclics are capable of swimming further 30 minutes.

This initial assay gives qualitative results suggesting there is a bias towards macrophages by both procyclic and metacyclic promastigotes. This result gives clear evidence and suggests it is worth pursuing further experimentation. There is obvious importance and relevance for this chemotaxis concept for metacyclic promastigotes as is could influence their ability to infect macrophages immediately after transmission. In order to prove this mechanism a more quantitative approach was needed and hence the development of the second assay.

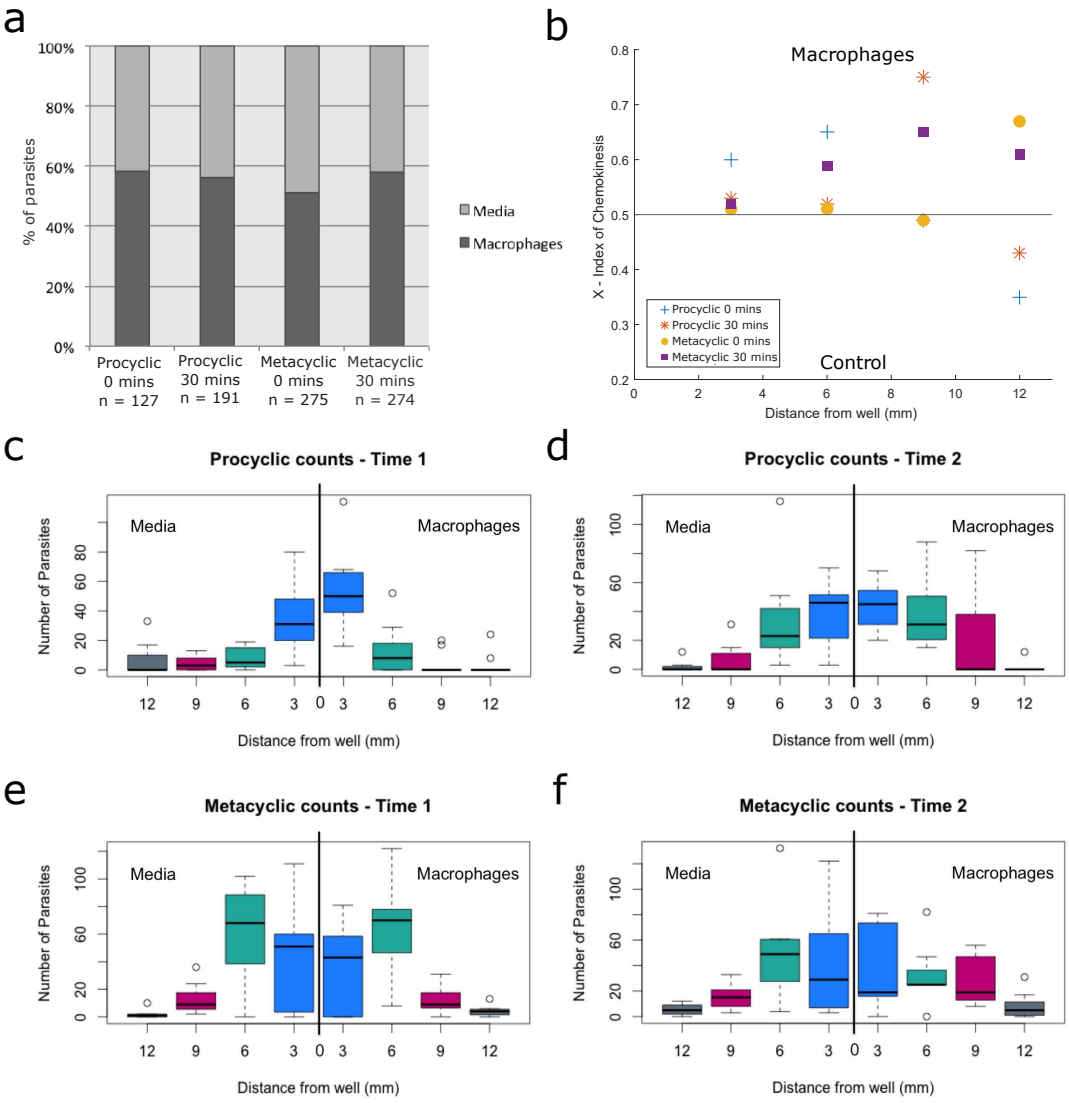

Figure 7.2.2: **a** Analysis of the percentage of parasites from all experiments in the test versus control channels. **b** Calculating the index of chemokinesis, where the line at 0.5 is the null hypothesis, showing that there is definite bias towards macrophages at all distances and time points analysed (with the exception of procyclics at the furthest distance). Panels **c-f** show boxplots detailing the variation in our experiments for procyclics (**c** - 0 mins, **d** - 30 mins) and metacyclics (**e** - 0 mins, **f** - 30 mins) at various distances along each channel. These results suggest their is a bias of promastigotes towards macrophages as a result of their motility, which is more exaggerated among metacyclic promastigotes.

7.3 3D Tracking Reveals Parasites' Kinematics in Reaction to Chemoattractants

This more in-depth approach aimed to understand how the parasites were changing their motility patterns when they were in the presence of a potential chemoattractants. The assay used DIHM (as described in chapter 4 and section 5.1.2) to track the cells in 3D and analyse their response to a gradient of potential chemotaxic substrates and controls. The experiment and subsequent analysis overcomes many of the drawbacks of previous studies mentioned giving us accurate quantitative information in addition to qualitative.

7.3.1 Methods

Cell Culture

Parasites and macrophages were cultured and prepared identically to the previous chemotaxis experiment. Details are described in section 7.2.1.

Establishing a Chemotaxic Gradient

Although caution must be used in direct comparisons of eukaryotic and prokaryotic behaviour, adaptation is a fundamental characteristic of taxic responses of bacterial cells [142]. This is the capacity of the cells to stop responding to a stimulus when it becomes constant, that is, when there is no variation in the concentration of the taxic agent or osmolarity of the medium. In order to avoid over-compensating for a transient stimulus, a cell's adaptation time scale is often much longer than the initial chemotaxic time scale. In bacteria, if the concentration of the attractant stops varying, adaption occurs within five minutes and their re-orientation frequency returns to the 'no stimulus' value of around one re-orientation per second, regardless of swimming direction. As long as the gradient persists, the bacteria will keep climbing it.

For this reason, it was important to establish and test chemotaxic gradients for our assay with *Leishmania* as it is possible they also exhibit adaptation. In order to establish this gradient the putative chemoattractant was dissolved in a 1% agar solution. While still liquid, 10μl of the solution was drawn into a 10 μl pipette tip and allowed to set at room temperature. The tip containing the agar-chemoattractant solution was then inserted into custom-made chamber slides (section 5.1.2) already containing parasites in M199 and sealed with petroleum jelly.

To test the establishment of this gradient over time, fluorescein and fluorescence microscopy were used. Fluorescein is a fluorophore commonly used in microscopy and dye tracing. Its diffusion coefficient of 4.36×10^{-6} [146] is in similar range to those of many small-molecule signals such as cytokines [147], so we use it to visualise molecular diffusion from the agar-filled pipette tip. It has a maximum absoption of 494 nm and emission maximum of 512 nm. 10mM of fluorescein was dissolved into 1% agar and inserted into a pipette tip, prepared identically to the chemotaxis assay. Fluorescence microscopy images were then captured every 15 minutes to analyse the diffusion of the fluorophore from the tip over 60 minutes (Fig. 7.3.1a).

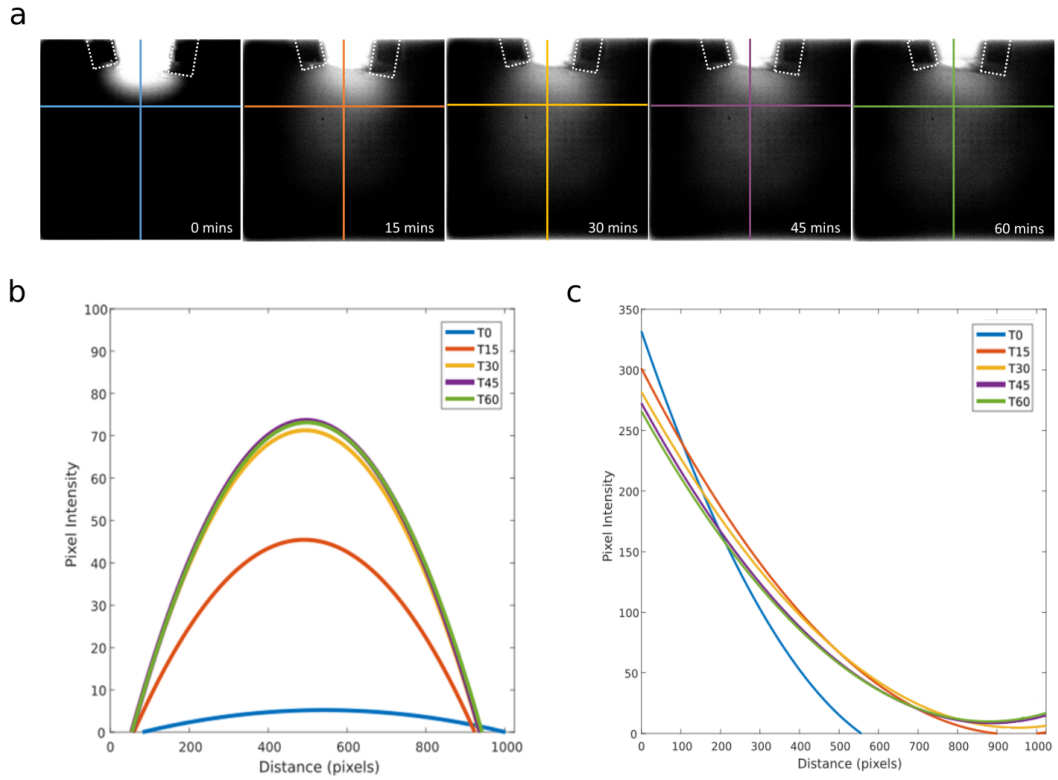

Figure 7.3.1: Testing the establishment of gradient using fluorescein-agar solution. **a** Fluorescent imaging captures the diffusion of fluorescein from the pipette tip over a 60 minute time frame. **b** Horizontal line profile and **c** vertical line profiles quantify the development of the gradient over time. Each colour corresponds to a particular time point as indicated and the line profile location is overlayed on the fluorescent images. The pixel intensity is higher in the horizontal centre and vertically closer to the tip, increasing with time and proving that the gradient and is sufficiently established by 30 minutes.

Analysing the vertical and horizontal pixel intensity of the images taken showed how the fluorescein diffused over time (a higher pixel intensity corresponding to a higher concentration of fluorescein) and confirmed the establishment of the gradient (Fig. 7.3.1b, c). The gradient was well established after approximately 30 minutes, hence this was the lag time allowed after the insertion of the tip into the sample chamber for the chemotaxis experiments.

Choosing Chemoattractants

Firstly, a negative control using 1% agar only was used in the tips. This was to check that the parasites did not react to the experimental setup differently to the M199-only results (section 5).

Fetal calf serum (FCS) was used as a positive control for this assay. Previous chemotaxis studies have shown possible chemoattractant effects of sugars with procyclic *Leishmania* [138, 139]. However, these experiments were never replicated with metacyclic promastigotes. The media used in previous experiments was washing and incubation solution (WIS buffer). We found the metacyclic promastigotes did not respond or swim in this media, potentially due to starvation. Hence, M199 media was used for this chemotaxis assay, with the additional advantage of allowing comparison with other results within this study. M199 was

supplemented with FCS, a liquid fraction of clotted blood that contains a large number of nutritional and macromolecular factors essential for cell growth. It also contains many other small molecules such as amino acids, lipids, hormones and, importantly, sugars in unknown quantities. Hence, setting up a well-controlled sugar gradient would have been difficult as the background sugar concentration in the media was unknown. Instead we used a higher concentration of 30% w/v FCS dissolved in 1% agar, to act as a positive control.

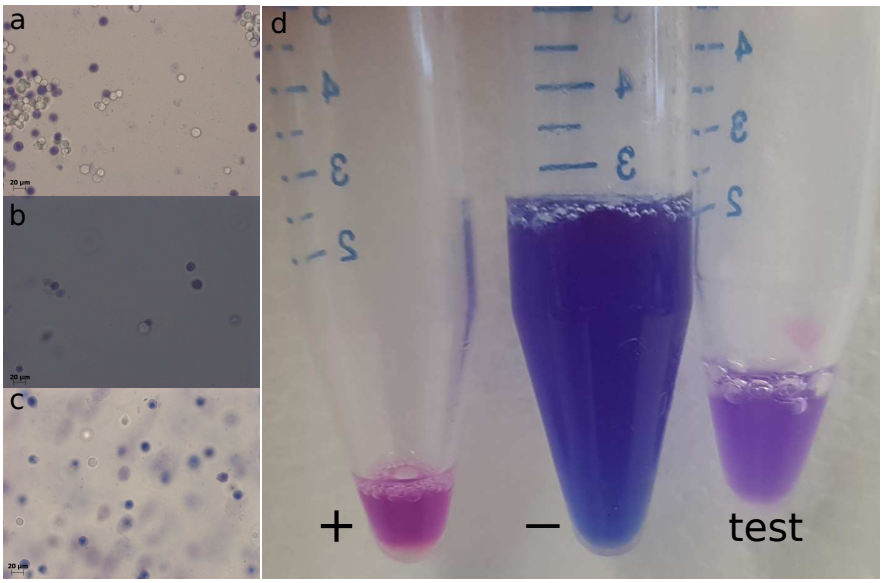

Figure 7.3.2: Using Trypan blue and alamarBlue we were able to test the viability of the macrophages in agar. **a** Trypan blue positive control, *i.e.* macrophages with no agar showing only a fraction of the cells are alive before in agar. **b** Trypan blue negative control, *i.e.* macrophages were fixed with PFA to show how the dye reacts to dead cells. **c** Trypan blue test with macrophages in agar. A significant proportion of the macrophages are still alive and the results comparable to the positive control in **a**. **d** Qualitative results from the alamarBlue tests with the same controls as the Trypan blue in **a, b, c**. The colour change of alamarBlue in the test condition was ample to prove a fraction of macrophages were still capable of breaking down the dye, hence healthy within agar.

The main test targets of this assay were the macrophages due to their implications with infection within the mammalian host. J774.2 macrophages were used due to ethical considerations and for increased speed and efficiency to optimise this assay. 1×10^6 cells were added to 1% agar and pipetted into tips. These macrophages were cultured in DMEM until they adhered to the cell culture plate. The excess DMEM media was removed by pipetting off the plate before scraping the cells resulting in the high concentrations used without the interference of any additives that are in the media. They were then resuspended in agar. In order to check the agar did not effect the viability of the macrophages Trypan blue and alamarBlue were used. Trypan blue is a dye exclusion test to determine the viability of cells present in a cell suspension. It is based on the principle that live cells possess an intact membrane that exclude the dye, whereas dead cells do not [148]. Trypan blue gave us an idea of the fraction of live vs dead cells but no further information on if the cells are reacting normally within the agar. AlamarBlue is a proven cell viability indicator that uses the natural reducing power of living cells to convert resazurin to the fluorescent molecule, resorufin. The active ingredient of alamarBlue (resazurin) is a nontoxic, cell permeable compound that

is blue in colour and virtually nonfluorescent. Upon entering cells, resazurin is reduced to resorufin, which produces very bright red fluorescence. Viable cells continuously convert resazurin to resorufin, thereby generating a measure of viability. Figure 7.3.2a-c (Trypan blue test) show that there is a fraction of live cells in the initial solution and figure 7.3.2d (alamarBlue test) shows that there is a fraction of viable, healthy cells when the macrophages are within agar. This qualitative result confirmed that there were enough viable cells to continue with the chemotaxis assay using macrophages.

Assay Setup and Cell Tracking (DIHM)

To DIHM assay was set up as follows. Pipette tips containing 10 μl of test substrate in 1% agar were made and allowed to set at room temperature. The majority of this task was carried out in a 50°C water bath to ensure the agar was kept liquid allowing easy pipetting.

Approximately 300 μl of a suspension of parasites in M199, at a concentration of 5×10^4 cells/ml, were added to sealed custom-made chamber slides prepared as previously described (section 5.1.1).The pipette tip containing chemoattractant-agar solution was added before sealing one end. The chambers were then kept lying flat in a 26°C incubator for 30 minutes to allow the gradient to form. Note that if any air bubbles formed within the slides at any time these were discarded because the bubbles were observed to cause unpredictable convective flows within samples.

The slides were then imaged using DIHM (as described in section 5.1.2). Two videos were captured as far from the source as possible, at the opposite end of the sample chamber to the tip (described from here on as 'away'). Then five videos were captured at the tip (but excluding the tip to remove unwanted light-scattering) before taking another three videos at the 'away' distance. As there should be no chemoattractant at the 'away' distance, these measurements constitute an additional control and help detect distance at which effects occur.

Analysis Methods

The speed, curvature and motile fraction analysis was performed as described in chapter 5. In addition to the previously used analysis methods, further analysis was needed to determine whether taxis was occurring in our experiments.

We began the analysis with a quantitative analysis of 'run and tumble' swimming mechanism previously observed in metacyclic promastigotes (chapter 5). In-house LabVIEW code was used to locate 'tumbles' within the swimming trajectories (as marked on Fig. 7.3.3). A tumble is characterised as a change in direction and a reduction of speed. When both these events occur at the same time in one location along the track it was given a higher score corresponding to its higher likelihood of being a tumbling event. Individual tracks were analysed to determine the accurate threshold score to pick up each tumble. We then calculated the change of direction resulting from each detected tumble. This was found by computing the angle between two vectors from a delay window of 0.5 seconds at either side of the tumble. This delay parameter was used as it appeared to be far enough away to give accurate measurement of the change in direction without another tumble occurring within that distance. The duration of the time in

between tumbling events, or 'runs', were also calculated. Bacteria such as *E. coli* are known to modify their run duration in the presence of a chemical stimulus; we examined whether *Leishmania* do the same.

We also examined the overall direction of the parasites we tracked, using in-house LabVIEW programmes. The 1.44×1.44 mm^2 field of view was split into a 10×10 grid using a standard binning arrangement. The tracks were smoothed (please see section 5.1.2 for more information on spline smoothing) using a slightly stiffer balance parameter (0.7) to eliminate slight fluctuations in direction. The average unit tangent vector was calculated for the segment of each trajectory while it passed inside a particular bin. The direction vector of all the cells within each bin were then averaged giving a single direction vector for each bin (displayed on the figures 7.3.12, 7.3.14 and 7.3.16).

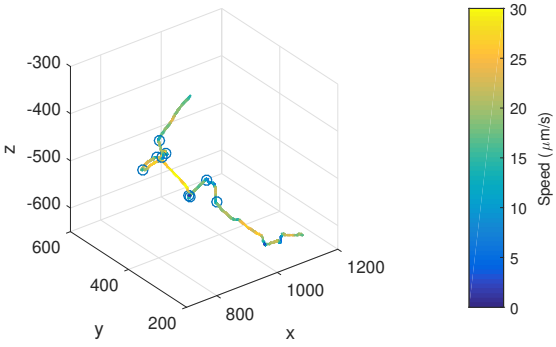

Figure 7.3.3: Metacyclic track with its distinctive 'run and tumble' swimming path. The colourbar represents instantaneous speed along the trajectory. This is used along with change in direction to calculate the probability of a 'tumble', nine of which were found for this trajectory and are marked with blue circles. The angle of each tumble and the duration between each were calculated for analysis.

7.3.2 Results

In line with previous experiments we first analysed the average speed of the *L. mexicana* procyclic and metacyclic promastigotes in the defined experimental conditions. The histograms in figure 7.3.4 allow comparison to be made between the two locations, 'tip' and 'away', and include log-normal fits to each data set. The speed of procyclic promastigotes is constant, regardless of the conditions and proximity to potential attractant tested, with an average similar to the M199 media control (Chapter 5, Fig. 5.2.2a) of 12-14 μms^{-1}. The speed of the metacyclic promastigotes in our negative control and the other conditions is on average slower than that in M199. The average speed for metacyclics in media was 31 μms^{-1} whereas in these experiments it ranged from 12-17 μms^{-1}, the higher end of which
was observed in our macrophage chemotaxis assays. There is also a noticable decrease in speed at the tip compared to the 'away' results in the FCS and macrophage assays, which is not observed in the agar control. This distinction is more prevalent for one of the three replicates tested in the macrophage assay (Fig. 7.3.5). Sample one has a higher number of cells swimming at slower rate than sample two and three. We ascribe these discepancies to biological variation. Sample one was therefore treated as an outlier, this is not due to it being unimportant - the lack of motility suggests chemokinesis instead of chemotaxis and this will be considered in following sections. As these cells were experiencing reduced speed and motility the displacement, and hence length of tracks, was decreased. Therefore these cells produced limited amount of data which could not be analysed further using our mathematical framework (run and tumble anal-

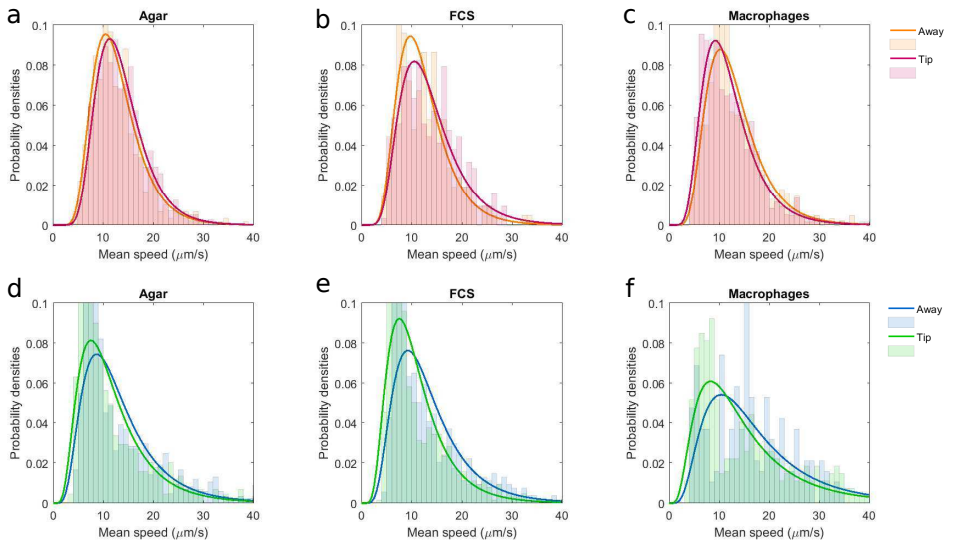

Figure 7.3.4: Histograms show the average swimming speed of procyclic (**a-c**) and metacyclic (**d-f**) in the three different chemotaxis experiments executed (agar - **a, d**, FCS - **b, e** and macrophages - **c, f**). To allow comparison between tracks at the 'away' position (orange/blue) and 'tip' position (red/green), both are shown on the same graph along with the log-normal fit for each. The only data showing a noticable difference the results shown in **e** and **f**. These graphs show the average speed of the metacyclics at the tip is reduced in comparison to the 'away' position.

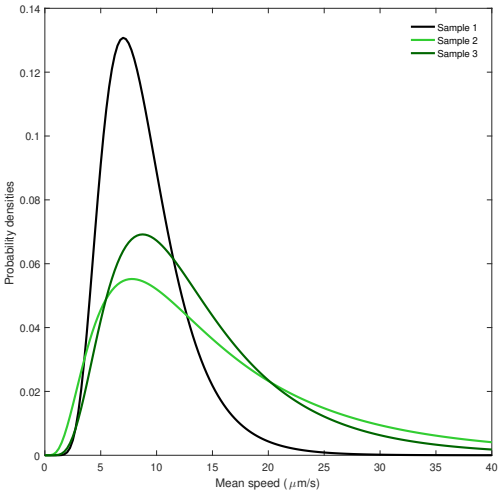

Figure 7.3.5: Graph shows the log-normal fits of corresponding speed data for the three different replicates of the experiments tracking metacyclic promastigotes in potential macrophage chemical gradients. Sample 1 has a significantly different probability distribution than samples 2 and 3.

ysis). Henceforth, this replicate was removed from further analysis but was not regarded as unimportant.

In addition to speed, the other main distinction in the swimming behaviours between procyclic and metacyclic promastigotes is in the curvature of the trajectories. Procyclic promastigotes have a helical swimming pattern, hence higher curvature, in comparison to metacyclics in M199 media alone (Fig. 5.2.2b, e). We also calculated curvature for the 3D trajectories in our chemotaxis assays to determine whether the chemical stimulus has an affect on this aspect of the parasites motility. The histograms in figure 7.3.6 show there is no change in procyclic promastigote curvature in any condition tested and resemble results of M199 (Fig. 5.2.2b). However, the curvature of the metacyclic trajectories is different to that previously observed in M199 media (Fig. 5.2.2e), a result which is seen in all our conditions. This considerable difference is unexpected in the negative control. However, it could be a result of very small convection currents within our setup.

The plastic tip inserted into the sample conducts heat differently to the media surrounding it, causing small convection to occur. Our results indicate that the convection currents affect the metacyclic cells more than procyclic cells because our agar control results match those in M199. Perhaps this is due to morphological differences or because the procyclics are more capable of controlling their motility better in different flow conditions. This is biologically relevant as the procyclic stage experiences higher fluid flows in the midgut of the sandfly. These currents could also explain the metacyclics slower speed within this experimental setup (Fig. 7.3.4d); the increased flow preventing the metacyclic promastigotes from reaching their highest speed. Instead of comparison to the data in M199, our agar control gives a better comparison as the convection will be consistent throughout all conditions, proven by the repeatability of the agar-fluorescein tests. There is still a higher number of metacyclic cells which exhibit higher curvature in comparison to the agar negative control (Fig. 7.3.7). There are three non-exclusive possibilities that could cause this increase; higher tumble angles, more frequent tumbles, and/or more curved runs.

To address the first possibility, the histograms in figure 7.3.8 show the different angles between 0-180 degrees exhibited during the tumble events found in metacyclic trajectories. This analysis is only executed for the metacyclic parasites, because the procyclic cells do not appear to exhibit 'run and tumble' motility. In M199 we observe broad range of tumble angles, the average tumble angle is 72 degrees with a slight skew towards more acute angles hence the peak at around 30 degrees. This does not appear to change in most of different conditions tested to analyse chemotaxis. However, figure 7.3.8d shows a higher number of cells exhibit smaller tumble angles further away from the macrophages potentially correcting their trajectory in smaller increments. However, this suggests the trajectories are mainly straighter and the higher curvature observed in metacyclics is not due to the angle of tumbles.

The second possibility which could explain higher curvature is a higher frequency of tumbles. Figure 7.3.9a, b show the number of tumbles analysed per distance (μm) and time (s) respectively. The results clearly show the cells undergo higher number of tumbling events in the 'away' location testing with FCS and macrophages. Combined with our data showing a smaller tumble angle at this location, this suggests the cells are capable of sensing the chemoattractant

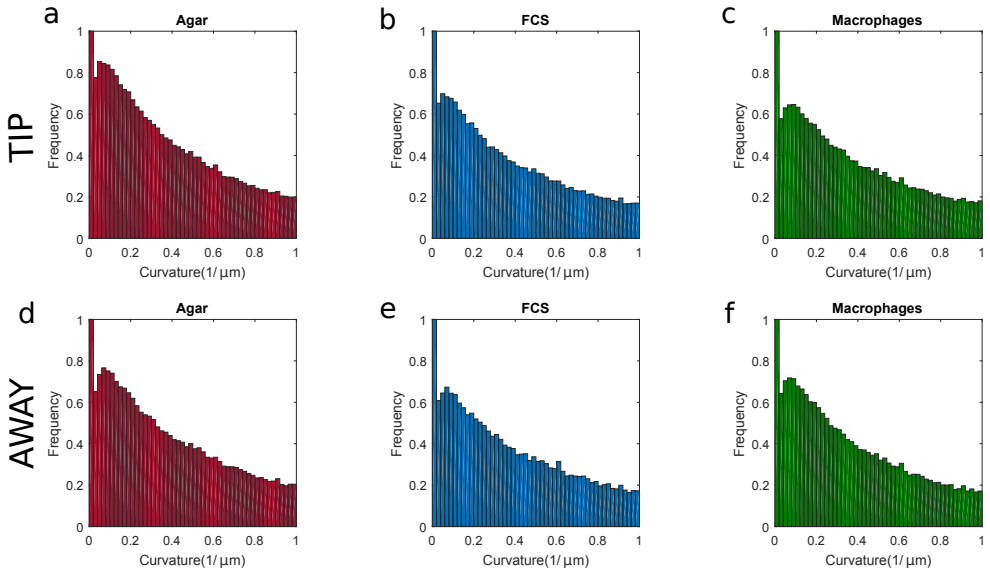

Figure 7.3.6: Curvature of procyclic promastigote cell trajectories when exposed to: agar (red histograms **a, d**), FCS (blue histograms **b, e**) and macrophages (green histograms **c, f**). Panels **a-c** are results from measurements close to the tip, and **d-f** show measurements far from the tip. Trajectory is unchanged for all the conditions we have tested.

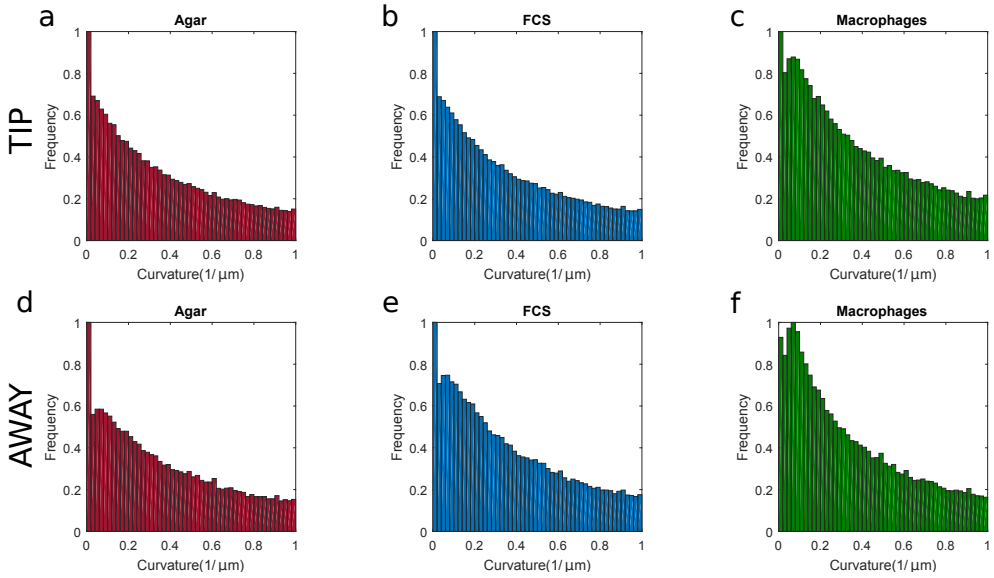

Figure 7.3.7: Curvature of metacyclic promastigote cell trajectories when exposed to: agar (red histograms **a, d**), FCS (blue histograms **b, e**) and macrophages (green histograms **c, f**). Panels **a-c** are results from measurements close to the tip, and **d-f** show measurements far from the tip. Metacyclics exhibit a higher curvature, particularly in **c**, when they are in close proximity to macrophages.

at this distance and are searching the environment, changing their direction incrementally and more frequently to move closer to the attractant. Once they reach the attractant the number of tumbles decreases. This is reminiscent of mechanisms bacteria use during chemotaxis [149]. As the frequency of tumbles is reduced nearer the attractant and the angle is unchanged, by elimination, this leaves the higher curvature to be a result of increased overall curvature during the 'runs' in between the tumbles.

We are also able to analyse the duration of 'runs' which are delimited by two distinct tumbling events. An example is shown in figure 7.3.10a which gives the distribution of runs for metacyclic promastigotes in control conditions, without stimulus. We find two exponential regimes, denoted by lines of best fit (non-linear least squares regressions over each domain). This phenomenon is only observed in the M199 experiment data and is not as obviously prevalent in the chemotaxis results.

We investigated the reorientation events in more detail in figure 7.3.11, which is a histogram relating the run duration to the subsequent tumble event. We observe two distinct populations: the first where small angle tumbles are most often associated with long runs. This is shown by the broad maximum in the bottom right of the figure peaking around 5 seconds/45 degrees. The second population correlates short runs punctuated by tumbles of more widely varying angle; this is represented by the tall, narrow region peaking at around 0.3 seconds, but extending up to 150 degrees.

In line with our initial chemotaxis experiments (section 7.2) we also analyse the overall direction of the promastigotes in these distinct conditions. Dividing the 1.44×1.44 mm^2 area into a 10×10 grid we examine local speed and direction within each region. Figure 7.3.12 combines a 'heatmap' of the local swimming speed and arrows representing the average swimming direction of all cells in the region. The speed and swimming direction of procyclic and metacyclic promastigotes in M199 media alone is isotropic. The unbiased direction highlighted by rearranging the arrows to a central origin in a compass plot (Fig. 7.3.13).

Interestingly, analysing overall direction of the procyclic parasites in agar, FCS and macrophages shows a clear bias of swimming towards the tip when macrophages are present in agar (Fig. 7.3.14c, 7.3.15c). Some bias is also seen in the agar and FCS but these results are not as exaggerated as with macrophages. This suggests the procyclics are capable of sensing chemical gradients even though they do not use the same 'run and tumble' mechanisms as metacyclics.

Similarly, the metacyclics show the same directional bias to macrophages (Fig. 7.3.16c, 7.3.17c). The metacyclics in other conditions tested appear to be swimming aimlessly, including in all the 'away' locations where tumbling is more frequent. This implies the cells are tumbling in all directions in the absense of a chemical stimulus, refining their trajectories as they get closer to the macrophage stimulus.

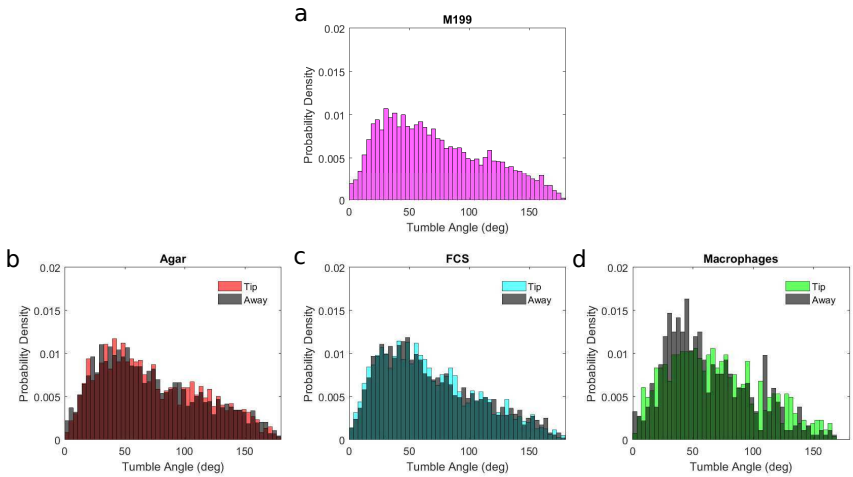

Figure 7.3.8: Tumble angles exhibited by metacyclic promastigotes in **a** M199, **b** agar, **c** FCS and **d** macrophages. The away position data in conditions **b-d** are shown in grey. The uncertainty represents standard deviation between replicates. The angles can range from 0-180 degrees, with a mean around 70 degrees and the higher peak shows a bias towards smaller angles. There are no distinct differences in the angle of the tumbles for most of the potential chemoattractants tested. More cells exhibit smaller angles further from macrophages.

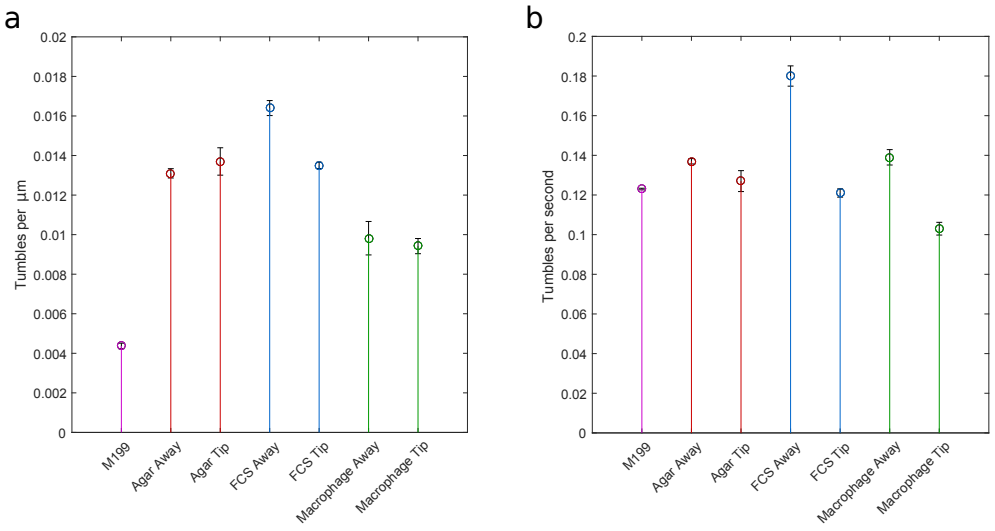

Figure 7.3.9: Number of metacyclic tumbles detected in all conditions tested. **a** Number of tumbles per unit distance travelled ($1/\mu$m) and **b** Number of tumbles per second. As the metacyclic promastigotes swim closer to FCS and macrophages the number of tumbles is decreased. We also observe higher frequency of tumbles at the furthest distance from the chemoattractant compared to both M199 and agar controls.

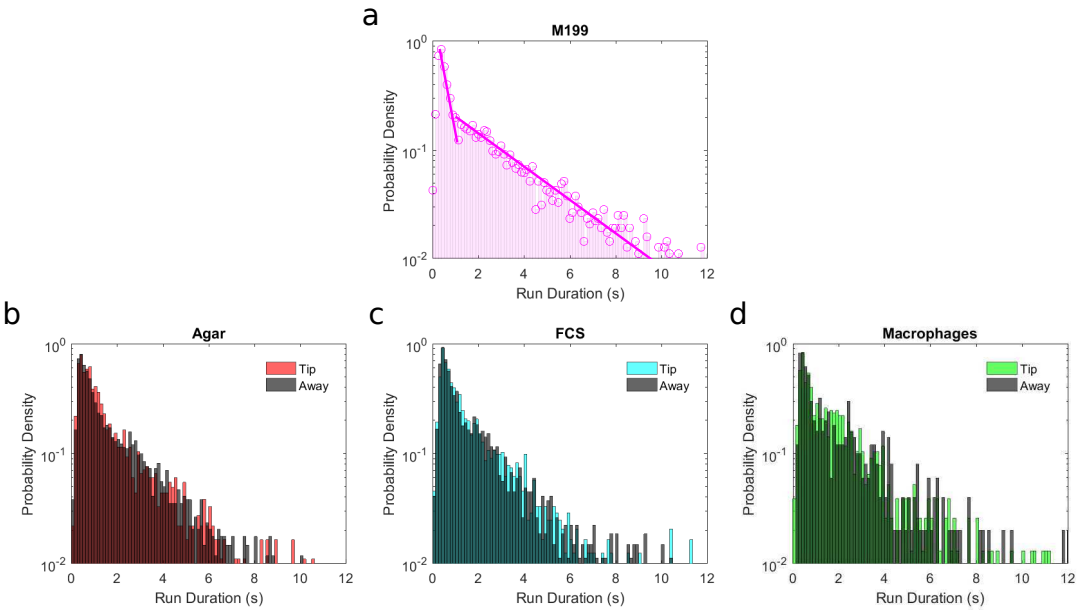

Figure 7.3.10: Distribution of metacyclic run durations in M199 media (**a**), and in the presence of agar-filled tip (**b**), FCS (**c**), and macrophages (**d**).The away position data in conditions (**b-d**) are shown in grey. Although these figures only show up to 12 second run duration, occasional runs of durations up to or beyond 25 seconds are observed. In M199 we observe two exponential regimes, indicated by lines of best fit for each domain, which are unambiguously assignable in other histograms.

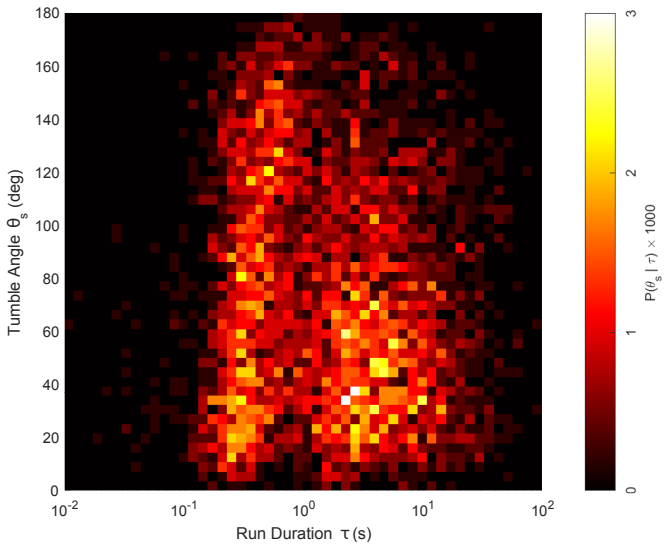

Figure 7.3.11: Histogram relating metacyclic run duration to subsequent tumble angle. The colourbar represents the probability of the corresponding run duration and tumble angle. We observe two distinct populations of cells. In the population to the left we see short runs are followed by a more varied degree of tumble. Whereas the cells in the population to right exhibit small angles after long runs.

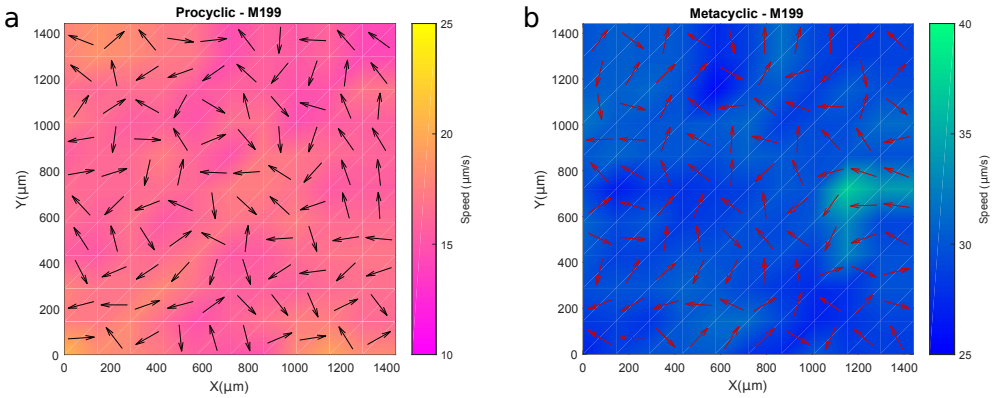

Figure 7.3.12: Average direction within 1.44×1.44 mm^2 region of **a** procyclic and **b** metacyclic promastigotes in M199 media. The heatmap in the background represents local swimming speed and the arrows in the quiver plot show the average direction in that region. Although the metacyclics swim faster than procyclics (hence the different colourbars) the direction in these control measurements are isotropic.

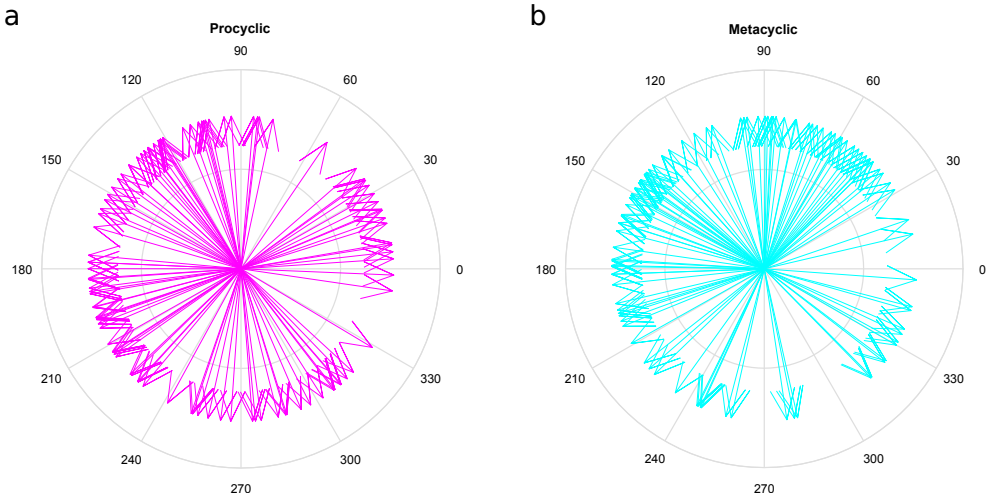

Figure 7.3.13: These compass plots rearrange the arrows from the quiver plot in figure 7.3.12 to start from the origin, to show any directional bias more clearly. Both **a** procyclic and **b** metacyclic data is uniform in all directions in M199 media alone.

7.4 Conclusions

To allow a clearer description of taxis in *Leishmania* promastigotes we established new methods and analysis possible due to our unique experimental approach which advances previous studies. Firstly, the assay distinguishes between verified, molecularly distinct procyclic and metacyclic promastigotes. This is important to contextualise behaviour within different physiological and environmental conditions during the lifecycle. DIHM is high throughput and gives a large amount of information in three-dimensions. The hundreds of cells analysed per experiment gives us a more complete insight into the motility of a large population of parasites. In addition, the reliable duplication and the 3D nature establishes new methods of analysis for *Leishmania* chemotaxis. We are able to analyse the instantaneous and average velocity of individual cells and hence the total population. This allows us to determine whether chemokinesis is involved; a mechanism which affects speed and cannot be determined through the qualitative

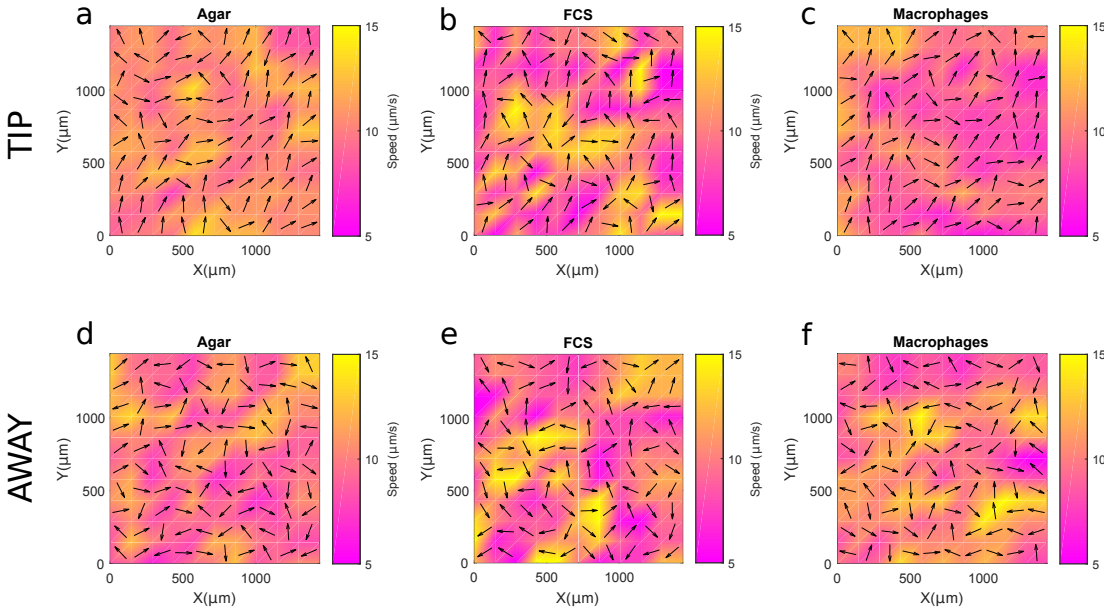

Figure 7.3.14: Average direction within 1.44×1.44 mm^2 region of procyclic cells located towards the tip (**a-c**) and away from the tip (**d-f**). The heatmap in the background represents local swimming speed and the arrows in the quiver plot show the average direction in that region for different conditions in agar (**a, d**), FCS (**b, e**) and macrophages (**c, f**).

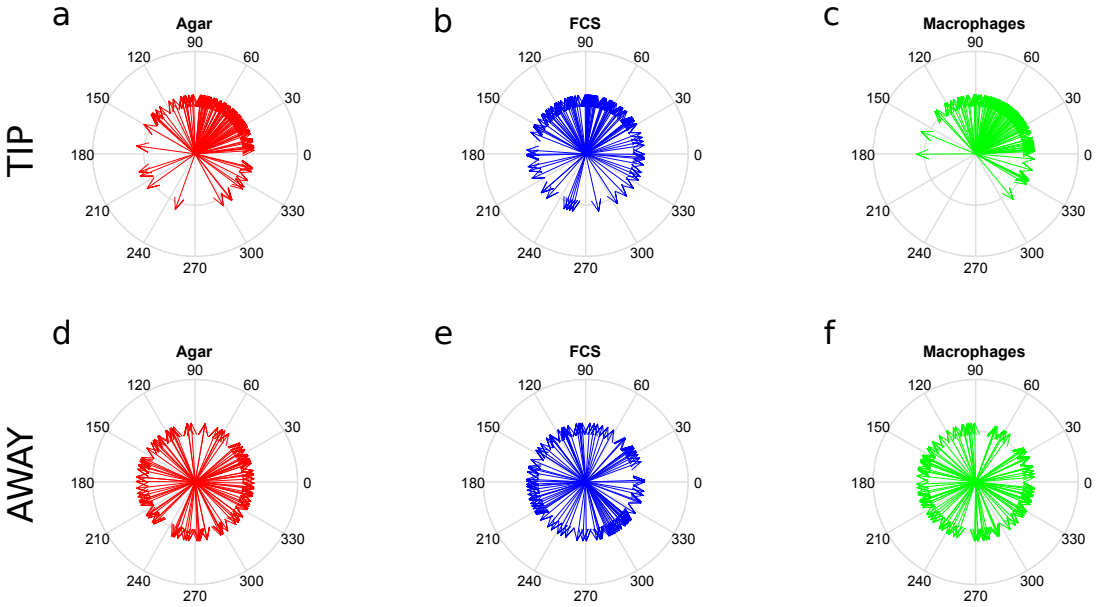

Figure 7.3.15: Procyclic compass plots in agar (**a, d**), FCS (**b, e**) and macrophages (**c, f**) at both tip (**a-c**) and away from the tip (**d-f**). There is a bias at the tip location towards the chemoattractant source. This is clearly more exaggerated in **c** where most cells are swimming towards the tip containing agar and macrophages.

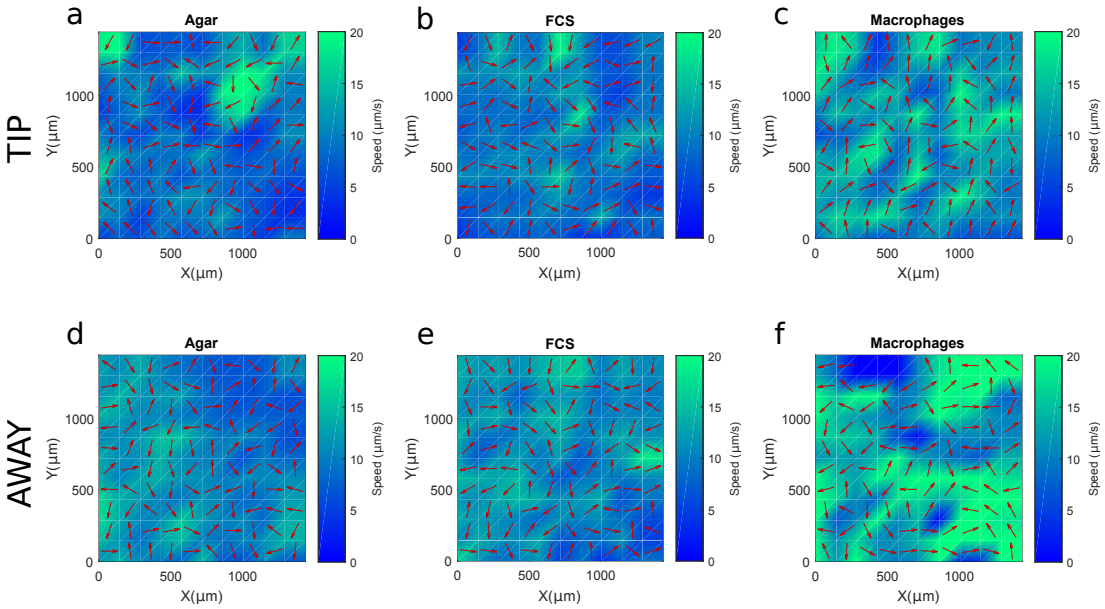

Figure 7.3.16: Average direction within 1.44×1.44 mm^2 region of metacyclic cells located towards the tip (**a-c**) and away from the tip (**d-f**). The heatmap in the background represents local swimming speed and the arrows in the quiver plot show the average direction in that region for different conditions in agar (**a, d**), FCS (**b, e**) and macrophages (**c, f**).

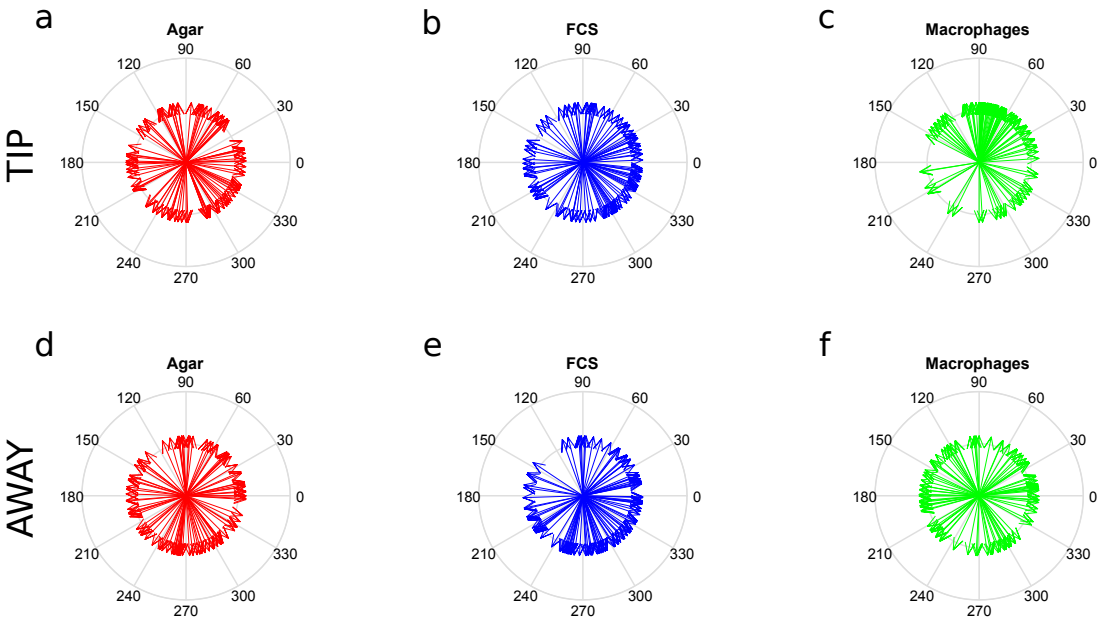

Figure 7.3.17: Metacyclic compass plots in agar (**a, d**), FCS (**b, e**) and macrophages (**c, f**) at both tip (**a-c**) and away from the tip (**d-f**). The only figure which shows some bias is **c** where there are more cells swimming towards the tip containing agar and macrophages.

experiments in previous studies. The tracking also gave insight into the direction of the cells' swimming to determine whether they are swimming towards, or away from, potential chemoattractants. The orientation of the cells' swimming paths was not considered in previous studies but is important to confirm taxis.

Overall, our experiments suggest taxic behaviour is present in both *L. mexicana* procyclic and metacyclic cells. The procyclics show a directional bias towards all solute gradients which is more pronounced towards macrophages. This is in line with previous studies testing chemotaxis with promastigote populations [139]. Our results indicate that promastigotes exhibit a non-specific attraction towards any of the substances tested, suggesting the cells are undergoing osmotaxis as apposed to chemotaxis. We were unable to determine precise motility mechanisms used by the procyclic cells to achieve taxic behaviour. However, this information is potentially within our data and additional aspects of the swimming patterns could reveal significant mechanistic insight as the analysis is further developed in the future.

No previous study has tested a purified population of metacyclic promastigotes in response to solute gradients. Our unique high-throughput methods produced large volumes of three-dimensional swimming trajectories. Our in-depth analysis of these trajectories suggest *L. mexicana* metacyclic cells have a chemotaxic bias towards J774.2 macrophages and use a 'run and tumble' motility method to achieve this. Analysing the swimming patterns at two locations ('away' and 'tip') allowed us to observe how their behaviour changes at different distances from potential attractants. At the 'away' position the metacyclic cells exhibit high speed swimming involving higher frequency of small degree tumbles in equally random directions suggesting a 'searching' phenotype. Once the cells reach the 'tip' location, the frequency of tumbles and swimming speed is reduced, and they are predominantly swimming in the same direction towards the attractant chemicals emitted by the macrophages. The reduced swimming speed also suggests chemokinesis, an outcome that could not have been previously considered without our improved method and in-depth analysis. The observed deceleration of the metacyclics in response to stimuli from macrophages promotes these cells to remain in close proximity to macrophages while saving energy and increasing likelihood of macrophage phagocytosis.

As discussed this 'run and tumble' behaviour is reminiscent of swimming patterns observed in bacteria [117]. In the absense of a stimulus, *E. coli* bacteria tumble every 1-10 s depending on strain and growth phase [150]. This pattern is altered in the presence of chemoattractants or chemorepellents. Increased attractant gradient reduces the probability of tumbling and decreasing attractant gradient increases tumbling [149]. This property ensures that during positive chemotaxis, runs towards stimuli are longer, while runs away are shorter. The random walk thus takes the bacteria towards attractants or away from repellents. These bacteria are able to measure gradients by measuring concentration differences relative to current and past chemical environments. Comparitively, our results suggest that these eukaryotic *Leishmania* promastigotes sense their environment and use a pattern similar to bacteria to achieve locomotion towards positive stimuli and a more beneficial environment.

The capability of cells to perform chemotaxis has clear implications for the infection of macrophages by the mammalian infective parasites. This work would

benefit from testing with activated mammalian macrophages which would provide a more biologically relevant result. Studies suggest the metacyclic promastigotes intially invade neutrophils [133]. Therefore, it would also be of interest to test whether a similar phenomenon is observed with neutrophils. In addition to this it may be advantageous to explore how a higher temperature, closer to body temperature, would impact observed results.

Chapter 8

Conclusions and Outlook

In this final chapter, I summarise the main findings of my experiments, and suggest some interesting possibilities for future work.

8.1 Conclusions and their Impact

The work in this thesis describes the use of a three-dimensional imaging technique to track the motility of *Leishmania mexicana* promastigote parasites of specific lifecycle stages. Digital holographic microscopy has the unique ability to record quantitative three-dimensional position data at high speeds. Within this thesis I have demonstrated that these cells swim in a 3D landscape, however the 3D trajectories of *Leishmania* species have not been analysed previously. This additional dimension revealed distinct swimming parameters that cannot be measured accurately with two-dimensional data. Using this technique, this study analyses the position of the motile promastigote forms under various biologically-relevant conditions to reveal information about how these cells utilise motility throughout their lifecycle.

In chapter 5 we described methods used to track and analyse distinct-molecularly validated populations of procyclic and metacyclic cells in M199 culture media. These two lifecycle stages have obvious morphological differences and have very different environments and survival strategies. Importantly, of these promastigote stages they have different swimming patterns. This section aimed to test this hypothesis and quantitatively characterise any distinctions. Our data showed that there are clear, quanitifiable differences between the procyclic and metacyclic promastigotes motility. The procyclics swim at moderate speed in a helical, corkscrew-like motion, whereas the metacyclics swim faster and straighter. This rapid, more direct method of motility potentially promotes metacyclic transmission, which is biologically irrelevant for the procyclics. It would be interesting to test whether these swimming patterns are observed *in vivo*. Although our analysis is optimised for *in vitro* conditions, these are controlled for both lifecycle stages. Hence, differentiation during metacyclogenesis not only alters *Leishmania* parasite morphology, but also the means by which they execute motility.

In order to understand precisely which proteins cause different motility in *Leishmania* it would be advantageous to begin characterising motility mutants. This study set this in motion by analysing a BBS9 knock out. Not only did this confirm that a mutation of this subunit of the BBSome impacts parasite

swimming capacity, it also confirmed our method is sensitive enough to detect motility mutants. Until more is known about the specific function of BBS9, it is difficult to draw a more specific conclusion from this data other than that this gene knockout causes a severe motility defect.

The data from optimised motility experiments in complete M199 media was then used as comparison to decipher how motility changes in different environments. The first of the environments, tested in chapter 6, has relevance to transmission through the promastigote secretory gel plug in the sandfly. 86-98% of the promastigotes egested into the skin are the mammalian-infective metcyclic promastigotes [27]. This suggests that the metacyclics are more capable of remaining motile and swimming through this highly viscous solution than other promastigote stages. Due to high variability and limited quantity of PSG we initially tested the effects of viscosity on procyclic and metacyclic promastigotes using Ficoll and PVP polymers of different molecular weights dissolved in M199. Using these polymers allowed us to control the viscosity to reveal how viscous and elastic forces effected the promastigotes' swimming in comparison to M199 only data (see Chapter 5). Quantifying the speed and motile fraction concluded that the metacyclic promastigotes were inhibited less by the viscosity of these two polymers and implies they are more capable of swimming in higher viscosities than procyclic promastigotes.

Although these provisional results using polymers complement our hypothesis, the same was not observed on testing in PSG. The speed and motile fraction of procyclic cells was unaffected whereas both relative speed and motility were reduced in the metacyclic experiments. Despite no biological relevance of PSG, we would still expect to see some inhibitory affects upon procyclic motility in response to higher viscosity, such as seen in polymer tests. This study would clearly benefit from additional information regarding the structure and physical properties of PSG, including viscosity, in order to make accurate comparisons to Ficoll and PVP. As such a molecular investigation into PSG components is beyond the scope of this investigation we can only discuss potential implications of our results. As we have characterised the effects of viscosity on the motility of promastigotes and have not observed comparable results in PSG, our data would suggest that it is not only viscosity impacting the motility of promastigotes in PSG. Further testing, discussed in the next section on future work, is needed to draw precise conclusions on how the cells motility impacts transmission.

Although no study has yet to verify the relationship between *Leishmania* motility and transmission, we did discover some intriguing results regarding motility in lifecycle stages associated with early infection in the mammalian host. In chapter 7, we used our optimised DIHM imaging techniques along with additional analytical framework to test for chemotaxic bias towards leukocytes. We previously observed potential 'run and tumble' methods used by metacyclics in chapter 5. By analysing parameters of this run and tumble swimming pattern we revealed that, similar to bacteria, metacyclic promastigotes use this type of random walk to relocate themselves closer to macrophages (J774.2). By tracking the cells at two distances from any chemoattractant emitted from these macrophages we discovered at the furthest distance the cells swim rapidly exhibiting a high frequency of tumbles. This is reminiscent of a 'searching' phenotype. Once the cells reach a closer proximity to the chemoattractant, their speed and number of

tumbles is reduced. Additionally, there was a clear bias in the overall direction of motility: the cells close to the chemoattractant swim towards it whereas there was no distinct direction further from the chemoattractant. This suggests the cells can remain in the vicinity of macrophages while saving energy and increasing their chances of being engulfed by macrophages which is essential for survival and lifecycle progression in the host. Although these results are not validated *in vivo*, this has clear consequences for infection and indicates a chemotaxic response to environmental stimuli can alter swimming behaviour.

Overall, this work gives the field of leishmaniasis research a well-suited, accurate method to analyse the motility of *Leishmania* promastigotes, a previously neglected study of a clearly important mechanism. The results can be related to relevant situations that the parasites experience throughout their lifecycle, informing potential future treatments and therapeutics.

8.2 Future Work

A number of possibilities exist for the extension and improvement of the work described in this document. Intially, the 3D data from post-processing DIHM images is in abundance of information, some of which was not analysed due to the limited time available for this study. For example, implementing fourier analysis, to generate the average power spectrum, could reveal principal frequency components conserved in specific lifecycle stages. These components could inform us about the beating of the flagellum and the rotation of the cell body ('beat plane') about the swimming direction and hence explain physics governing these parameters. Further analysis could reveal additional swimming parameters and properties giving us a greater understanding of parasite motility and also alternative distinguishing features and functional implications of swimming behaviour.

Our tracking of parasites in PSG indicates that physical properties of the gel do not strongly influence motility and alternative mechanisms such as a receptor-mediated process is more likely to impact swimming capabilities. Further testing with fPPG, the main component of PSG, would be useful. This component is easily extracted in media [28] and could provide a biologically-relevant comparison to observe effects without unknown factors in PSG. During transmission and upon feeding, blood and other factors are imbibed through a small channel in the PSG (unpublished work on observations by Dr. Matthew Rogers). This blood contains many factors and there are additional factors in the microenvironment of the sandfly (saliva, microbiota etc) which may be necessary to allow metacyclic promastigotes motility through PSG and hence be transmitted. Additionally, it would be useful to compare biologically-relevant lifecycle stages. This would require advancing culture techniques to acquire purified populations of leptomonads. Overall, key information is missing in order to define how motility promotes *Leishmania* transmission; the ultimate goal of this strand of research would be to impede its occurrence.

For our analysis of chemotaxis in *L. mexicana* promastigotes, it would be desirable to use the same assay to test gradients of specific factors emitted from macrophages (chemokines, cytokines etc.). This would provide precise information on parasite response to leukocyte factors and parasite:host dynamics. It

would also be advantageous to analyse the effects of other leukocytes. Recent research suggests neutrophils are important during early uptake of metacyclic promastigotes in the skin [133]. Testing with neutrophils as well as activated human macrophages could increase our understanding of the infection process substantially and could have serious implications for potential treatments. As most current developing treatments focus on eliminating the non-motile amastigote stages after infection is established, this could offer an alternative route of focus as a preventative control measure before infection is established.

This study analyses two of the main environmental conditions during processes where motility is involved during the parasites lifecycle. However, it could also be adapted to measure motility in multiple other relevant circumstances. An obvious and important condition would be temperature. All our experiments have been performed consistently at room temperature, however the parasite experiences a range of climates. Within the sandfly, *Leishmania* parasites will experience temperatures as low as 27°C, whereas once transmitted into the mammalian skin it experiences typical temperatures in the range of 34-37°C. Analysing these varied temperatures could potentially reveal interesting, heat-responsive features of motility in other biologically-relevant conditions and increase our understanding.

Regarding comparative, it would be useful to couple the 3D tracks with data regarding the oscillations of the flagellum during specific movements and/or in particular conditions. For example, how the flagella waveform is altered during a tumbling event, how it returns to a state of 'running' and whether this changes in the presence of chemoattractant. Reconstruction of the flagella in 3D using the same DIHM technique may also be possible. Using different settings and a higher magnifications this technique could reconstruct the shape of individual cells and reveal the 3D flagellar waveforms. Some of the issues with noise, due to the large cell body of *Leishmania*, have already begun to be overcome in the study by Farthing et al. (2017) [101]. Data from this thesis was used to advance the technique described in this article however due to lack of time to optimise and automate the procedures it was not included in this thesis.

All the work in this study and the future suggestions described are examined *in vitro* which has obvious drawbacks. DIHM is a long way from being used *in vivo* and significant advances would be required to reduce light-scattering from tissues and other features within the sandfly or mammalian host. However, technology is advancing rapidly and biophysics research is expanding so it may not be long before this technique could three-dimensionally track the position of *Leishmania* promastigotes in their natural hosts.

Appendix A

Torsion

Due to the three-dimensionality of our tracks we were also able to calculate the inherently 3D parameter torsion, *i.e.* the amount by which the curve is coming out of the plane which it lies. However, this quantity is not ideal for our purposes as it is difficult to interpret the result and relate biological meaning.

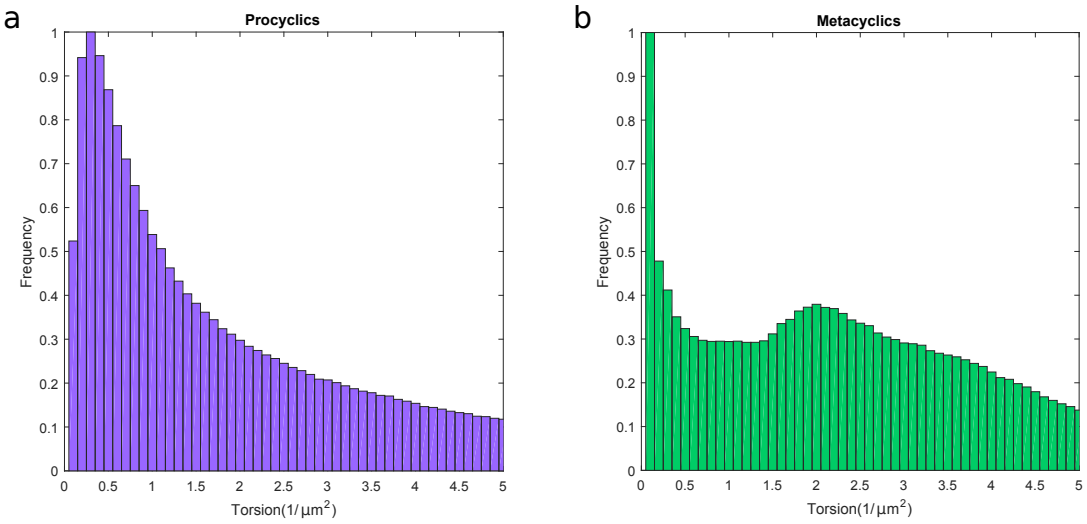

Figure A.0.1: Torsion histograms of **a** procyclic and **b** metacyclic promastigotes in M199. These graphs are included for reference however it is difficult to interpret any conclusions from this analysis therefore we calculated the helicity instead.

Bibliography

[1] G. Dawit. A Review on Biology, Epidemiology and Public Health Significance of Leishmaniasis. *Journal of Bacteriology & Parasitology*, 04:2–7, 2013.

[2] World Health Organization. Investing to overcome the global impact of neglected tropical diseases. *World Health Organization*, 2015.

[3] World Health Organization. Accelerating Work to Overcome the Global Impact of Neglected Tropical Diseases: A Roadmap for Implementation. *World Health Organization*, pages 1–42, 2012.

[4] World Health Organization. Control of the leishmaniases. *World Health Organization technical report series*, (949), 2010.

[5] F. Chappuis, S. Sundar, A. Hailu, H. Ghalib, S. Rijal, R. W. Peeling, J. Alvar, and M. Boelaert. Visceral leishmaniasis: what are the needs for diagnosis, treatment and control? *Nature reviews. Microbiology*, 5(11):873–82, 2007.

[6] P. Kaye and P. Scott. Leishmaniasis: complexity at the host-pathogen interface. *Nature reviews. Microbiology*, 9(8):604–615, 2011.

[7] P. A. Bates. Leishmania sand fly interaction: progress and challenges. *Current Opinion in Microbiology*, 11(4):340–344, 2008.

[8] M. H. Wakid and P. A. Bates. Flagellar attachment of Leishmania promastigotes to plastic film in vitro. *Experimental Parasitology*, 106(3-4):173–178, mar 2004.

[9] C. L. Forestier, C. MacHu, C. Loussert, P. Pescher, and G. F. Spath. Imaging host cell-leishmania interaction dynamics implicates parasite motility, lysosome recruitment, and host cell wounding in the infection process. *Cell Host and Microbe*, 9(4):319–330, 2011.

[10] S. Besteiro, R. A. M. Williams, G. H. Coombs, and J. C. Mottram. Protein turnover and differentiation in Leishmania. *International Journal for Parasitology*, 37(10):1063–1075, 2007.

[11] S. M. Landfear and M. Ignatushchenko. The flagellum and flagellar pocket of trypanosomatids. *Molecular and Biochemical Parasitology*, 115(1):1–17, jun 2001.

[12] A. P. R. Gadelha, N. L. Cunha-e Silva, and W. De Souza. Assembly of the Leishmania amazonensis flagellum during cell differentiation. *Journal of Structural Biology*, 184(2):280–292, nov 2013.

[13] E. Gluenz, M. L. Ginger, and P. G. McKean. Flagellum assembly and function during the Leishmania life cycle. *Current Opinion in Microbiology*, 13(4):473–479, 2010.

[14] T. D. Serafim, I. V. Coutinho-Abreu, F. Oliveira, C. Meneses, S. Kamhawi, and J. G. Valenzuela. Sequential blood meals promote Leishmania replication and reverse metacyclogenesis augmenting vector infectivity. *Nature Microbiology*, pages 1–8, mar 2018.

[15] K. J. Esch and C. A. Petersen. Transmission and epidemiology of zoonotic protozoal diseases of companion animals. *Clinical Microbiology Reviews*, 26(1):58–85, 2013.

[16] S. Kamhawi. Phlebotomine sand flies and Leishmania parasites: friends or foes? *Trends in Parasitology*, 22(9):439–445, 2006.

[17] P. A. Bates. Transmission of Leishmania metacyclic promastigotes by phlebotomine sand flies. *International Journal for Parasitology*, 37(10):1097–1106, 2007.

[18] M. E. Rogers. The role of Leishmania proteophosphoglycans in sand fly transmission and infection of the mammalian host. *Frontiers in Microbiology*, 3:1–13, 2012.

[19] D. M. Mosser and A. Brittingham. Leishmania, macrophages and complement: a tale of subversion and exploitation. *Parasitology*, 115:9–23, 1997.

[20] D. L. Sacks and P. V. Perkins. Development of infective stage Leishmania promastigotes within phlebotomine sand flies. *American Journal of Tropical Medicine and Hygiene*, 34(3):456–459, 1985.

[21] A. Dostálová and P. Volf. Leishmania development in sand flies: Parasite-vector interactions overview. *Parasites and Vectors*, 5(1):1, 2012.

[22] D. L. Sacks and P. V. Perkins. Identification of an infectove stage of Leishmania Promastigotes. *Science*, 223(4643):1417–9, 1984.

[23] D. L. Sacks, S. Hieny, and A. Sher. Identification of cell surface carbohydrate and antigenic changes between noninfective and infective developmental stages of Leishmania major promastigotes. *The Journal of Immunology*, 135(1):564–569, 1985.

[24] M. L. Cunningham. Regulation of Differentiation to the Infective Stage of the Protozoan Parasite Leishmania major by Tetrahydrobiopterin. *Science*, 292(5515):285–287, 2001.

[25] J. M. Ramalho-Ortigao, A. N. Pitaluga, E. L. Telleria, C. Marques, A. A. Souza, and Y. M. Traub-Cseko. Cloning and characterization of a V-ATPase

subunit C from the American visceral leishmaniasis vector Lutzomyia longipalpis modulated during development and blood ingestion. *Memorias do Instituto Oswaldo Cruz*, 102(4):509–515, 2007.

[26] P. Volf, M. Hajmova, J. Sadlova, and J. Votypka. Blocked stomodeal valve of the insect vector: Similar mechanism of transmission in two trypanosomatid models. *International Journal for Parasitology*, 34(11):1221–1227, 2004.

[27] M. E. Rogers, T. Ilg, A.V. Nikolaev, M. A. J. Ferguson, and P. A. Bates. Transmission of cutaneous leishmaniasis by sand flies is enhanced by regurgitation of fPPG. *Nature*, 430(6998):463–7, 2004.

[28] T. Ilg, Y. D. Stierhof, D. Craik, R. Simpson, E. Handman, and A. Bacic. Purification and structural characterization of a filamentous, mucin- like proteophosphoglycan secreted by Leishmania parasites. *Journal of Biological Chemistry*, 271(35):21583–21596, 1996.

[29] Y. D. Stierhof, P. A. Bates, R. L. Jacobson, M. E. Rogers, Y. Schlein, E. Handman, and T. Ilg. Filamentous proteophosphoglycan secreted by Leishmania promastigotes forms gel-like three-dimensional networks that obstruct the digestive tract of infected sandfly vectors. *European Journal of Cell Biology*, 78(10):675–689, 1999.

[30] P. G. Lawyer, P. M. Ngumbi, C. Anjili, S. Odongo, Y. B. Mebrahtu, J. I. Githure, K. Davy, and C. R. Roberts. Development of Leishmania Major in and Sergentomyja. *American Journal of Tropical Medicine and Hygiene*, 43(1):31–43, 1990.

[31] E. Giraud, T. Lestinova, T. Derrick, O. Martin, R. J. Dillon, P. Volf, I. Műller, P. A. Bates, and M. E. Rogers. Leishmania proteophosphoglycans regurgitated from infected sand flies accelerate dermal wound repair and exacerbate leishmaniasis via insulin-like growth factor 1-dependent signalling. *PLoS Pathogens*, 14(1), 2018.

[32] R. Titus and J. Ribeiro. Salivary gland lysates from the sand fly Lutzomyia longipalpis enhance Leishmania infectivity. *Science*, 239(4845):1306–1308, mar 1988.

[33] M. G. Rittig, G. R. Burmester, and A. Krause. Coiling phagocytosis: When the zipper jams, the cup is deformed. *Trends in Microbiology*, 6(10):384–388, 1998.

[34] M. G. Rittig and C. Bogdan. Leishmania-host-cell interaction: Complexities and alternative views. *Parasitology Today*, 16(7):292–297, 2000.

[35] M. C. Diniz, M. P. Costa, A. C. L. Pacheco, M. T. Kamimura, S. C. Silva, L. D. G. Carneiro, A. P. L. Sousa, C. E. A. Soares, C. S. F. Souza, and D. M. de Oliveira. Actin-interacting and flagellar proteins in Leishmania spp.: Bioinformatics predictions to functional assignments in phagosome formation. *Genetics and Molecular Biology*, 32(3):652–665, 2009.

[36] K. M. Tyler, A. Fridberg, K. M. Toriello, C. L. Olson, J. A. Cieslak, T. L. Hazlett, and D. M. Engman. Flagellar membrane localization via association with lipid rafts. *Journal of Cell Science*, 122(6):859–866, 2009.

[37] N. Singla and V. K. Vinayak. Leishmania donovani flagellum-specific mediating host-parasite interactions epitopes. *FEMS Immunology and Medical Microbiology*, 8:175–182, 1994.

[38] B. Rotureau, M. A. Morales, P. Bastin, and G. F. Späth. The flagellum-mitogen-activated protein kinase connection in Trypanosomatids: A key sensory role in parasite signalling and development? *Cellular Microbiology*, 11(5):710–718, 2009.

[39] J. A. Champion and S. Mitragotri. Role of target geometry in phagocytosis. *Proceedings of the National Academy of Sciences*, 103(13):4930–4934, 2006.

[40] J. A. Champion and S. Mitragotri. Shape Induced Inhibition of Phagocytosis of Polymer Particles. *Pharmaceutical Research*, 26(1), 2009.

[41] C. Yao, J. E. Donelson, and M. E. Wilson. The major surface protease (MSP or GP63) of Leishmania sp. Biosynthesis, regulation of expression, and function, nov 2003.

[42] A. Brittingham, C. J. Morrison, W. R. McMaster, B. S. McGwire, K. P. Chang, and D. M. Mosser. Role of the Leishmania surface protease gp63 in complement fixation, cell adhesion, and resistance to complement-mediated lysis. *Journal of immunology*, 155(6):3102–11, sep 1995.

[43] P. B. Joshi, D. L. Sacks, G. Modi, and W. R. McMaster. Targeted gene deletion of Leishmania major genes encoding developmental stage-specific leishmanolysin (GP63). *Molecular microbiology*, 27(3):519–30, feb 1998.

[44] J. Blanchette, N. Racette, R. Faure, K. A. Siminovitch, and M. Olivier. Leishmania-induced increases in activation of macrophage SHP-1 tyrosine phosphatase are associated with impaired IFN-γ-triggered JAK2 activation. *European Journal of Immunology*, 29(11):3737–3744, nov 1999.

[45] M. Olivier, D. J. Gregory, and G. Forget. Subversion mechanisms by which Leishmania parasites can escape the host immune response: A signaling point of view, apr 2005.

[46] M. Jaramillo, M. A. Gomez, O. Larsson, M. T. Shio, I. Topisirovic, I. Contreras, R. Luxenburg, A. Rosenfeld, R. Colina, R. W. McMaster, M. Olivier, M. Costa-Mattioli, and N. Sonenberg. Leishmania repression of host translation through mTOR cleavage is required for parasite survival and infection. *Cell Host and Microbe*, 9(4):331–341, apr 2011.

[47] S. M. Puentes, R. P. Da Silva, D. L. Sacks, C. H. Hammer, and K. A. Joiner. Serum resistance of metacyclic stage Leishmania major promastigotes is due to release of C5b-9. *Journal of immunology*, 145(12):4311–6, dec 1990.

[48] D. L. Sacks, G. Modi, E. Rowton, G. Späth, L. Epstein, S. J. Turco, and S. M. Beverley. The role of phosphoglycans in Leishmania-sand fly interactions. *Proceedings of the National Academy of Sciences*, 97(1):406–411, 2000.

[49] D. L. Sacks. Leishmania-sand fly interactions controlling species-specific vector competence. *Cellular microbiology*, 3(4):189–96, apr 2001.

[50] B. Leader, L. Epstein, S. J. Turco, S. M. Singer, S. M. Beverley, G. F. Spath, and H. A. Avila. Lipophosphoglycan is a virulence factor distinct from related glycoconjugates in the protozoan parasite Leishmania major. *Proceedings of the National Academy of Sciences*, 97(16):9258–9263, 2002.

[51] D. L. Sacks, E. M. Saraiva, E. Rowton, S. J. Turco, and P. F. Pimenta. The role of the lipophosphoglycan of Leishmania in vector competence. *Parasitology*, 108:55–62, 1994.

[52] E. Inbar, V. K. Hughitt, L. A. L. Dillon, K. Ghosh, N. M. El-Sayed, and D. L. Sacks. The transcriptome of Leishmania major developmental stages in their natural sand fly vector. *mBio*, 8(2), may 2017.

[53] P. F. Pimenta, S. J. Turco, M. J. McConville, P. G. Lawyer, D. L. Sacks, and P. V. Perkins. Stage-specific adhesion of Leishmania promastigotes to the sandfly midgut. *Science*, 256(5065):1812–1815, mar 1992.

[54] G. F. Späth, L. A. Garraway, S. J. Turco, and S. M. Beverley. The role(s) of lipophosphoglycan (LPG) in the establishment of Leishmania major infections in mammalian hosts. *Proceedings of the National Academy of Sciences of the United States of America*, 100(16):9536–41, aug 2003.

[55] M. E. Wilson and R. D. Pearson. Evidence that Leishmania donovani utilizes a mannose receptor on human mononuclear phagocytes to establish intracellular parasitism. *Journal of immunology*, 136(12):4681–8, jun 1986.

[56] G. F. Spath, L. Lye, H. Segawa, D. L. Sacks, S. J. Turco, and S. M. Beverley. Persistence Without Pathology in Phosphoglycan-Deficient Leishmania major. *Science*, 301(5637):1241–1243, 2003.

[57] R. J. Wheeler, E. Gluenz, and K. Gull. The cell cycle of Leishmania: Morphogenetic events and their implications for parasite biology. *Molecular Microbiology*, 79(3):647–662, 2011.

[58] G. Langousis and K. L. Hill. Motility and more: the flagellum of Trypanosoma brucei. *Nature reviews. Microbiology*, 12(7):505–18, 2014.

[59] G. Taylor. Analysis of the Swimming of Microscopic Organisms. *Proceedings of the Royal Society A: Mathematical, Physical and Engineering Sciences*, 209(1099):447–461, 1951.

[60] E. M. Purcell. Life at low Reynolds number. *American Journal of Physics*, 45:3–11, 1977.

[61] H. C. Berg. The Rotary Motor of Bacterial Flagella. *Annual Review of Biochemistry*, 72(1):19–54, 2003.

[62] E. A. Gaffney, H. Gadêlha, D. J. Smith, J. R. Blake, and J. C. Kirkman-Brown. Mammalian Sperm Motility: Observation and Theory. *Annual Review of Fluid Mechanics*, 43(1):501–528, 2011.

[63] K. Y. Wan, K. C. Leptos, and R. E. Goldstein. Lag, lock, sync, slip: the many "phases" of coupled flagella. *Journal of the Royal Society, Interface*, 11(94), may 2013.

[64] N. Heddergott, T. Krüger, S. B. Babu, A. Wei, E. Stellamanns, S. Uppaluri, T. Pfohl, H. Stark, and M. Engstler. Trypanosome Motion Represents an Adaptation to the Crowded Environment of the Vertebrate Bloodstream. *PLoS Pathogens*, 8(11), 2012.

[65] S. Uppaluri, J. Nagler, E. Stellamanns, N. Heddergott, S. Herminghaus, M. Engstler, and T. Pfohl. Impact of microscopic motility on the swimming behavior of parasites: Straighter Trypanosomes are more directional. *PLoS Computational Biology*, 7(6):1–8, 2011.

[66] R. J. Wheeler. Use of chiral cell shape to ensure highly directional swimming in trypanosomes. *PLOS Computational Biology*, 13, 2017.

[67] J. Elgeti, R. G. Winkler, and G. Gompper. Physics of microsimmers - single particle motion and collective behavior: a review. *Reports on Progress in Physics*, 78, 2015.

[68] C. Brennen and H. Winet. Fluid Mechanics of Propulsion by Cilia and Flagella. *Annual Review of Fluid Mechanics*, 9(1):339–398, 1977.

[69] C. J. Brokaw. Swimming with three-dimensional flagellar bending wave. *Second Int.Sympos. Aqua-Biomech.*, pages Honolulu, HI,, 2003.

[70] C. Gadelha, B. Wickstead, and K. Gull. Flagellar and ciliary beating in trypanosome motility. *Cell Motility and the Cytoskeleton*, 64(8):629–643, 2007.

[71] S. Schuster, T. Krüger, I. Subota, S. Thusek, B. Rotureau, A. Beilhack, and M. Engstler. Developmental adaptations of trypanosome motility to the tsetse fly host environments unravel a multifaceted in vivo microswimmer system. *eLife*, 6, aug 2017.

[72] J. L. Höög, C. Bouchet-Marquis, J .R. McIntosh, A. Hoenger, and K. Gull. Cryo-electron tomography and 3-D analysis of the intact flagellum in Trypanosoma brucei. *Journal of Structural Biology*, 178(2):189–198, may 2012.

[73] J. A. Rodríguez, M. A. Lopez, M. C. Thayer, Y. Zhao, M. Oberholzer, D. D. Chang, N. K. Kisalu, M. L. Penichet, G. Helguera, R. Bruinsma, K. L. Hill, and J. Miao. Propulsion of African trypanosomes is driven by bihelical waves with alternating chirality separated by kinks. *Proceedings of the National Academy of Sciences*, 106(46):19322–19327, 2009.

[74] R. Cerbino and V. Trappe. Differential dynamic microscopy: Probing wave vector dependent dynamics with a microscope. *Physical Review Letters*, 100(18):1–4, 2008.

[75] V. A. Martinez, R. Besseling, O. A. Croze, J. Tailleur, M. Reufer, J. Schwarz-Linek, L. G. Wilson, M. A. Bees, and W. C. K. Poon. Differential dynamic microscopy: A high-throughput method for characterizing the motility of microorganisms. *Biophysical Journal*, 103(8):1637–1647, 2012.

[76] M. Reufer, V. A. Martinez, P. Schurtenberger, and W. C. K. Poon. Differential dynamic microscopy for anisotropic colloidal dynamics. *Langmuir*, 28(10):4618–4624, 2012.

[77] V. A. Martinez, J. Schwarz-Linek, M. Reufer, L. G. Wilson, A. N. Morozov, and W. C. K. Poon. Flagellated bacterial motility in polymer solutions. *Proceedings of the National Academy of Sciences*, 111(50):17771–6, 2014.

[78] S. Weisse, N. Heddergott, M. Heydt, D. Pflasterer, T. Maier, T. Haraszti, M. Grunze, M. Engstler, and A. Rosenhahn. A quantitative 3D motility analysis of Trypanosoma brucei by use of digital in-line holographic microscopy. *PLoS ONE*, 7(5):1–13, 2012.

[79] L. G. A. Alves, D. B. Scariot, R. R. Guimarães, C. V. Nakamura, R. S. Mendes, and H. V. Ribeiro. Transient Superdiffusion and Long-Range Correlations in the Motility Patterns of Trypanosomatid Flagellate Protozoa. *PloS ONE*, 11(3), 2016.

[80] U. Schnars and W. Jüptner. Direct recording of holograms by a CCD target and numerical reconstruction. *Applied optics*, 33(2):179–181, 1994.

[81] W. Xu, M. H. Jericho, I. A. Meinertzhagen, and H. J. Kreuzer. Digital in-line holography for biological applications. *Proceedings of the National Academy of Sciences*, 98(20):11301–5, sep 2001.

[82] F. Merola, L. Miccio, P. Memmolo, G. Di Caprio, A. Galli, R. Puglisi, D. Balduzzi, G. Coppola, P. Netti, and P. Ferraro. Digital holography as a method for 3D imaging and estimating the biovolume of motile cells. *Lab on a Chip*, 13(23), oct 2013.

[83] F. Saglimbeni, S. Bianchi, A. Lepore, and R. Di Leonardo. Three-axis digital holographic microscopy for high speed volumetric imaging. *Optics Express*, 22(11):13710, jun 2014.

[84] A. Wang, R. F. Garmann, and V. N. Manoharan. Tracking E. coli runs and tumbles with scattering solutions and digital holographic microscopy. *Optics Express*, 24(21):23719–23725, 2016.

[85] J. F. Jikeli, L. Alvarez, B. M. Friedrich, L. G. Wilson, R. Pascal, R. Colin, M. Pichlo, A. Rennhack, C. Brenker, and U. B. Kaupp. Sperm navigation along helical paths in 3D chemoattractant landscapes. *Nature Communications*, 6:7985, 2015.

[86] L. G. Wilson, L. M. Carter, and S. E. Reece. High-speed holographic microscopy of malaria parasites reveals ambidextrous flagellar waveforms. *Proceedings of the National Academy of Sciences*, 110(47):18769–18774, 2013.

[87] J. Gray. *Ciliary movement*. The University Press, Cambridge [England], 1928.

[88] J. Gray and G. J. Hancock. The Propulsion of Sea-Urchin Spermatozoa. *Journal of Experimental Biology*, 32(4):802–814, 1955.

[89] D. J. Smith, E. A. Gaffney, H. Gadelha, N. Kapur, and J. C. Kirkman-Brown. Bend propagation in the flagella of migrating human sperm, and its modulation by viscosity. *Cell Motility and the Cytoskeleton*, 66(4):220–236, 2009.

[90] S. M. Duncan, N. G. Jones, and J. C. Mottram. Recent advances in Leishmania reverse genetics: Manipulating a manipulative parasite. *Molecular and Biochemical Parasitology*, 216:30–38, sep 2017.

[91] L. Sollelis, M. Ghorbal, C. R. MacPherson, R. M. Martins, N. Kuk, L. Crobu, P. Bastien, A. Scherf, J. Lopez-Rubio, and Y. Sterkers. First efficient CRISPR-Cas9-mediated genome editing in Leishmania parasites. *Cellular Microbiology*, 17(10):1405–1412, oct 2015.

[92] T. Beneke, R. Madden, L. Makin, J. Valli, J. Sunter, and E. Gluenz. A CRISPR Cas9 high-throughput genome editing toolkit for kinetoplastids. *Royal Society Open Science*, 4(5):170095, may 2017.

[93] N. G. Kolev, C. Tschudi, and E. Ullu. RNA interference in protozoan parasites: achievements and challenges. *Eukaryotic cell*, 10(9):1156–63, sep 2011.

[94] N. Kraeva, A. Ishemgulova, J. Lukeš, and V. Yurchenko. Tetracycline-inducible gene expression system in Leishmania mexicana. *Molecular and Biochemical Parasitology*, 198(1):11–13, nov 2014.

[95] A. Ishemgulova, N. Kraeva, D. Faktorová, L. Podešvová, J. Lukeš, and V. Yurchenko. T7 polymerase-driven transcription is downregulated in metacyclic promastigotes and amastigotes of Leishmania mexicana. *Folia Parasitologica*, 63(16), 2016.

[96] S. Dean, J. Sunter, R. J. Wheeler, I. Hodkinson, E. Gluenz, and K. Gull. A toolkit enabling efficient, scalable and reproducible gene tagging in trypanosomatids. *Open biology*, 5(1), jan 2015.

[97] R. J. Wheeler, E. Gluenz, and K. Gull. Basal body multipotency and axonemal remodelling are two pathways to a 9+0 flagellum. *Nature Communications*, 6(8964), 2015.

[98] T. Lang, S. Goyard, M. Lebastard, and G. Milon. Bioluminescent Leishmania expressing luciferase for rapid and high throughput screening of drugs

acting on amastigote-harbouring macrophages and for quantitative real-time monitoring of parasitism features in living mice. *Cellular Microbiology*, 7(3):383–392, mar 2005.

[99] M. E. Wilson, L. Love-Homan, S. M. Beverley, S. M. Hickerson, N. Craft, J. W. Graff, and C. J. Thalhofer. In vivo Imaging of Transgenic Leishmania Parasites in a Live Host. *Journal of Visualized Experiments*, (41), 2010.

[100] S. Thiberge, S. Blazquez, P. Baldacci, O. Renaud, S. Shorte, R. Ménard, and R. Amino. In vivo imaging of malaria parasites in the murine liver. *Nature Protocols*, 2(7):1811–1818, jul 2007.

[101] N. E. Farthing, R. C. Findlay, J. F. Jikeli, P. B. Walrad, M. A. Bees, and L. G. Wilson. Simultaneous two-color imaging in digital holographic microscopy. *Optics Express*, 25(23):28489–28500, nov 2017.

[102] D. Gabor. A new microscopic principle. *Nature*, 161(4098):777–778, 1948.

[103] K. L. Thornton, R. C. Findlay, P. B. Walrad, and L. G. Wilson. Investigating the Swimming of Microbial Pathogens Using Digital Holography. *Biophysics of Infection*, 8(3):17–32, 2016.

[104] G. Corkidi, B. Taboada, C. D. Wood, A. Guerrero, and A. Darszon. Tracking sperm in three-dimensions. *Biochemical and Biophysical Research Communications*, 373(1):125–129, aug 2008.

[105] C. B. Giuliano, R. Zhang, and L. G. Wilson. Digital Inline Holographic Microscopy (DIHM) of Weakly-scattering Subjects Video Link. *Journal of Visualized Experiments*, 8450488(10), 2014.

[106] L. Mandel and E. Wolf. *Optical coherence and quantum optics*. Cambridge University Press, 1995.

[107] S-H. Lee and D. G. Grier. Holographic microscopy of holographically trapped three-dimensional structures. *Optics express*, 15(4):1505–1512, 2007.

[108] M. K. Kim. Principles and techniques of digital holographic microscopy. *SPIE Reviews*, 1(1):018005, 2010.

[109] L. G. Wilson and R. Zhang. 3D Localization of weak scatterers in digital holographic microscopy using Rayleigh-Sommerfeld back-propagation. *Optics Express*, 20(15):16735, jul 2012.

[110] M. Molaei, M. Barry, R. Stocker, and J. Sheng. Failed escape: Solid surfaces prevent tumbling of Escherichia coli. *Physical Review Letters*, 113(6), 2014.

[111] M. E. Rogers, P. Kropf, B. S. Choi, R. Dillon, M. Podinovskaia, P. A. Bates, and I. Müller. Proteophosophoglycans regurgitated by Leishmania-infected sand flies target the L-arginine metabolism of host macrophages to promote parasite survival. *PLoS Pathogens*, 5(8), 2009.

[112] M. E. Rogers, K. Corware, I. Müller, and P. A. Bates. Leishmania infantum proteophosphoglycans regurgitated by the bite of its natural sand fly vector, Lutzomyia longipalpis, promote parasite establishment in mouse skin and skin-distant tissues. *Microbes and Infection*, 12(11):875–879, 2010.

[113] G. F. Späth and S. M. Beverley. A lipophosphoglycan-independent method for isolation of infective Leishmania metacyclic promastigotes by density gradient centrifugation. *Experimental Parasitology*, 99:97–103, 2001.

[114] E. Knuepfer, Y. D. Stierhof, P. G. M. C. Kean, and D. F. Smith. Characterization of a differentially expressed protein that shows an unusual localization to intracellular membranes in Leishmania major. *Biochemistry Journal*, 356:335–344, 2001.

[115] A. Down. The Frenet-Serret Theorem. pages 1–7, 2006.

[116] G. S. Reddy, A. G. Mukhopadhyay, and C. S. Dey. The p38 MAP kinase inhibitor, PD 169316, inhibits flagellar motility in Leishmania donovani. *Biochemical and Biophysical Research Communications*, 493(4):1425–1429, sep 2017.

[117] H. C. Berg and D. A. Brown. Chemotaxis in Escherichia coli analysed by three-dimensional tracking. *Nature*, 239(5374):500–504, 1972.

[118] P. Satir, L. B. Pedersen, and S. T. Christensen. The primary cilium at a glance. *Journal of Cell Science*, 123(4):499–503, feb 2010.

[119] H. P. Price, D. Paape, M. R. Hodgkinson, K. Farrant, J. Doehl, M. Stark, and D. F. Smith. The Leishmania major BBSome subunit BBS1 is essential for parasite virulence in the mammalian host. *Molecular Microbiology*, 90(3):597–611, nov 2013.

[120] M. E. Rogers and P. A. Bates. Leishmania manipulation of sand fly feeding behavior results in enhanced transmission. *PLoS Pathogens*, 3(6):0818–0825, 2007.

[121] D. L. Sacks. Metacyclogenesis in Leishmania promastigotes. *Experimental Parasitology*, 69:100–103, 1989.

[122] M. Meyers and K. Chawla. *Mechanical Behaviour of Materials*. 1999.

[123] K. Sankaranarayanan and N. Meenakshisundaram. Micro-viscosity induced conformational transitions in poly-L-lysine. *Royal Society of Chemistry Advances*, 6(78):74009–74017, aug 2016.

[124] D. Zhang, X. Li, H. Tan, G. Zhang, Z. Zhao, H. Shi, Li. Zhang, W. Yu, and Z. Sun. Photocatalytic reduction of Cr(VI) by polyoxometalates/TiO2 electrospun nanofiber composites. *Royal Society of Chemistry Advances*, 4(84):44322–44326, 2014.

[125] W. R. Schneider and R. N. Doetsch. Effect of Viscosity on Bacterial Motility. *Journal of Bacteriology*, 71(8):3253–3254, 1974.

[126] H. C. Berg and L. Turner. Movement of microorganisms in viscous environments. *Nature*, 278(5702):349–351, 1979.

[127] Y. Magariyama and S. Kudo. A mathematical explanation of an increase in bacterial swimming speed with viscosity in linear-polymer solutions. *Biophysical Journal*, 83(2):733–739, 2002.

[128] M. E. Rogers, M. L. Chance, and P. A. Bates. The role of promastigote secretory gel in the origin and transmission of the infective stage of Leishmania mexicana by the sandfly Lutzomyia longipalpis. *Parasitology*, 124(Pt 5):495–507, 2002.

[129] D. Sacks and S. Kamhawi. Molecular Aspects of Parasite-Vector and Vector-Host Interactions in Leishmaniasis. *Annual Review of Microbiology*, 55(1):453–483, 2001.

[130] S. Adler and O. Theodor. Attempts to transmit leishmania tropica by bite: The transmission of L. Tropica by phlebotomus: Sergenti. *Annals of Tropical Medicine and Parasitology*, 23(1):1–18, apr 1929.

[131] E. D. Franke, P. B. McGreevy, S. P. Katz, and D. L. Sacks. Growth cycle-dependent generation of complement-resistant Leishmania promastigotes. *Journal of immunology*, 134(4):2713–2718, apr 1985.

[132] T. Laskay, G. van Zandbergen, and W. Solbach. Neutrophil granulocytes–Trojan horses for Leishmania major and other intracellular microbes? *Trends in microbiology*, 11(5):210–4, may 2003.

[133] N. C. Peters, J. G. Egen, N. Secundino, A. Debrabant, S. Kamhawi, P. Lawyer, M. P. Fay, R. N. Germain, and D. Sacks. In vivo imaging reveals an essential role for neutrophilis in Leishmaniasis transmitted by sand flies. *Science*, 321(5891):970–974, 2009.

[134] J. S. P. Doehl, Z. Bright, S. Dey, H. Davies, J. Magson, N. Brown, A. Romano, J. E. Dalton, A. I. Pinto, J. W. Pitchford, and P. M. Kaye. Skin parasite landscape determines host infectiousness in visceral leishmaniasis. *Nature Communications*, 8(1):57, dec 2017.

[135] L. H. Franco, S. M. Beverley, and D. S. Zamboni. Innate Immune Activation and Subversion of Mammalian Functions by Leishmania Lipophosphoglycan. *Journal of Parasitology Research*, pages 1–11, 2012.

[136] R. S. Bray. Leishmania: chemotaxic responses of promastigotes and macrophages in vitro. *Journal of Protozoology*, 30(2):322–329, 1983.

[137] C. Grabher, A. Cliffe, K. Miura, R. Pepperkok, P. Rorth, and J. Wittbrodt. Birth and life of tissue macrophages and their migration in embryogenesis and inflammation in medaka. *Journal of Leukocyte Biology*, 81(1):263–271, 2006.

[138] J. S. Oliveira, M. N. Melo, and N. F. Gontijo. A sensitive method for assaying chemotaxic responses of Leishmania promastigotes. *Experimental parasitology*, 96(3):187–189, 2000.

[139] G. Leslie, M. Barrett, and R. Burchmore. Leishmania mexicana: Promastigotes migrate through osmotic gradients. *Experimental Parasitology*, 102(2):117–120, 2002.

[140] A. A. Ahmed, A. Wahbi, K. Nordlind, A. Kharazmi, K. G. Sundqvist, V. Mutt, and S. Lidé. In vitro Leishmania major promastigote-induced macrophage migration is modulated by sensory and autonomic neuropeptides. *Scandinavian Journal of Immunology*, 48(1):79–85, 1998.

[141] V. C. Barros, J. S. Oliveira, M. N. Melo, and N. F. Gontijo. Leishmania amazonensis: Chemotaxic and osmotaxic responses in promastigotes and their probable role in development in the phlebotomine gut. *Experimental Parasitology*, 112(3):152–157, 2006.

[142] R. M. Macnab and D. E. Koshland. The Gradient-Sensing Mechanism in Bacterial Chemotaxis. *Proceedings of the National Academy of Sciences*, 69(9):2509–2512, 1972.

[143] Y. Rikitake and Y. Takai. Directional Cell Migration. Regulation by Small G Proteins, Nectin-like Molecule-5, and Afadin. *International Review of Cell and Molecular Biology*, 287:97–143, jan 2011.

[144] U. B. Kaupp and T. Strünker. Signaling in Sperm: More Different than Similar. *Trends in Cell Biology*, 27(2):101–109, 2017.

[145] P. Ralph, J. Prichard, and M. Cohn. Reticulum cell sarcoma: an effector cell in antibody-dependent cell-mediated immunity. *J Immunol*, 114:898–905, 1975.

[146] Z. Petrasek and P. Schwille. Precise measurement of diffusion coefficients using scanning fluorescence correlation spectroscopy. *Biophysical Journal*, 94(4):1437–1448, feb 2008.

[147] G. J. Goodhill. Diffusion in axon guidance. *European Journal of Neuroscience*, 9(7):1414–1421, jul 1997.

[148] M. U. Shiloh, J. Ruan, and C. Nathan. Evaluation of Bacterial Survival and Phagocyte Function with a Fluorescence-Based Microplate Assay. *Infection and Immunity*, 65(8):3193–3198, 1997.

[149] S. H. Larsen, R. W. Reader, E. N. Kort, W. W. Tso, and J. Adler. Change in direction of flagellar rotation is the basis of the chemotactic response in Escherichia coli. *Nature*, 249(5452):74–77, 1974.

[150] J. F. Staropoli and U. Alon. Computerized analysis of chemotaxis at different stages of bacterial growth. *Biophysical Journal*, 78(1):513–519, 2000.